Theoretical study of real-gas effects on shock wave phenomena

2011

Shigeru TANIGUCHI

Nagoya Institute of Technology

Theoretical study of real-gas effects on shock wave phenomena

(衝撃波現象における実在気体効果に関する理論的研究)

A dissertation for the Doctor Degree of Engineering

Submitted To

Department of Scientific and Engineering Simulation,
Nagoya Institute of Technology,
Japan

Written By

Shigeru TANIGUCHI

2011

Supervised By

Professor

Masaru SUGIYAMA

Abstract

Compared to shock waves in rarefied gases, shock waves in condensed matters, namely, dense gases, liquids and solids, have not been fully understood. In order to construct the basic theoretical framework of shock wave phenomena in condensed matters, we propose the following strategy with two steps:

(i) We study shock wave phenomena in a hard-sphere system which is a good reference system of materials in liquid state.

(ii) By using all the results obtained in step (i) and by using the perturbation method developed in the theory of liquid-state physics, we study shock wave phenomena in physical systems with more realistic interatomic potential with both repulsive and attractive parts.

Shock wave phenomena are theoretically and numerically studied on the basis of the system of Euler equations with the caloric and thermal equations of state for several models of condensed matters. First Rankine-Hugoniot conditions are analyzed. The quantitative classification of Hugoniot types in terms of the thermodynamic quantities of the unperturbed state (the state before a shock wave) and the degrees of freedom is made. Second the admissibility (stability) of shock waves is studied by means of the results obtained by T.-P. Liu in the theory of hyperbolic systems. Last numerical calculations have been performed in order to confirm the theoretical results in the case of admissible shocks and to obtain the actual evolution of the wave profiles in the case of inadmissible shocks.

The organization of this thesis is summarized as follows:

In Chap. 1, The purpose of the present study and the applications of shock wave phenomena are summarized. It is pointed out there exist shock wave phenomena which can not be explained even qualitatively within the well-known framework of the ideal-gas model. The effects inducing such differences are called as the real-gas effects on shock wave phenomena. The typical phenomena due to the real-gas effects are shock-induced phase transitions, shock splitting phenomena and rarefaction (negative) shock waves.

In Chap. 2, Shock waves in a polytropic hard-sphere system with and without internal degrees of freedom are investigated. The important role of the internal degrees of freedom for shock-induced phase transition from the liquid to the solid phase (Alder transition) is made clear. It is shown that another type of instability of a shock wave can exist even though the perturbed state is thermodynamically stable.

In Chap. 3, we predict and simulate a new type of compressive shock wave in a real gas. For simplicity, we adopt a real gas modeled the van der Waals constitutive equation which can be regarded as a simplified model of a system of hard-spheres with attractive force. This shock produces a phase transition from the gas to the liquid phase and, under some special circumstances, back to the gas phase. This shock has the following quite unusual property: When the perturbed pressure (the pressure after a shock) increases, the perturbed density decreases and tends to a limit value *from above*, in contrast with the ordinary compressive shock in which the density tends to the limit value *from below*.

In Chap. 4, shock waves in a system of hard-spheres with attractive force are analyzed. By using this model, we can analyze shock wave phenomena in the three phases, namely, gas, liquid and solid phases within a unified way. It is confirmed that the analysis based on this model can explain both the results obtained in a hard-sphere system and in a van der Waals fluid. Two possible scenarios of shock-induced phase transition from the gas to the solid phase have been presented and the condition of such phase transition is made clear.

In Chap. 5, by adopting a simplified model of a non-polytropic hard-sphere system where heat capacity depends on the temperature, we demonstrate the importance of non-polytropic effect on the shock wave phenomena. We show explicitly that with the increase of the shock strength the perturbed temperature (the temperature after a shock) increases and the vibrational modes are gradually excited, and as a result, shock-induced phase transitions and the admissibility of shock wave are qualitatively and quantitatively different from the phase transitions observed in a simple polytropic model.

In Chap. 6, general summary of the present study and concluding remarks are made.

Contents

NOTATIONS

t: time

x: position

ρ: mass density

m: mass of a constituent particle

V: volume

$\mathcal{V}$: specific volume

η: packing fraction

v: velocity

p: pressure

T: temperature

e: specific internal energy

s: specific entropy

h: specific enthalpy

c: sound velocity

U_{s}: velocity of a shock wave

c_{v}: specific heat capacity at constant volume

λ: characteristic velocity

$\mathcal{D}$: degrees of freedom

f: internal degrees of freedom

k_{B}: Boltzmann constant

$\mathbf{u}$: density of conservative quantities

$\mathbf{F}$: flux of conservative quantities

Chapter 1

Introduction

1.1 Background of the present study

Shock waves, which are characterized by the steep and rapid changes of physical quantities such as mass density, velocity, temperature, pressure at a shock front, are typical nonlinear waves that have been studied from many aspects experimentally, theoretically and numerically [1–3]. Concerning the theoretical studies, for example, the rapid change of physical quantities at a shock front has been studied based on the theories of non-equilibrium thermodynamics and statistical physics [4–6] and also their nonlinear properties have been investigated based on the theories of nonlinear wave propagation [7, 8].

The motivation to study shock waves comes from not only the interest in such properties but also the fact that shock wave phenomena can be observed in wide area. The examples of shock waves in nature and the man-made shock waves can be summarized as follows.

Examples of shock waves in nature

The most familiar shock wave phenomenon is a thunder after the lightening. Shock waves are also related to Earthquakes and volcanic eruptions. Shock waves are much frequently generated in cosmic space. For example, meteoroids entering in the atmosphere around the earth generate shock waves. The flow of ionized gas particles emitted from the sun's corona (so-called solar wind) can be accelerated by the magnetic field of the earth and be developed to be a bow shock.

Examples of man-made shock waves

The typical example of man-made shock waves is a detonation of explosive materials. The other typical example is the complex shock wave structure observed around a supersonic passenger plane. Shock waves can also be observed during the atmosphere entry of a space shuttle. The strength of man-made shock waves have large variety from weak shocks generated by firearms, to very strong shock generated nuclear explosions.

1.1.1 Applications of shock wave study

There are many applications of shock wave studies in engineering, physical and chemical fields. We here summarize typical examples of the applications of shock wave phenomena briefly.

Supersonic airplane

As mentioned above, the complex shock structure can be observed around a supersonic airplane. The shock wave study becomes important when we design the shape of the supersonic airplane because efficiency of the flight and noise due to such waves strongly depend on the property of shock waves generated by the airplane.

Detonation

The detonation wave is a supersonic wave phenomena accompanying chemical reactions with the rapid change of pressure and temperature after the shock front. The studies have been concentrated on the technique to avoid detonation phenomena for the safety because such kind of rapid increasing of the physical quantities may be dangerous. Recently detonation phenomena can be used positively, for example, in pulse detonation engines and also pulse detonation rocket.

Calculus fragmentation, Shock focusing

Shock waves are also used for the fragmentation of the calculus in the human body. The technique, which make us to destroy the calculus without any surgeries, are well established. In such cases the technique of focusing of a shock wave using convex lens plays an essential role in order to avoid to injure any organs except the calculus and therefore the detailed study of shock wave propagation becomes very important.

Space science

The basic researches of shock wave phenomena are also important for the space engineering and space science. As we mentioned in above examples, the body of space shuttle involves shock waves during the atmosphere entry and therefore the detailed study of flows around the body is important to design the shape of a space shuttle. Moreover, there exists an important problem of serious damage of the frames of space shuttles or space satellite due to space debris, that is the garbage or dust moving at high velocities in the cosmic space. The response to the impact of space debris are important in order to prepare the safe frame of space shuttles.

Land-mine removal

The response to shock waves generated by the explosive materials is also important especially in the field of engineering. The land-mine removal is quite important, however, is dangerous due to the risk of accidents. In order to remove land mines much more safely, the shape of the machine for the land-mine removal and the quality of materials should be designed carefully. The studies of shock wave phenomena can provide the basic knowledge of such kind of applications.

1.1.2 Study of Shock waves in condensed matters

As is seen from the above examples and applications, the studies of shock wave phenomena in condensed matters, namely, dense gases, liquids and solids are necessary. In recent years, shock wave phenomena in condensed matters have also attracted much interest of researchers in various fields. See, for example, the review paper [9] and books [10–18] and references cited therein. However, Compared to shock waves in rarefied gases, shock waves in condensed matters have not been fully studied until now.

Many studies of shock waves in condensed matters have been done mainly from the experimentally and numerically. Some theoretical studies were also made by using the models with realistic interatomic potentials. However, most of the previous works are based on more or less qualitative models. An unified framework of theoretical studies is highly required in order to understand shock wave phenomena in condensed matters deeply. Such kind of theoretical framework can be essentially important for the development of shock wave study as the theoretical study played an essential role at the early stage of the development of shock wave studies. Jouguet

wrote the usefulness of the theoretical predictions of shock waves as follows [19]: "*The shock wave represents a phenomenon of rare peculiar such that it has been uncovered by the pen of mathematicians, first by Riemann, then by Hugoniot. The experiments followed not until afterwards.* "

In this thesis we will propose the basic theoretical framework to analyze shock wave phenomena in condensed matters. Based on that framework, we will investigate the shock wave phenomena which can not be explained even qualitatively within the well-known framework of the ideal gas model.

1.2 Theory of shock wave phenomena

In this section, we will discuss the basis of the present theoretical studies. In order to make the physical implications of our analysis clear, here we summarize the typical theoretical studies briefly [20].

The first-order approximation of shock wave phenomena is the analysis based on the Euler fluids in which the dissipative effects, namely, viscosity and heat conduction are neglected. The solution of a shock wave in Euler fluids can be obtained as a weak solution which represents the jump of physical quantities before and after a shock front without any shock structures. The relation between the propagation speed and the jump of physical quantities before and after a shock front is the central problem within this approximation. The compatibility conditions of the jump of physical quantities can be derived from the conservation laws of mass, momentum and energy. These conditions are well known as the Rankine-Hugoniot conditions.

In the higher-order approximation of shock wave phenomena, the shock structure, that is the wave profile in terms of the time and the position, is one of the interesting problem in the field of the non-equilibrium thermodynamics and statistical physics. Because physical quantities change rapidly with steep gradient at a shock front, many information about highly non-equilibrium phenomena can be obtained through the analysis of shock structure. In order to make the validity range of several theories clear, the studies of shock structures have been done theoretically [22–33], experimentally [34–37] and numerically [38–42]. From these studies, it is shown that the theoretical prediction by the well-known Navier-Stokes and Fourier theory is not valid for strong shock waves (or large Knudsen number) and therefore the results imply that we need other theories which have larger validity range.

The dimensionality dependence is also one of the important problems. Pla-

nar shock waves can be analyzed easily and can be generated by the shock tubes, however, spherical or cylindrical shock waves are more frequently observed for the applications of shock waves generated by explosive materials.

In this thesis we concentrate on one-dimensional waves (plane shock waves) traveling only along the x direction in the Euler fluid for the first step. In the following, we summarize the system of Euler equations and the compatibility condition of jump of physical quantities before and after a shock front. Moreover, the admissibility (stability) conditions of a shock wave are also discussed.

1.2.1 The system of Euler equations

The system of Euler equations describing the conservation of mass, momentum and energy for a compressible fluid in the one-dimensional case can be expressed as

$$\mathbf{u}_t + \mathbf{F}_x(\mathbf{u}) = 0, \tag{1.1}$$

where the subscripts (time t and position x) denote partial differentiation. Here the density $\mathbf{u}$ and the flux $\mathbf{F}$ of conservation quantities are given by

$$\mathbf{u} = \begin{pmatrix} \rho \\ \rho v \\ \rho e + \frac{1}{2}\rho v^2 \end{pmatrix}, \qquad \mathbf{F} = \begin{pmatrix} \rho v \\ \rho v^2 + p \\ \left(\rho e + \frac{1}{2}\rho v^2 + p\right) v \end{pmatrix}, \tag{1.2}$$

with ρ, v, p and e being the mass density, the velocity, the pressure and the specific internal energy, respectively. The characteristic velocities of the hyperbolic system (1.1) and (1.2) can be summarized as follows:

$$\lambda^{(1)} = v - c, \qquad \lambda^{(2)} = v, \qquad \lambda^{(3)} = v + c, \tag{1.3}$$

where $c = \sqrt{(\partial p/\partial \rho)_s}$ represents the sound velocity and s is the specific entropy.

1.2.2 The Rankine-Hugoniot conditions

The system of Euler equations (1.1)-(1.2) admits a plane shock wave provided that the jump of the physical quantities between the states before and after the shock front satisfies the well-known Rankine-Hugoniot (RH) conditions:

$$\begin{aligned} -U_s[\![\rho]\!] + [\![\rho v]\!] &= 0, \\ -U_s[\![\rho v]\!] + \left[\!\!\left[\rho v^2 + p\right]\!\!\right] &= 0, \\ -U_s\left[\!\!\left[\rho e + \frac{1}{2}\rho v^2\right]\!\!\right] + \left[\!\!\left[\left(\rho e + \frac{1}{2}\rho v^2 + p\right) v\right]\!\!\right] &= 0, \end{aligned} \tag{1.4}$$

where U_s is the propagation velocity of the shock front and $[\![\psi]\!] = \psi_1 - \psi_0$ represents the jump of a generic quantity ψ across the shock front, being ψ_1 the quantity in the state after the shock *(perturbed state)* and ψ_0 in the state before the shock *(unperturbed state)*.

The Mach number at the unperturbed state, M_0, is defined by

$$M_0 = \frac{U_\mathrm{s} - v_0}{c_0} \tag{1.5}$$

where the quantities with the subscript 0 are the so-called *unperturbed quantities*, i.e. the quantities evaluated in the unperturbed state (analogously, the quantities with the subscript 1 are evaluated in the perturbed state and are called *perturbed quantities*).

In the following, we shall consider only shocks propagating in the positive x direction ($M_0 > 0$) and, due to the Galilean invariance, we shall also assume, without any loss of generality, $v_0 = 0$, then we have

$$\begin{aligned}
\hat{v}_1 &\equiv \frac{v_1}{c_0} \\
&= M_0 \frac{\rho_1 - \rho_0}{\rho_1}, \\
\hat{p}_1 &\equiv \frac{p_1}{p_0} \\
&= 1 + c_0^2 M_0^2 \frac{\rho_0 (\rho_1 - \rho_0)}{p_0 \rho_1}, \\
M_0 &= \frac{1}{c_0} \sqrt{\frac{2\rho_1}{\rho_0 (\rho_1 - \rho_0)} \left[p_1 - \frac{\rho_0 \rho_1 (e_1 - e_0)}{\rho_1 - \rho_0} \right]}.
\end{aligned}$$

The specific entropy production rate can also be given by

$$\varsigma = -U_s [\![\rho s]\!] + [\![\rho s v]\!].$$

Using the RH condition $(1.4)_1$ and the definition of the unperturbed Mach number (1.5), this relation can be rearranged as follows:

$$\begin{aligned}
\varsigma &= \rho_0 (U_\mathrm{s} - v_0) [\![s]\!] \\
&= \rho_0 c_0 M_0 [\![s]\!].
\end{aligned} \tag{1.6}$$

Since we will focus on the fastest wave traveling in the positive x-direction, we define a dimensionless characteristic velocity $\hat{\lambda}$ as follows:

$$\hat{\lambda} \equiv \frac{\lambda_1^{(3)}}{c_0} = \hat{v} + \hat{c}, \tag{1.7}$$

where $\hat{c}$ is the dimensionless sound speed defined by

$$\hat{c} = \frac{c_1}{c_0}.$$

Weak shock waves

Let us also study shock waves with the small jumps of physical quantities. Such shock waves are called as the *weak shock waves*. Here we introduce the specific enthalpy h as follows:

$$h \equiv e + \frac{p}{\rho}.$$

Using the RH conditions, we can obtain the expression of the jump of the specific enthalpy as follows:

$$h_1 - h_0 = \frac{1}{2}(\mathcal{V}_0 - \mathcal{V}_1)(p_1 - p_0), \tag{1.8}$$

where $\mathcal{V}$ is the specific volume. On the other hand, expanding the jump of the specific enthalpy $(h_1 - h_0)$ with respect to $(p_1 - p_0)$ within third order and with respect to $(s_1 - s_0)$ within first order for the consistency and then we have

$$\begin{aligned} h_1 - h_0 = &\left(\frac{\partial h}{\partial s_0}\right)_p (s_1 - s_0) + \left(\frac{\partial h}{\partial p_0}\right)_s (p_1 - p_0) \\ &+ \frac{1}{2}\left(\frac{\partial^2 h}{\partial p_0^2}\right)_s (p_1 - p_0)^2 + \frac{1}{6}\left(\frac{\partial^3 h}{\partial p_0^3}\right)_s (p_1 - p_0)^3. \end{aligned}$$

Using the expression of the partial differential of the specific enthalpy

$$\left(\frac{\partial h}{\partial s}\right)_p = T, \qquad \left(\frac{\partial h}{\partial p}\right)_s = \mathcal{V},$$

we obtain

$$\begin{aligned} h_1 - h_0 = &T_0(s_1 - s_0) + \mathcal{V}_0(p_1 - p_0) \\ &+ \frac{1}{2}\left(\frac{\partial \mathcal{V}}{\partial p_0}\right)_s (p_1 - p_0)^2 + \frac{1}{6}\left(\frac{\partial^2 \mathcal{V}}{\partial p_0^2}\right)_s (p_1 - p_0)^3. \end{aligned} \tag{1.9}$$

Similarly the jump of specific volume $(\mathcal{V}_1 - \mathcal{V}_0)$ can be expanded with respect to $(p_1 - p_0)$ within second order and we obtain

$$\mathcal{V}_1 - \mathcal{V}_0 = \left(\frac{\partial \mathcal{V}}{\partial p_0}\right)_s (p_1 - p_0) + \frac{1}{2}\left(\frac{\partial^2 \mathcal{V}}{\partial p_0}\right)_s (p_1 - p_0)^2. \tag{1.10}$$

Inserting the relations (1.8) and (1.9) into the relation (1.10), we can obtain the jump of the specific entropy $(s_1 - s_0)$ as follows:

$$s_1 - s_0 = \frac{1}{12T_0}\left(\frac{\partial^2 \mathcal{V}}{\partial p_0^2}\right)_s (p_1 - p_0)^3. \tag{1.11}$$

From the basic knowledge of nonequilibrium thermodynamics, the entropy production rate should have non-negative value in all physical processes in order to satisfy

the second law of thermodynamics. Because in this case the entropy production rate is proportional to the entropy jump (see (1.6)), the solution is physically meaningful only in the case the entropy jump is positive. Therefore we can conclude that only compressive shock waves can propagate in the case that derivative $(\partial^2\mathcal{V}/\partial p_0^2)_s$ is positive, however, a negative shock wave may be observed if the derivative $(\partial^2\mathcal{V}/\partial p_0^2)_s$ is negative. The derivative $(\partial^2\mathcal{V}/\partial p_0^2)_s$ is sometimes called as the *fundamental derivative* and in many researches the dimensionless form

$$\mathcal{G} = \frac{c^4}{2\mathcal{V}^3}\left(\frac{\partial^2\mathcal{V}}{\partial p^2}\right)_s$$

was used for the analysis.

1.2.3 Admissibility of shock waves

According to the theory of hyperbolic systems, not every solution of the Rankine-Hugoniot conditions corresponds to a physically meaningful shock wave. Thus, we need a criterion to select which states $\mathbf{u}_1 \in \mathcal{H}(\mathbf{u}_0)$ are the perturbed states that, together with $\mathbf{u}_0$ form *admissible* shocks. Since admissible shocks propagate with no change in shape when they are given as initial data, these solution are sometimes called *stable shocks*.

In order to provide a selection rule to evaluate the admissibility of shocks, it is necessary to recall that in the theory of hyperbolic systems a wave associated to a characteristic velocity λ (eigenvalue of the characteristic system) is called *genuinely non-linear*, if $\nabla\lambda \cdot \mathbf{r} \neq 0 \ \ \forall\mathbf{u}$; *linearly degenerate* (or *exceptional*), if $\nabla\lambda \cdot \mathbf{r} \equiv 0 \ \ \forall\mathbf{u}$; *locally linearly degenerate* (or *locally exceptional*), if $\nabla\lambda \cdot \mathbf{r} = 0$ for some $\mathbf{u}$, where $\mathbf{r}$ is the corresponding eigenvector of λ.

The issue of shock admissibility when genuinely non-linear and linearly degenerate waves are involved has been largely investigated; the hyperbolic system of conservation laws of mass, momentum and energy for an ideal gas, for example, features only waves belonging to these two types and it has been deeply analyzed in the past decades (see, among others, [20]). On the contrary, the hyperbolic system of the van der Waals fluid, for example, features linearly degenerate and locally linearly degenerate waves. Focusing on the fastest wave associated to $\lambda \equiv \lambda^{(3)}$, the locus such that $\nabla\lambda = 0$ for the present system can be obtained given by

$$\rho\left(\frac{\partial^2 p}{\partial\rho^2}\right)_s + 2\left(\frac{\partial p}{\partial\rho}\right)_s = 0.$$

It can be proved that this locus is equivalent to the curve such that the fundamental derivative is zero ($\mathcal{G} = 0$).

The selection rule useful to study the admissibility of shocks depends on the type of the involved non-linear waves. Thus, it is necessary to discuss separately the cases of genuinely non-linear, linearly degenerate and locally linearly degenerate waves.

When we deal with genuinely non-linear waves, the selection rule is given by the *Lax condition* [43], according to which a shock wave is admissible if the shock speed satisfies

$$\lambda_0 < U_\mathrm{s} < \lambda_1$$

where $\lambda_0 \equiv \lambda(\mathbf{u}_0)$ and $\lambda_1 \equiv \lambda(\mathbf{u}_1)$. The Lax condition turns out to be equivalent (at least for *weak shocks*) to the condition of entropy growth across the shock [20]. When we deal with a linearly degenerate wave, admissible shocks are called *characteristic shocks* and they propagate with velocity $s = \lambda_0 = \lambda_1$. In this case, there is no entropy production across the shock.

When the system features locally linearly degenerate waves, the selection rule is given by the *Liu condition* [44, 45], which asserts that a shock wave connecting an unperturbed state $\mathbf{u}_0$ and a perturbed state $\mathbf{u}_1$ is *admissible* (*stable*) if its velocity of propagation, s, is not decreasing as we move along $\mathcal{H}(\mathbf{u}_0)$, which is the locus of the perturbed states satisfying the RH conditions, starting from the unperturbed state, $\mathbf{u}_0$, towards the perturbed state $\mathbf{u}_1$, i.e.:

$$U_\mathrm{s}(\mathbf{u}_0, \tilde{\mathbf{u}}) \leq U_\mathrm{s}(\mathbf{u}_0, \mathbf{u}_1) \;\; \forall \tilde{\mathbf{u}} \in \mathcal{H}(\mathbf{u}_0) \,\text{between}\, \mathbf{u}_0 \,\text{and}\, \mathbf{u}_1.$$

If the Liu condition is not satisfied, the shock is *unstable*, or *inadmissible*. It is well known that the Liu condition implies the Lax condition, and at least for moderate shocks, the entropy growth, and therefore stable shocks satisfy the second law of the thermodynamics (see, e.g. [8]). Conversely, the entropy growth is not sufficient to imply the Liu condition, and we need an additional condition [8, 46].

1.3 Shock wave phenomena in an ideal gas

Shock wave phenomena in a rarefied gas has widely been studied by using the well-known framework of an ideal gas model (See, for example, [20, 21]). We here summarize the typical properties of shock waves in an ideal gas in detail.

Equations of state

The basic equations are the Euler equations with the thermal and caloric equations of state for an ideal gas. Caloric equation of state for an ideal gas is summarized as follows:

$$e = \frac{RT}{\delta}, \tag{1.12}$$

where T is the temperature; $\delta = R/c_v$, $R = k_B/m$, being k_B the Boltzmann constant, m the mass of a constituent molecule and c_v the specific heat capacity at constant volume related to the internal degrees of freedom. Thermal equation of state is given by

$$p = RT\rho. \tag{1.13}$$

Using the Gibbs relation

$$\mathrm{d}s = \frac{1}{T}\mathrm{d}e + \frac{p}{T}\mathrm{d}\left(\frac{1}{\rho}\right),$$

we can obtain the explicit expression of the sound speed as follows:

$$c = \sqrt{\frac{(1+\delta)p}{\rho}}.$$

Note that there is no phase transitions in an ideal gas model.

Rankine-Hugoniot conditions

Inserting the thermal and caloric equations of state for an ideal gas (1.12) and (1.13) into the general form of Rankine-Hugoniot conditions, we can obtain the expression of the perturbed velocity divided by the unperturbed sound speed $\hat{v}_1$ and the expression of the ratio between pressures in the perturbed and the unperturbed state as follows:

$$\begin{aligned} \hat{v}_1 &= M_0\left(1 - \frac{1}{\hat{\rho}_1}\right) \\ &= \sqrt{\frac{2\hat{\rho}_1}{2+\delta(1-\hat{\rho}_1)}}\left(1 - \frac{1}{\hat{\rho}_1}\right), \end{aligned} \tag{1.14}$$

$$\begin{aligned} \hat{p}_1 &= 1 + c_0^2 M_0^2 \frac{\rho_0\left(\rho_1 - \rho_0\right)}{p_0\rho_1} \\ &= 1 + \frac{2\left(1+\delta\right)\left(\hat{\rho}_1 - 1\right)}{2 - \delta\left(\hat{\rho}_1 - 1\right)}, \end{aligned} \tag{1.15}$$

where $\hat{\rho}_1$ is the ratio between densities in the perturbed and unperturbed state and expressed as follows:

$$\hat{\rho}_1 = \frac{\rho_1}{\rho_0}.$$

The expression of the unperturbed Mach number can be obtained as follows:

$$\begin{aligned} M_0 &= \frac{1}{c_0}\sqrt{\frac{2\rho_1 p_0\,(1+\delta)}{\rho_0\,[2\rho_0 - \delta\,(\rho_1 - \rho_0)]}} \\ &= \sqrt{\frac{2\hat{\rho}_1}{2+\delta(1-\hat{\rho}_1)}}. \end{aligned} \tag{1.16}$$

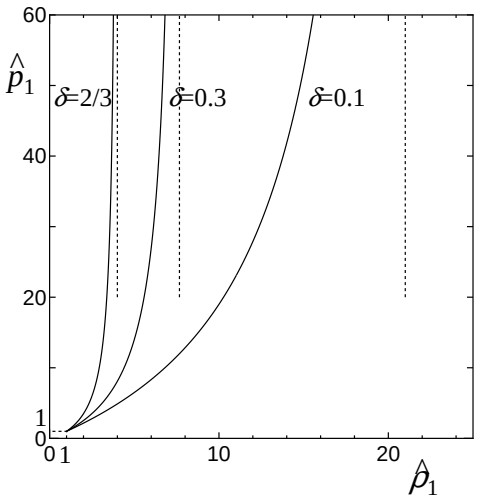

Figure 1.1: Dependence of the perturbed pressure on the perturbed density for several $\delta(\delta = 2/3, 0.3, 0.1)$. Vertical dotted lines are asymptotes, $\hat{\rho}_1 = \hat{\rho}_1^{\infty}$.

It can be seen from Fig. 1.1 that the perturbed pressure increase monotonically as the increase of the perturbed density (strength of the shock wave). In the strong shock limit the perturbed pressures diverge, however, the perturbed density approach a finite critical value which depend on δ (internal degrees of freedom). The ratio between densities in the strong shock limit and the unperturbed state is called as ultimate compression ratio, $\hat{\rho}_1^{\infty}$. From the expressions of Rankine-Hugoniot conditions (1.14), (1.15) and (1.16), the value of $\hat{\rho}_1^{\infty}$ can be obtained explicitly as follows:

$$\hat{\rho}_1^{\infty} = 1 + \frac{2}{\delta}. \tag{1.17}$$

From Fig. 1.2 and also (1.17), $\hat{\rho}_1^{\infty}$ increase as the decrease of δ (which corresponds to the increase of the internal degrees of freedom). This result can be physically interpreted that as the increase of the internal degrees of freedom. the energy

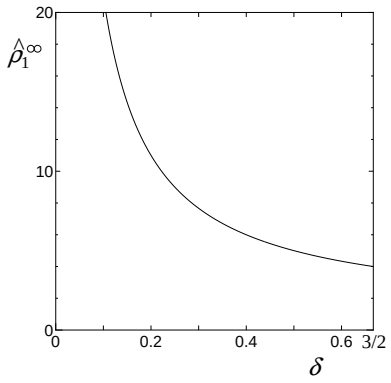

Figure 1.2: The dependence of $\hat{\rho}_1^{\infty}$ on δ.

flow into the internal motion becomes larger and therefore the increasing rate of perturbed temperature and perturbed pressure, due to a shock compression, become comparatively smaller.

Admissibility of shock waves

We have derived the Rankine-Hugoniot conditions for an ideal gas. As is pointed out in Sec. 1.2.3, the Rankine-Hugoniot conditions are only necessary conditions for the physically meaningful solution and therefore we need other admissibility conditions.

We discuss the admissibility of a shock wave by using the Lax condition which is obtained in terms of the propagation speed of a shock and the characteristic speed. The unperturbed Mach number M_0 (1.5) and the dimensionless characteristic speed $\hat{\lambda}$ (1.7) are the propagation speed of a shock wave $U_{\rm s}$ divided by the unperturbed sound speed and the fastest characteristic speed divided by the unperturbed sound speed. Therefore we can conclude the admissibility from the magnitude relation between M_0 and $\hat{\lambda}$ based on the Lax condition. From the definitions, the values of M_0 and $\hat{\lambda}$ at the unperturbed state are always one. The derivative of M_0 with respect to the perturbed density ρ_1 can be given by

$$\frac{{\rm d}M_0^2}{{\rm d}\hat{\rho}_1} = \frac{4+2\delta}{\left[2-\delta(1-\hat{\rho}_1)\right]^2} > 0$$

and therefore we have

$$M_0 = \begin{cases} > 1 & for \quad \hat{\rho}_1 > 1 \\ 1 & for \quad \hat{\rho}_1 = 1 \\ < 1 & for \quad \hat{\rho}_1 < 1. \end{cases} \tag{1.18}$$

We can conclude that $\lambda_0 < U_{\rm s}$ when $\hat{\rho}_1 > 1$.

The difference between M_0 and $\hat{\lambda}$ can be expressed by

$$\begin{aligned}\hat{\lambda} - M_0 &= \hat{v} + \hat{c} - M_0 \\ &= \sqrt{\frac{\hat{\rho}_1(2+\delta) - \delta}{\hat{\rho}_1\left[2 - \delta(\hat{\rho}_1 - 1)\right]}} - \sqrt{\frac{2}{\hat{\rho}_1\left[2 - \delta(\hat{\rho}_1 - 1)\right]}}.\end{aligned}$$

The magnitude relation between the unperturbed Mach number M_0 and the dimensionless characteristic speed $\hat{\lambda}$ is summarized as follows:

$$\hat{\lambda} = \begin{cases} > M_0 & \text{for} \quad \hat{\rho}_1 > 1 \\ M_0 & \text{for} \quad \hat{\rho}_1 = 1 \\ < M_0 & \text{for} \quad \hat{\rho}_1 < 1. \end{cases}$$

This fact can also be seen from Fig. 1.3. We can conclude that $U_\mathrm{s} < \lambda_1$ when $\hat{\rho}_1 > 1$.

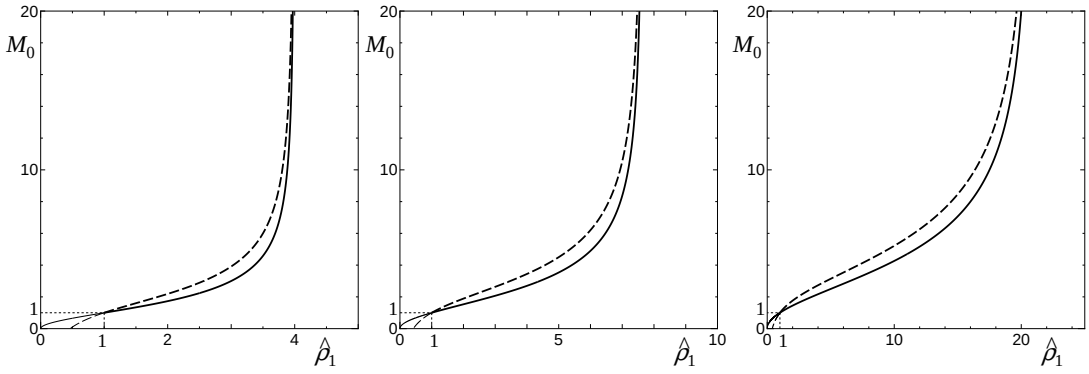

Figure 1.3: The dependence of the unperturbed Mach number M_0 (solid line) and the dimensionless characteristic speed $\hat{\lambda}$ (dashed line) on the perturbed density ρ_1 for several δ (Left: $\delta = 2/3$, center: $\delta = 0.3$, right: $\delta = 0.1$).

From the Lax condition, it is shown that a shock wave is admissible only when the perturbed density is larger than the unperturbed density. We can conclude that all and only compressive shock waves are admissible in an ideal gas based on the Lax condition.

Typical properties of shock waves in an ideal gas

The typical property of shock wave phenomena in an ideal gas are summarized as follows:

- Shock-induced phase transition can not occur.
- All and only compressive shock waves are admissible.

1.4 Typical real-gas effects on shock wave phenomena

The typical properties of wave phenomena in an ideal gas were summarized in the previous sections. As the validity range of the ideal gas model is limited, shock wave in condensed matters are more or less different from the ones in an ideal gas. However, it is known that there exists shock wave phenomena which are not only quantitatively but also even qualitatively different from shock waves an ideal gas. In this thesis we will call the effects inducing such differences as the *real-gas effects* on shock wave phenomena.

Here we list the typical examples of the real-gas effects on shock wave phenomena.

1.4.1 Shock-induced phase transition

Physical quantities can be changed rapidly at a shock front, therefore, the states before and after a shock front can be in different phases, in the other words, shock waves can induce phase transitions.

Several studies of the shock-induced phase transitions were made by experiments. Experiments of liquefaction shock waves [47] freezing and crystallization of liquid benzene [48], melting of Iron [49], melting of vanadium [50] and structural phase transition between two solid phases in Molybdenum [51] have already been investigated.

Several studies were made by computer simulations of microscopic models. Molecular dynamics simulations for shock-induced freezing in a hard-sphere system [52], melting of Argon [53], melting of Al [54], melting of Cu, Pd, Pt [55], melting of many metals [56] and structural phase transition between two solid phases [57] have been performed.

Some theoretical studies were also made by using the models with realistic interatomic potentials [9, 58–60]. A review article [61] is also available. Material synthesis, for example, sometimes makes use of such dynamic phase transitions [62].

1.4.2 Rarefaction (negative) shock waves

All and only compressive shock waves in an ideal gas are admissible. However, in condensed matters, rarefaction (negative) shock waves can propagate stably. This shock waves are shock waves of which the density in the state after the shock is smaller than the density in the state before the shock.

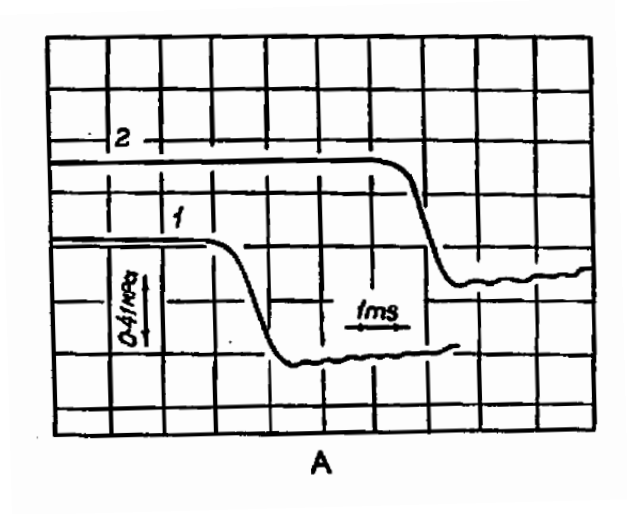

Figure 1.4: Direct observation of rarefaction shocks by the experiments in the pressure - time plane [67]. It is clearly seen that the pressure decrease rapidly after the shock fronts.

The existence of the negative shock wave and the condition for these shock waves were investigated [63]. More detailed discussions have also been done [64, 65]. The negative shock waves were observed directly by the experiment [66, 67]. A review paper [68] is also available.

1.4.3 Shock splitting phenomena

Shock splitting phenomena are the other typical phenomena due to the real-gas effect. This phenomena are that an unstable shock wave eventually splits into several waves composed of shock waves, rarefaction waves and constant states in the course of its propagation.

Shock splitting phenomena in a gas [69–71] and in a solid [57] have already been studied.

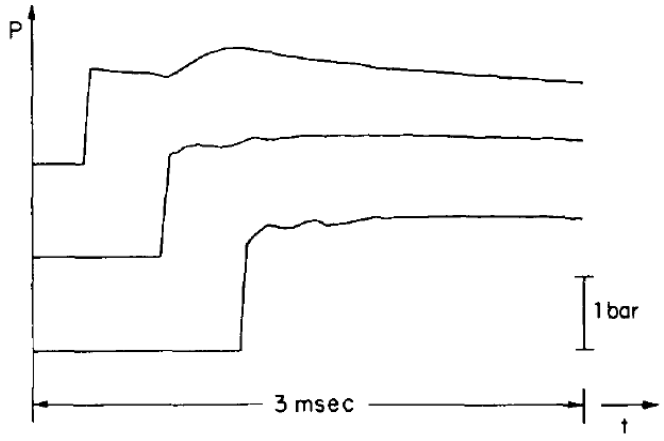

Figure 1.5: Several experimental results of shock wave profile [69] in a vapor-liquid phase are shown in the pressure - time plane. Shock splitting phenomena can be observed.

1.5 Theoretical studies of shock wave phenomena in two models of condensed matters

Here we show theoretical studies which can explain typical real-gas effects on shock wave phenomena by using the framework of models of condensed matters.

1.5.1 Shock wave phenomena in a hard-sphere system

The shock waves in a hard-sphere system without internal degrees of freedom have widely been studied. Especially, in the recent paper [83], shock wave phenomena and shock-induced phase transition from liquid phase to solid phase were studied in detail.

Because we will analyze shock wave phenomena in a hard-sphere system with internal degrees of freedom in Chap. 2 as a direct consequence of this study and we will derive more general relations which include all relations derived in that paper, we here summarize only the typical results briefly.

The caloric equation of state for a hard-sphere system has the same form as the one of an ideal gas. Only the thermal equation of state is different. From Fig. 1.6, we can see that there exists the first-order phase transition (*Alder transition*) which can be regarded as the prototype of the liquid / solid phase transition.

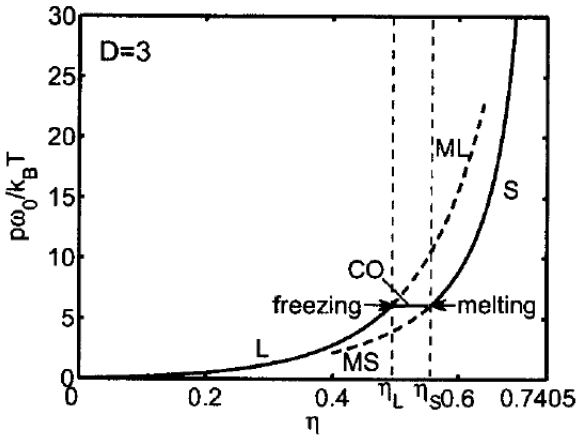

Figure 1.6: Liquid phase and solid phase branches of the $p\omega/k_BT - \eta$ curve for a hard-sphere system [83] (L: stable liquid branch, ML: metastable liquid branch, S: stable solid branch, MS: metastable solid branch, CO: liquid-solid coexistence branch). η_L and η_S are the packing fractions at the freezing and melting points, respectively.

Shock-induced phase transition

The two possibilities of shock-induced phase transition from liquid phase to solid phase were discussed. The case P-1 is the phase transition between a metastable liquid state and a stable solid state, and the case P-2 is the phase transition through coexistence states when the shock strength changes.

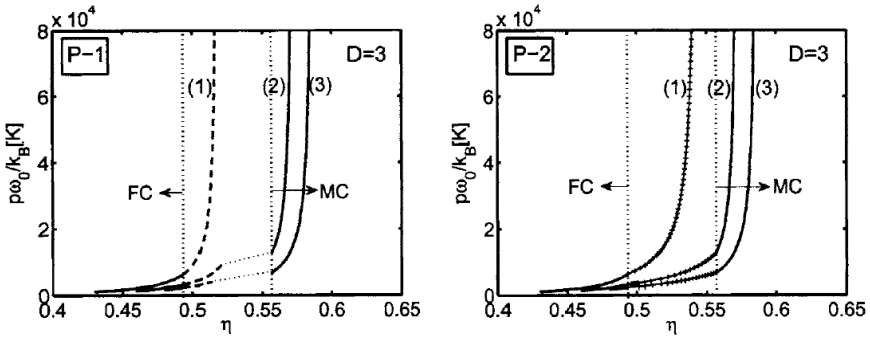

Figure 1.7: Typical Rankine-Hugoniot curves for several unperturbed states in the pressure - density plane. Left: RH curves in the case P-1. Right: RH curves in the case P-2. FC and MC represent the freezing curve and the melting curve, respectively.

The selection rule to choose more promising case was proposed. The selection rule is expressed in terms of the maximum entropy production rate: *The relevant case, from a physical point of view, is the one that involves the largest specific entropy*

production rate at a shock front as a function of the unperturbed Mach number. It is concluded that the possibility P-2 is more promising according to the selection rule.

The admissibility of a shock wave was also analyzed based on the Liu condition, however, rarefaction shock waves and shock splitting phenomena were not be reported in that paper.

1.5.2 Shock wave phenomena in a van der Waals fluid

In a real gas it is possible to observe several features related to shock phenomena, such as rarefaction (negative) shock waves, shock-splitting phenomena and shock-induced phase transitions. Despite its simplicity, the van der Waals model is able to explain all these phenomena. On these topics, several reviews are available; for instance, the papers by Menikoff & Plohr [72], Dahmen et al. [73], Meier [47] (see also the references cited therein) and the monograph by Zel'dovich and Reizer [74]. Zhao et al. [94] made a complete classification of *admissible* shocks (sometimes called *stable* shocks, with regard to the fact that such shocks may propagate with no change in shape) in a van der Waals fluid in terms of the unperturbed state.

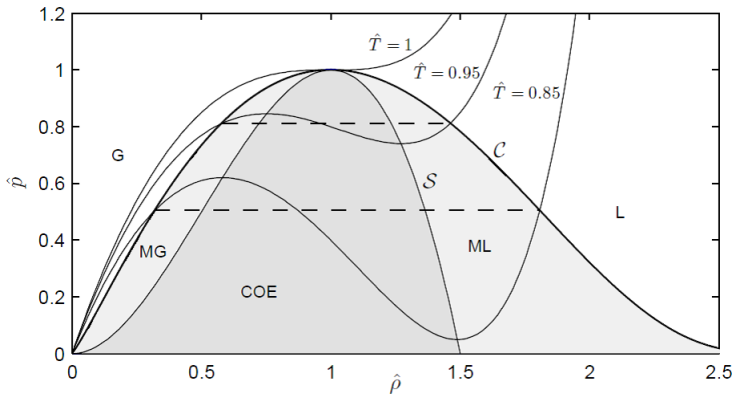

Figure 1.8: The isotherms for several temperatures ($\hat{T} = 0.85, 0.95, 1.0$) in the $\hat{p} - \hat{\rho}$ plane [94]. The Spinodal($\mathcal{S}$) and coexistence($\mathcal{C}$) curves are also shown. The dashed lines are the isotherms by means of Maxwell construction. (G: gas phase, L: liquid phase, MG: metastable gas phase, ML: metastable liquid phase, COE: gas/liquid coexistence phase).

1.6 Purpose and organization of this thesis

As we showed above, several real-gas effects on shock wave phenomena can be explained based on the Euler equations with thermal and caloric equations of state

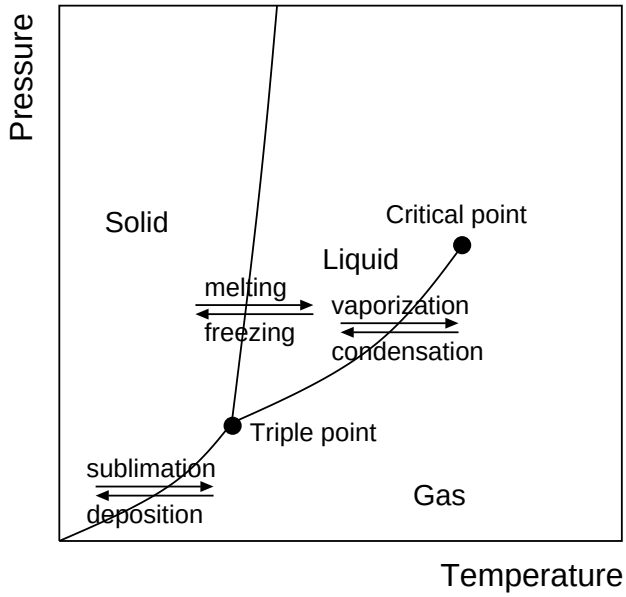

Figure 1.9: Schematic representation of the phase diagram for a simple system in which structural phase transitions can never be observed. The validity ranges of a hard-sphere system and of a van der Waals fluid are near the liquid / solid coexistence curve and near the gas / liquid coexistence curve, respectively.

for a hard-sphere system or a van der Waals system. However, the validity ranges of these analyses are limited. The validity ranges of a hard-sphere system and of a van der Waals fluid are only near the liquid / solid coexistence curve and only near the gas / liquid coexistence curve, respectively.

The purpose of the present study is to construct the framework of more realistic model and to study the real-gas effects on shock wave phenomena by using this framework. In order to construct such framework, we propose the following strategy with two steps:

(i) We study shock wave phenomena in a hard-sphere system which is a good reference system of materials in liquid state.

(ii) By using all the results obtained in step (i) and by using the perturbation method developed in the theory of liquid-state physics, we study shock wave phenomena in physical systems with more realistic interatomic potential with both repulsive and attractive parts.

The organization of this thesis can be summarized as follows:

In Chap. 1, which is this chapter, we summarized the applications of shock wave study. We pointed out that there exists shock wave phenomena which can not be

analyzed even qualitatively within the well-known framework of ideal gas model. We call the effects inducing such differences as the real-gas effects on shock wave phenomena. We summarized typical real-gas effects and showed the usefulness of the theoretical studies of shock wave phenomena in a hard-sphere system and a van der Waals fluid.

In Chap. 2, we will analyze the shock waves in a polytropic hard-sphere system with and without internal degrees of freedom as a direct consequence of the previous study of a hard-sphere system. We will make clear the crucial role of internal degrees of freedom on shock wave phenomena. The complete classification of shock wave phenomena will be made from the viewpoint of the admissibility of a shock wave.

In Chap. 3, we will analyze the new type of compressive shock wave in a van der Waals fluid which can be regarded as the simplified model of a system of hard-spheres with attractive force. This shock has the following quite unusual property: when the perturbed pressure (the pressure after a shock) increases, the perturbed density decreases and tends to a limit value from above, in contrast with the ordinary well-known compressive shock in which the density tends to the limit value from below. The admissibility of a shock wave will be also analyzed based on the Liu condition and we will show that this unusual shock wave can exist.

In Chap. 4, we will analyze the shock waves in a system of hard-spheres with attractive force. It is well known that this system is a suitable realistic model of condensed matters and the validity of this system has already been confirmed. By using this model, we will analyze shock wave phenomena in the three phases, namely, gas, liquid and solid phase, in a unified way.

In Chap. 5, we will analyze the shock waves in a non-polytropic hard-sphere system. We assume that the internal degrees of freedom are independent of the temperature in Chap.2, however, we will introduce the dependence of the internal degrees of freedom on the temperature in this chapter. We will see that this temperature dependence may affect on the shock-induced phase transition and the admissibility of a shock wave strongly.

In Chap. 6, general summary and concluding remarks of this thesis will be shown.

The flow chart of the present study is shown in Fig. 1.10

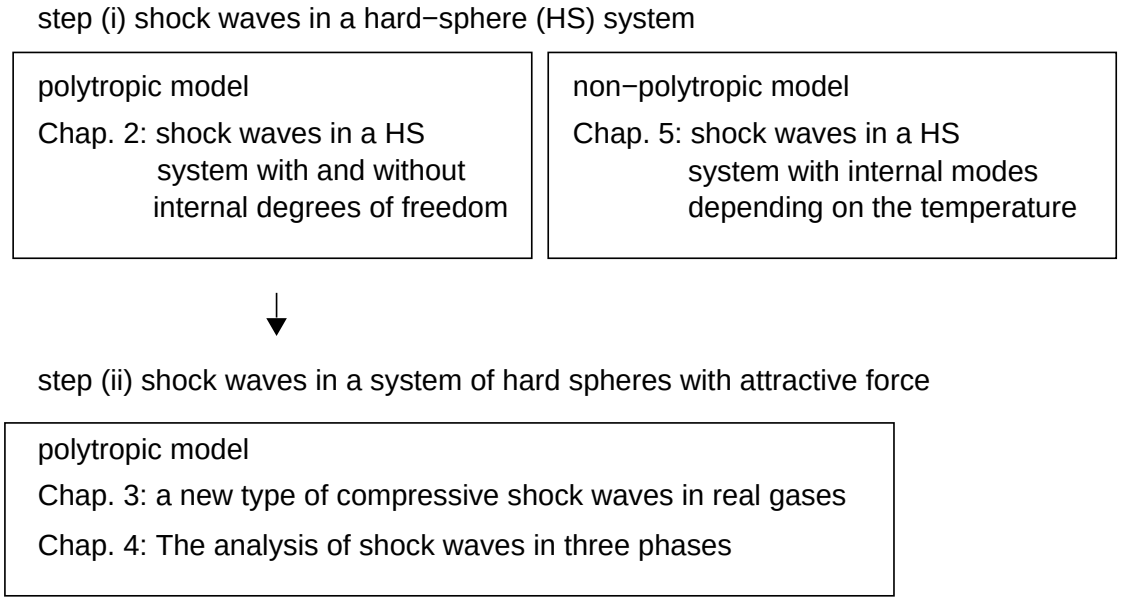

Figure 1.10: The flow chart of the present study.

Chapter 2

Shock waves in polytropic hard-sphere systems with and without internal degrees of freedom

2.1 Introduction

As we mentioned in Chap. 1, in a paper [83], dynamic phase transition induced by a shock wave was studied quantitatively on the basis of the system of Euler equations with caloric and thermal equations of state for a hard-sphere system in which the first-order phase transition (*Alder transition*) can be observed [75–77]. Rankine-Hugoniot (RH) conditions were analyzed in detail and the classification of Hugoniot types in terms of the thermodynamic quantities of the unperturbed state (the state before a shock wave) and of the shock strength was made. The admissibility (stability) of a shock wave was discussed from the viewpoint of the mathematical theory of hyperbolic systems. The importance of a hard-sphere system resides in the fact that it is a suitable reference system for studying shock wave phenomena including the shock-induced phase transitions in more realistic condensed matters with both attractive and repulsive parts of interatomic potential by using the perturbation theory of liquid state physics [78–80]. In the paper [83], for simplicity, any internal motion in the constituent hard-sphere particles was neglected.

In the present chapter, which is the sequel to the paper [83], we extend our study by introducing internal degrees of freedom in hard-sphere particles [84]. It is well-known that the ultimate compression ratio, i.e. the ratio of mass densities before and

after a shock in the strong shock limit, depends strongly on the internal degrees of freedom. In order to show the crucial importance of the internal degrees of freedom on shock-induced phase transitions, we may consider the possibility of shock-induced gas-liquid phase transitions. In § 132 of the text book [20], the authors expressed their negative opinion about this possibility by saying that *" [the compression of gas in an ordinary shock wave] cannot lead to condensation, since the increase of pressure in the shock wave has less effect on the degree of supersaturation than the increase of temperature"*. Shock-induced gas-liquid phase transitions, however, can be observed in some materials if unperturbed states are suitably chosen [47, 81]. Existence of shock-induced gas-liquid phase transitions can also be shown theoretically in a real gas model such as van der Waals gas, *if the constituent molecules have suitably many internal degrees of freedom* and if unperturbed states are suitably taken [94]. Roughly speaking, because of the energy flow into the internal motion, the increase of temperature of such a gas due to a shock compression is comparatively small, and then a gas-liquid phase transition may occur more easily. We naturally expect that the internal degrees of freedom have similar effects also on liquid-solid phase transitions, especially on Alder transition in a hard-sphere system. We will see below that our expectation is quite relevant.

The purpose of the present chapter is to study shock wave phenomena in a hard-sphere system with internal motion both theoretically and numerically. To be more specific, we will study the following three points in detail: (i) the dependence of the solution of RH conditions on the internal degrees of freedom of a hard-sphere system; (ii) the admissibility of shock waves; (iii) the effects of the internal degrees of freedom on shock-induced phase transitions.

2.2 Basic equations

In this section, we summarize the basic equations of the hard sphere system model. We consider hard spheres in a three-dimensional space, but we study shock-induced phase transitions and shock admissibility focusing on one-dimensional waves (plane waves) travelling only along the x-direction. Therefore, the system of equations that we study is written in the one-dimensional case but the equations of state are written assigning to the hard spheres three degrees of freedom connected to the translational motion.

2.2.1 Caloric and thermal equations of state

We adopt the following caloric equation of state:

$$e = \frac{\mathcal{D}}{2m} k_B T, \tag{2.1}$$

where e, $\mathcal{D}$, m, k_B and T are the specific internal energy, the degrees of freedom of a hard-sphere particle, the mass of a particle, the Boltzmann constant and the absolute temperature, respectively. The degrees of freedom, $\mathcal{D}$, is the sum of the space dimensionality (3, in our analysis), corresponding to the degrees of freedom of the translational motion of a particle and the internal degrees of freedom of a particle, f, so:

$$\mathcal{D} \equiv 3 + f. \tag{2.2}$$

Note that the internal degrees of freedom, f, corresponds to the number of excited eigenmodes of internal motion in a particle and it is assumed to be constant. In the derivation of Eq. (2.1), we have assumed that all the excited modes satisfy the equipartition law of energy in classical statistical mechanics. Although these assumptions are very strong, we believe that they are appropriate as a first step in our analysis. The results obtained below will show us a sound direction for the next steps of this study.

As in the paper [83], the thermal equation of state is given by

$$\frac{p\omega}{k_B T} = \eta \Gamma(\eta), \qquad \Gamma(\eta) \equiv 1 + \chi(\eta), \tag{2.3}$$

where p is the pressure, $\chi(\eta)$ is the deviation from the ideal gas law and η is the packing fraction related to the mass density, ρ, by

$$\eta \equiv \frac{\rho\omega}{m}$$

being ω the volume of a hard sphere ($\omega = \pi\sigma^3/6$, where σ is the diameter of a hard sphere). We adopt the Padé approximation (P(3,3)) for the liquid phase [82] and the results from the free volume theory for the solid phase [80] as follows:

$$\chi^L(\eta) = \frac{4\eta + 1.016112\eta^2 + 1.109056\eta^3}{1 - 2.245972\eta + 1.301008\eta^2},$$
$$\chi^S(\eta) = \frac{1}{\left(\frac{\sqrt{2}\pi}{6\eta}\right)^{1/3} - 1},$$

where superscripts L and S stand for the liquid phase and solid phase, respectively. Hereafter we also use these superscripts for the quantity Γ as follows:

$$\Gamma^L(\eta) \equiv 1 + \chi^L(\eta), \qquad \Gamma^S(\eta) \equiv 1 + \chi^S(\eta).$$

As seen in Fig. 2.1, the curve $p\omega/k_BT - \eta$ has two branches: one is the liquid phase branch and the other one is the solid phase branch. Both branches have thermodynamically metastable parts (ML and MS) as well as stable parts (L and S). The packing fractions η_L and η_S are, respectively, the values of η at the freezing point and at the melting point. In the range between η_L and η_S, there can be liquid-solid coexistence states (CO) with a common temperature, T^*, and a common pressure, p^*. According to the simulation data [77]

$$\frac{6}{\sqrt{2}\pi}\frac{p^*\omega}{k_BT^*} \approx 8.27,$$

and the values of η_L and η_S are given by

$$\eta_L \approx 0.4946, \qquad \eta_S \approx 0.5564.$$

As we have seen in this section, the only difference between the basic equations

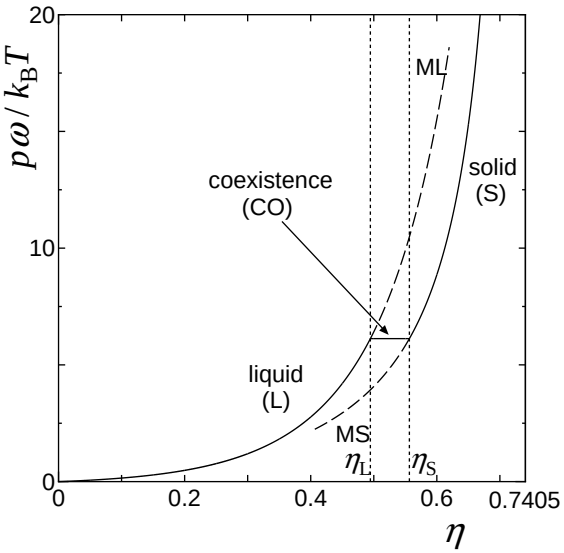

Figure 2.1: Liquid phase and solid phase branches of the $p\omega/k_BT - \eta$ curve for a hard-sphere system (L: stable liquid branch, ML: metastable liquid branch, S: stable solid branch, MS: metastable solid branch, CO: liquid-solid coexistence branch). η_L and η_S are the packing fractions at the freezing and melting points, respectively.

adopted here and those introduced in the paper [83] is in the expression of the caloric equation of state (Eq. (2.1)). This seemingly small difference, however, leads to some profound differences in shock wave phenomena as seen in the following.

2.2.2 The system of Euler equations

The system of Euler equations describing the conservation of mass, momentum and energy for a compressible fluid in the one-dimensional case can be expressed as

$$\mathbf{u}_t + \mathbf{F}_x(\mathbf{u}) = 0, \tag{2.4}$$

where the subscripts (time t and position x) denote partial differentiation. Here the density $\mathbf{u}$ and the flux $\mathbf{F}$ are given by

$$\mathbf{u} = \begin{pmatrix} \rho \\ \rho v \\ \rho e + \frac{1}{2}\rho v^2 \end{pmatrix}, \qquad \mathbf{F} = \begin{pmatrix} \rho v \\ \rho v^2 + p \\ \left(\rho e + \frac{1}{2}\rho v^2 + p\right) v \end{pmatrix} \tag{2.5}$$

with v being the velocity.

The characteristic velocities of the hyperbolic system (2.4)-(2.5) are given by

$$\lambda^{(1)} = v - c, \quad \lambda^{(2)} = v, \quad \lambda^{(3)} = v + c,$$

where $c = \sqrt{(\partial p/\partial \rho)_s}$ represents the sound velocity and s is the specific entropy.

2.3 The Rankine-Hugoniot conditions

The system of Euler equations (2.4)-(2.5) admits a plane shock wave provided that the jump of the physical quantities between the states before and after the shock front satisfies the well-known Rankine-Hugoniot (RH) conditions:

$$-U_s[\![\mathbf{u}]\!] + [\![\mathbf{F}(\mathbf{u})]\!] = 0, \tag{2.6}$$

where U_s is the propagation velocity of the shock front and $[\![\psi]\!] = \psi_1 - \psi_0$ represents the jump of a generic quantity ψ across the shock front, being ψ_1 the quantity in the state after the shock *(perturbed state)* and ψ_0 in the state before the shock *(unperturbed state)*. The conditions (2.6) are explicitly written by using the packing fraction η instead of the mass density ρ as follows:

$$\begin{aligned} -U_s[\![\eta]\!] + [\![\eta v]\!] &= 0, \\ -U_s[\![\eta v]\!] + \left[\!\!\left[\eta v^2 + \frac{p\omega}{m}\right]\!\!\right] &= 0, \\ -U_s\left[\!\!\left[\eta e + \frac{1}{2}\eta v^2\right]\!\!\right] + \left[\!\!\left[\left(\eta e + \frac{1}{2}\eta v^2 + \frac{p\omega}{m}\right) v\right]\!\!\right] &= 0. \end{aligned} \tag{2.7}$$

The Mach number in the unperturbed state, M_0, is defined by

$$M_0 \equiv \frac{U_s - v_0}{c_0},$$

where the quantities with the subscript 0 are the so-called *unperturbed quantities*, i.e. the quantities evaluated in the unperturbed state (analogously, the quantities with the subscript 1 are evaluated in the perturbed state and are called *perturbed quantities*). In the present case, we have

$$c_0 = \sqrt{\frac{k_B T_0}{m}\left(\Gamma_0 + \frac{2}{\mathcal{D}}\Gamma_0^2 + \eta_0 \Gamma_0'\right)},$$

where Γ_i and Γ_i' $(i = 0, 1)$ are defined by

$$\Gamma_i \equiv \Gamma(\eta_i), \qquad \Gamma_i' \equiv \left(\frac{d\Gamma(\eta)}{d\eta}\right)_{\eta_i}.$$

Without loss of generality, we hereafter assume for the Galilean invariance that $v_0 = 0$ and we will focus on the fastest shock wave propagating in the positive x-direction.

We summarize in the following how the RH conditions appear after introducing the equations of state, Eq. (2.1) and Eq. (2.3), into Eq. (2.7) (the details are essentially the same as in the paper [83]) and we discuss some related subjects. Throughout the present paper, we study only the case in which the unperturbed states are in the region of liquid phase (i.e. $\eta_0 < \eta_L$).

2.3.1 Liquid-liquid and liquid-solid RH conditions

Since the equations of state for both liquid and solid phases have the same form (see Eq. (2.1) and Eq. (2.3)), although the expressions of the function $\chi(\eta)$ are different, we write down the RH conditions in a unified way.

The ratios of the pressure and temperature in the perturbed and unperturbed states, and the velocity in the perturbed state divided by the unperturbed sound velocity, c_0, are given by

$$\begin{aligned}
\hat{p} &\equiv \frac{p_1}{p_0} = 1 + \frac{M_0^2(\hat{\eta} - 1)[\Gamma_0(\mathcal{D} + 2\Gamma_0) + \mathcal{D}\Gamma_0'\eta_0]}{\mathcal{D}\Gamma_0\hat{\eta}}, \\
\hat{T} &\equiv \frac{T_1}{T_0} = \frac{\hat{p}\Gamma_0}{\hat{\eta}\Gamma_1}, \\
\hat{v} &\equiv \frac{v_1}{c_0} = M_0\left(1 - \frac{1}{\hat{\eta}}\right),
\end{aligned} \tag{2.8}$$

where $\hat{\eta} \equiv \frac{\eta_1}{\eta_0}$ and M_0 is expressed as

$$M_0 = \sqrt{\frac{\mathcal{D}\hat{\eta}\{-\mathcal{D}\Gamma_0 + \Gamma_1[\mathcal{D}\hat{\eta} + 2(\hat{\eta} - 1)\Gamma_0]\}}{(\hat{\eta} - 1)[\Gamma_1(1 - \hat{\eta}) + \mathcal{D}](\mathcal{D}\Gamma_0 + 2\Gamma_0^2 + \mathcal{D}\eta_0\Gamma_0')}}. \tag{2.9}$$

Since we will be focusing on the fastest wave traveling in the positive x-direction, we define a dimensionless characteristic velocity $\hat{\lambda}$ as follows:

$$\hat{\lambda} \equiv \frac{\lambda_1^{(3)}}{c_0} = \hat{v} + \sqrt{\frac{\hat{T}(\Gamma_1 + \frac{2}{\mathcal{D}}\Gamma_1^2 + \eta_1\Gamma_1')}{\Gamma_0 + \frac{2}{\mathcal{D}}\Gamma_0^2 + \eta_0\Gamma_0'}}.$$

Note that, in all the above expressions,

$$\Gamma_0 \equiv \Gamma^L(\eta_0), \qquad \Gamma_0' \equiv \left(\frac{d\Gamma^L(\eta)}{d\eta}\right)_{\eta_0},$$

and

$$\Gamma_1 \equiv \begin{cases} \Gamma^L(\eta_1) & \text{for } \eta_1 \text{ on the liquid branch; L and ML} - \\ & \textit{liquid-liquid RH conditions}, \\ \Gamma^S(\eta_1) & \text{for } \eta_1 \text{ on the solid branch; S and MS} - \\ & \textit{liquid-solid RH conditions}, \end{cases}$$

$$\Gamma_1' \equiv \begin{cases} \left(\frac{d\Gamma^L(\eta)}{d\eta}\right)_{\eta_1} & \text{for } \eta_1 \text{ on the liquid branch; L and ML} - \\ & \textit{liquid-liquid RH conditions}, \\ \left(\frac{d\Gamma^S(\eta)}{d\eta}\right)_{\eta_1} & \text{for } \eta_1 \text{ on the solid branch; S and MS} - \\ & \textit{liquid-solid RH conditions}. \end{cases}$$

2.3.2 Liquid-coexistence Rankine-Hugoniot conditions

We summarize the RH conditions in the case in which the perturbed state is a coexistence state (L-CO RH conditions). The total packing fraction $\eta(\alpha)$ of a coexistence state is given by

$$\frac{1}{\eta(\alpha)} = \frac{1-\alpha}{\eta_L} + \frac{\alpha}{\eta_S}$$

with the parameter α running from 0 to 1 as the coexistence state moves from the freezing point to the melting point on the horizontal line in Fig. 2.1. The pressure, p^*, is common to both phases and it is related to a common temperature, T^*, as follows:

$$\frac{p^*\omega}{k_B} = T^*\eta_L\left(1 + \chi^L(\eta_L)\right) = T^*\eta_S\left(1 + \chi^S(\eta_S)\right).$$

The following relations are obtained:

$$\hat{p} = 1 + \frac{M_0^2\left(\hat{\eta}(\alpha) - 1\right)\left[\Gamma_0(\mathcal{D} + 2\Gamma_0) + \mathcal{D}\Gamma_0'\eta_0\right]}{\mathcal{D}\Gamma_0\hat{\eta}(\alpha)},$$

$$\hat{T} = \frac{\eta_0\left[\Gamma_0\hat{\eta}(\alpha) + M_0^2\left(\Gamma_0 + 2\Gamma_0^2/\mathcal{D} + \eta_0\Gamma_0'\right)\left(\hat{\eta}(\alpha) - 1\right)\right]}{\Gamma^L(\eta_L)\eta_L\hat{\eta}(\alpha)},$$

$$\hat{v} = M_0\left(1 - \frac{1}{\hat{\eta}(\alpha)}\right),$$

$$M_0 = \sqrt{\frac{\frac{\mathcal{D}\hat{\eta}(\alpha)^2(\Gamma^L(\eta_L)\eta_L - \Gamma_0\eta_0)}{\hat{\eta}(\alpha)-1} + 2\Gamma_0\hat{\eta}(\alpha)\Gamma^L(\eta_L)\eta_L}{(\Gamma_0 + 2\Gamma_0^2/\mathcal{D} + \eta_0\Gamma_0')\left[\Gamma^L(\eta_L)\eta_L(1-\hat{\eta}(\alpha)) + \mathcal{D}\eta_0\hat{\eta}(\alpha)\right]}},$$

$$\hat{\lambda} = \hat{v} + \sqrt{\frac{\frac{2}{\mathcal{D}}\hat{T}\left(\Gamma^L(\eta_L)\eta_L\right)^2}{\hat{\eta}^2(\alpha)\eta_0^2\left(\Gamma_0 + \frac{2}{\mathcal{D}}\Gamma_0^2 + \eta_0\Gamma_0'\right)}}.$$

2.3.3 Two possibilities of shock-induced phase transitions

In the paper [83], the *Hugoniot loci* for the unperturbed states $\mathbf{u}_0$, $\mathcal{H}(\mathbf{u}_0)$, i.e. the loci of the perturbed states satisfying the RH conditions for a given unperturbed state $\mathbf{u}_0$ (also known as *RH curves*), in the two possible cases, P-1 and P-2, of shock-induced phase transitions were analyzed in detail. The case P-1 is the phase transition with a jump between a metastable liquid state and a stable solid state, and the case P-2 is the phase transition through coexistence states when the shock strength changes. We concluded that the case P-2 is to be chosen, instead of the case P-1, by adopting the selection rule in terms of the maximum entropy production rate: *The relevant case, from a physical point of view, is the one that involves the largest specific entropy production rate at a shock front as a function of the unperturbed Mach number.*

Therefore, it is an interesting problem to study whether the conclusion drown in the paper [83] is still true for a hard sphere system with internal motion. We will study this problem in the next section and will conclude that the case P-2 is still to be chosen for any value of the internal degrees of freedom f.

Before applying the selection rule to the cases P-1 and P-2 (Section 2.4), we summarize the relations concerning the specific entropy production rate ς:

$$\varsigma = \eta_0 c_0 M_0 [\![s]\!],$$

where the jump of the specific entropy $[\![s]\!]$ for L-L, L-S and L-CO Hugoniot is given, respectively, by

$$\begin{aligned}
[\![s]\!]^{L-L} &= \tfrac{k_B}{m}\left(\tfrac{\mathcal{D}}{2}\ln\hat{T} - \textstyle\int_{\eta_0}^{\eta_1}\frac{\Gamma^L(\eta)}{\eta}\mathrm{d}\eta\right),\\
[\![s]\!]^{L-S} &= \tfrac{k_B}{m}\left(\tfrac{\mathcal{D}}{2}\ln\hat{T} - \left(\textstyle\int_{\eta_0}^{\eta_L}\frac{\Gamma^L(\eta)}{\eta}\mathrm{d}\eta + \right.\right.\\
&\qquad \left.\left.\textstyle\int_{\eta_S}^{\eta_1}\frac{\Gamma^S(\eta)}{\eta}\mathrm{d}\eta\right) + \chi^S(\eta_S) - \chi^L(\eta_L)\right),\\
[\![s]\!]^{L-CO} &= \tfrac{k_B}{m}\left(\tfrac{\mathcal{D}}{2}\ln\hat{T} - \textstyle\int_{\eta_0}^{\eta_L}\frac{\Gamma^L(\eta)}{\eta}\mathrm{d}\eta + \right.\\
&\qquad \left.\alpha\left(\chi^S(\eta_S) - \chi^L(\eta_L)\right)\right).
\end{aligned}$$

For details of these derivation, see the paper [83].

As a typical example, the dependence of the Hugoniot loci, $\mathcal{H}(\mathbf{u}_0)$, on the internal degrees of freedom, f, in the case P-2 with the unperturbed state $\eta_0 = 0.2$ is shown in Fig. 2.2 and Fig. 2.3. For the sake of brevity, the Hugoniot loci in the case P-1 are omitted. Noticeable points are summarized as follows:

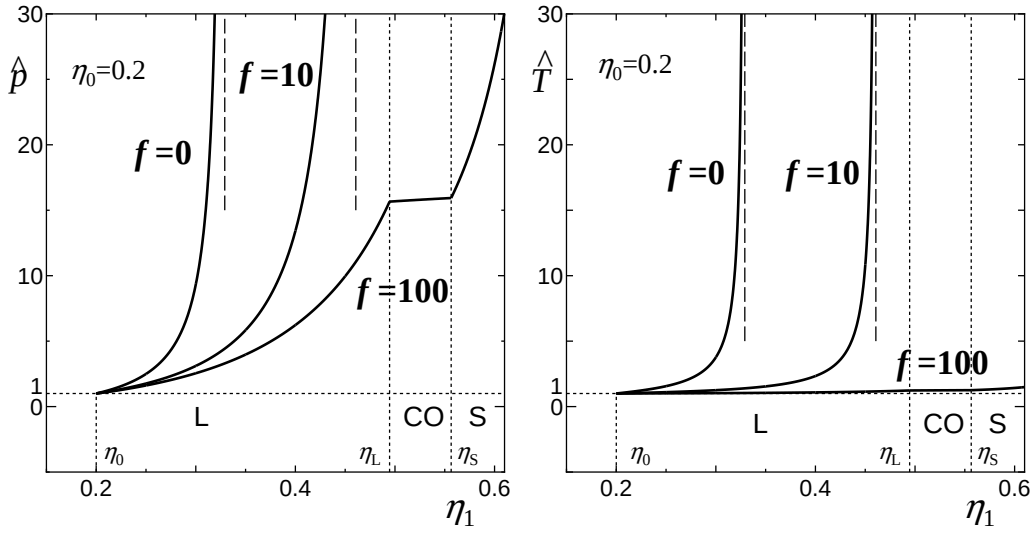

Figure 2.2: Hugoniot loci, represented in the $\hat{p} - \eta_1$ and $\hat{T} - \eta_1$ planes, for three different values of the internal degrees of freedom, f ($f = 0, 10, 100$). In the case $f = 100$, the Hugoniot loci cross the coexistence region, going from the liquid phase region to the solid phase region, as the shock strength increases (case P-2). The unperturbed packing fraction is $\eta_0 = 0.2$. Vertical dashed lines are asymptotes, $\eta_1 = \eta_1^\infty$, for $f = 0, 10$.

(i) As the strength of a shock wave increases (that is, as η_1 increases from η_0), the quantities $\hat{p}$ and $\hat{T}$ increase, but their increasing rates decrease with the increase of the internal degrees of freedom, f. Moreover, the decrease of the increasing-rate of $\hat{T}$ is larger than that of $\hat{p}$.

(ii) From Eq. (2.8) and Eq. (2.9), it may be seen that the RH conditions have real solutions only when the denominator of the right hand side of Eq. (2.9) is positive, i.e. when $\eta_0 \leq \eta_1 < \eta_1^\infty$, being η_1^∞ the perturbed packing fraction satisfying the relation

$$\Gamma(\eta_1^\infty)(1 - \eta_1^\infty/\eta_0) + \mathcal{D} = 0.$$

When η_1 tends to η_1^∞, $\hat{p}$ and $\hat{T}$, along with M_0, have a vertical asymptote (see Fig. 2.2); for this reason we call η_1^∞ the *strong shock limit*. It may be proved that η_1^∞ increases with the increase of the internal degrees of freedom, f.

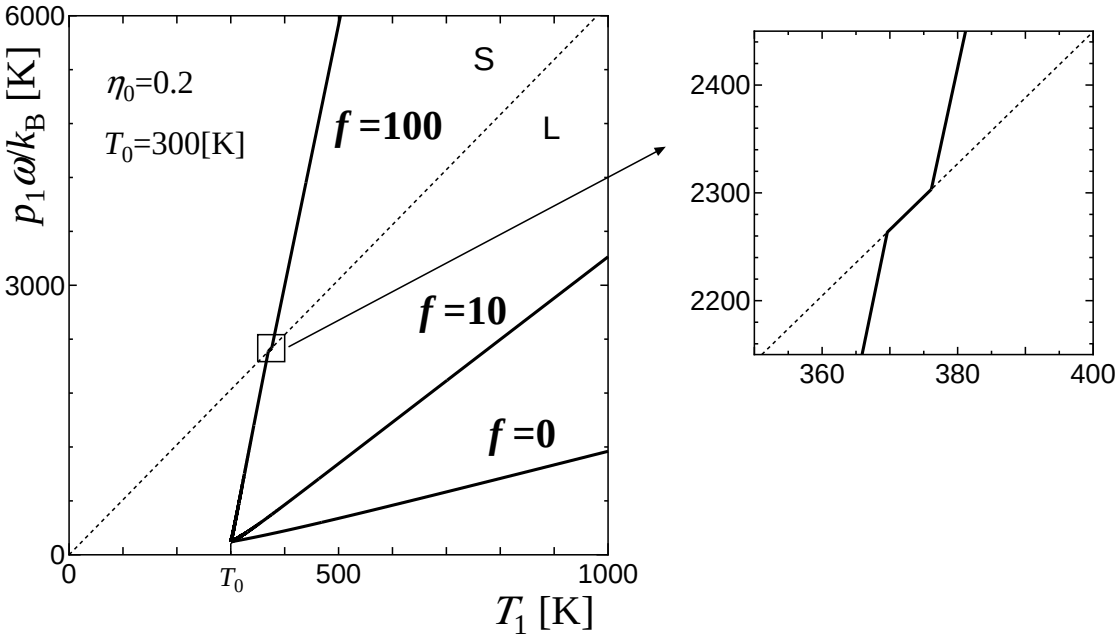

Figure 2.3: Hugoniot loci, represented in the $p_1\omega/k_B - T_1$ plane for three different values of the internal degrees of freedom, f ($f = 0, 10, 100$). In the case $f = 100$, the Hugoniot loci cross the coexistence line, going from the liquid phase region to the solid phase region, as the shock strength increases (case P-2). The unperturbed packing fraction and temperature are given, respectively, by $\eta_0 = 0.2$ and $T_0 = 300$K.

(iii) From a physical point of view, we can understand that a considerable portion of the energy supplied by a shock compression goes into the internal motions of the system, and therefore the temperature can not rise so much. This fact indicates that a shock-induced phase transition has a high possibility to take place in a hard-sphere system with large degrees of internal motion. In the figures, we can indeed observe a shock-induced phase transition when $f = 100$.

2.3.4 Characteristic quantities

In the paper [83], some quantities useful in the classification of shock wave phenomena were introduced. Since those quantities will be useful in the following, we recall their definitions in this section.

The quantity η_{01} (η_{02}) is defined as the unperturbed packing fraction that leads to a perturbed packing fraction equal to η_L (η_S) in the strong shock limit. In other words, η_{01} (η_{02}) is the largest unperturbed packing fraction for which the liquid-coexistence (liquid-solid) shock-induced phase transition never occurs, no matter how the shock is strong.

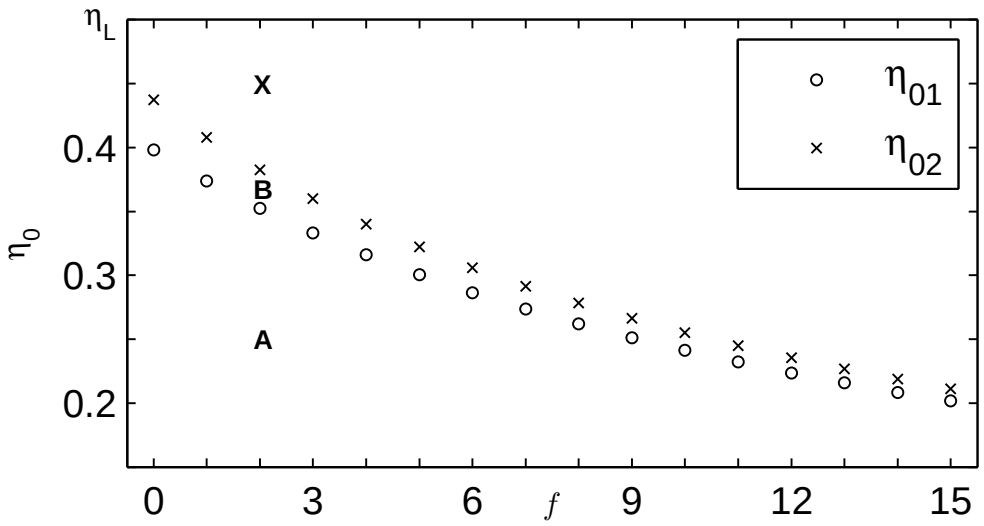

Figure 2.4: Dependence of the characteristic packing fractions η_{01} and η_{02} on the internal degrees of freedom, f. For each given value of f there are three distinct regions: **A**, **B** and **X**.

These characteristic packing fractions, η_{01} and η_{02}, may be expressed as follows:

$$\eta_{01} = \eta_L \frac{\Gamma^L(\eta_L)}{\mathcal{D} + \Gamma^L(\eta_L)}, \qquad \eta_{02} = \eta_S \frac{\Gamma^S(\eta_S)}{\mathcal{D} + \Gamma^S(\eta_S)}. \tag{2.10}$$

It is easily seen from Eq. (2.10) and Eq. (2.2) that η_{01} and η_{02} are decreasing (approaching zero) as f increases. This behavior is in agreement with the above-mentioned fact that the larger is f, the easier to obtain are the shock-induced phase transitions. As a consequence of the given definitions of η_{01} and η_{02}, we may define three distinct regions – graphically represented in Fig. 2.4 – over which the unperturbed packing fraction, η_0, can vary: region **A**$= \{(f, \eta_0) : f \in \mathbb{N}, 0 < \eta_0 < \eta_{01}\}$, region **B**$= \{(f, \eta_0) : f \in \mathbb{N}, \eta_{01} < \eta_0 < \eta_{02}\}$ and region **X**$= \{(f, \eta_0) : f \in \mathbb{N}, \eta_{02} < \eta_0 < \eta_L\}$. The dependence of η_{01} and η_{02} on the internal degrees of freedom, f, and the consequent effect of changing f on the extension of these three regions, may be appreciated in Fig. 2.4. A description of these three regions may be given as follows:

- Region **A**. When the unperturbed packing fraction, η_0, is in this region, the perturbed states on the Hugoniot locus never have a packing fraction equal or larger to the packing fraction of the freezing point, η_L, even in the strong shock limit (i.e. $\eta_1^\infty < \eta_L$). Therefore, only a thermodynamically stable liquid state can be observed after a shock front, that is, shock-induced phase transition never occurs.

- Region **B**. When the unperturbed packing fraction, η_0, is in this region, the perturbed states on the Hugoniot locus never have a packing fraction equal or larger than the packing fraction of the melting point, η_S, even thought it can be larger than the packing fraction of the freezing point, η_L (in other words, $\eta_L < \eta_1^\infty < \eta_S$). If the shock strength is large enough, we can observe a coexistence state after a shock front.

- Region **X**.When the unperturbed packing fraction, η_0, is in this region, the perturbed states on the Hugoniot locus may have a packing fraction larger than the packing fraction of the melting point, η_S (i.e. $\eta_1^\infty > \eta_S$). Therefore, if the shock strength is large enough, we can observe a stable solid state after a shock front. There can exist shock-induced liquid-solid phase transitions.

Other quantities, already introduced in the paper [83], that turn out to be useful in the present analysis are the following.

The quantity M_{01} (M_{02}) is defined as the unperturbed Mach number that leads to a perturbed state with a packing fraction equal to η_L (η_S). In other words, M_{01} (M_{02}) is the smallest unperturbed Mach number for which a liquid-coexistence (liquid-solid) shock-induced phase transition occurs, if ever.

The characteristic Mach numbers M_{01} and M_{02} may be expressed as follows:

$$M_{01} = \sqrt{\frac{\mathcal{D}\hat{\eta}_L\{-\mathcal{D}\Gamma_0 + \Gamma^L(\eta_L)[\mathcal{D}\hat{\eta}_L + 2(\hat{\eta}_L - 1)\Gamma_0]\}}{(\hat{\eta}_L - 1)[\Gamma^L(\eta_L)(1-\hat{\eta_L}) + \mathcal{D}](\mathcal{D}\Gamma_0 + 2\Gamma_0^2 + \mathcal{D}\eta_0\Gamma_0')}},$$

$$M_{02} = \sqrt{\frac{\mathcal{D}\hat{\eta}_S\{-\mathcal{D}\Gamma_0 + \Gamma^S(\eta_S)[\mathcal{D}\hat{\eta}_S + 2(\hat{\eta}_S - 1)\Gamma_0]\}}{(\hat{\eta_S} - 1)[\Gamma^S(\eta_S)(1-\hat{\eta_S}) + \mathcal{D}](\mathcal{D}\Gamma_0 + 2\Gamma_0^2 + \mathcal{D}\eta_0\Gamma_0')}}.$$

The dependence of M_{01} and M_{02} on the internal degrees of freedom, f, is shown in Fig. 2.5.

2.4 Admissibility of shock waves

From the theory of hyperbolic systems, it is well-known that some conditions (a selection rule) have to be satisfied in order for a shock to be allowed to propagate. Such a shock satisfying the proper selection rule will be referred to as an *admissible* shock. Since an admissible shock is a shock that does not change its wave profile during its propagation, while the wave profile of an inadmissible shock breaks into a combination of shocks, rarefaction waves and constant states evolving in time,

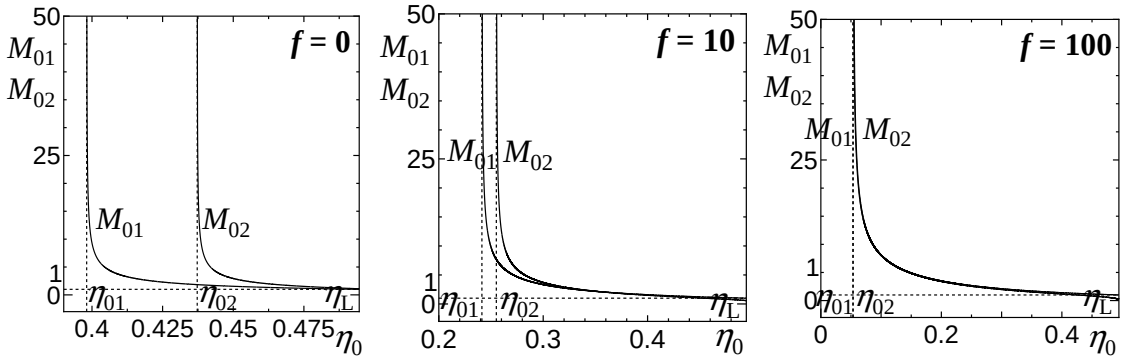

Figure 2.5: Characteristic Mach numbers M_{01} and M_{02} versus the unperturbed packing fraction η_0 for several values of the internal degrees of freedom: $f = 0$ (left), $f = 10$ (center), $f = 100$ (right).

an admissible shock is sometimes called a *stable* shock in the literature concerning hyperbolic system.

In the case of a genuinely nonlinear field, i.e. if the following condition is satisfied:

$$\nabla\lambda \cdot \mathbf{r} \neq 0 \qquad \forall \mathbf{u},$$

where λ is an eigenvalue of the hyperbolic systems, ∇ is the gradient made with respect to $\mathbf{u}$ and $\mathbf{r}$ is the corresponding eigenvector, the selection rule is given by the well-known Lax conditions [43], stating that a shock is admissible if its velocity of propagation, U_s, is such that

$$\lambda_0 < U_s < \lambda_1$$

being λ_0 and λ_1, respectively, the eigenvalues evaluated in the unperturbed and perturbed states.

In the case of a locally genuinely nonlinear field, i.e. when the genuine nonlinearity fails for some values of the field:

$$\nabla\lambda \cdot \mathbf{r} = 0 \qquad \text{for some } \mathbf{u},$$

the Lax conditions have to be replaced by the more general Liu conditions [44–46] asserting that a shock is admissible if and only if its velocity of propagation is not decreasing as we move on the Hugoniot locus starting from the unperturbed state, $\mathbf{u}_0$, towards the given perturbed state, $\mathbf{u}_1$:

$$U_s(\mathbf{u}_0, \tilde{\mathbf{u}}) \leq U_s(\mathbf{u}_0, \mathbf{u}_1) \;\; \forall \tilde{\mathbf{u}} \in \mathcal{H}(\mathbf{u}_0) \;\; \text{between } \mathbf{u}_0 \text{ and } \mathbf{u}_1.$$

First of all, let us consider two typical cases. In the first case (Fig. 2.6 and Fig. 2.7) the unperturbed packing fraction, η_0, is in the region **B** (see Fig. 2.4); in the second case (Fig. 2.8 and Fig. 2.9) the unperturbed packing fraction, η_0, lies in the region **X**.

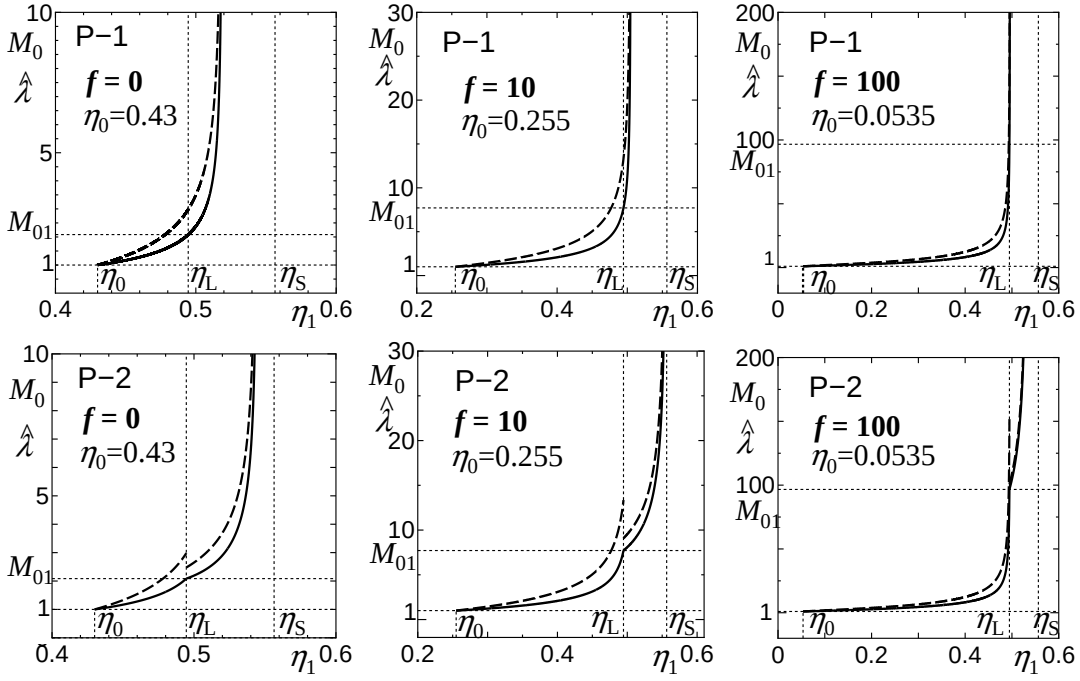

Figure 2.6: Dependence of the unperturbed Mach number, M_0, (solid curve) and of the dimensionless characteristic speed, $\hat{\lambda}$, (dashed curve) on the perturbed packing fraction η_1 for three different values of the internal degrees of freedom, f, ($f = 0, 10, 100$) according to the possibilities P-1 (above) and P-2 (below). The unperturbed packing fraction η_0 is in the region **B**.

From Fig. 2.6 and Fig. 2.8, we see that in both the two cases, both the possibilities P-1 and P-2 guarantee that the Liu conditions are satisfied. From Fig. 2.7 and Fig. 2.9, we can see that both the possibilities P-1 and P-2 satisfy also the thermodynamical requirement of the positivity of the entropy production rate, ς, in both the two cases. Therefore shock waves of both P-1 and P-2 are stable.

The problem to be solved now consist in understanding which of the two possibilities is the physically relevant one. It can be proved that the entropy production rate, ς, of P-2 is larger than that of P-1 for any value of the internal degrees of freedom, f, although the difference between P-1 and P-2 decreases with the increase of f. Here, for the sake of brevity, we omit the proof. Therefore, if we use the selection rule in terms of the maximum entropy production rate mentioned in the last sec-

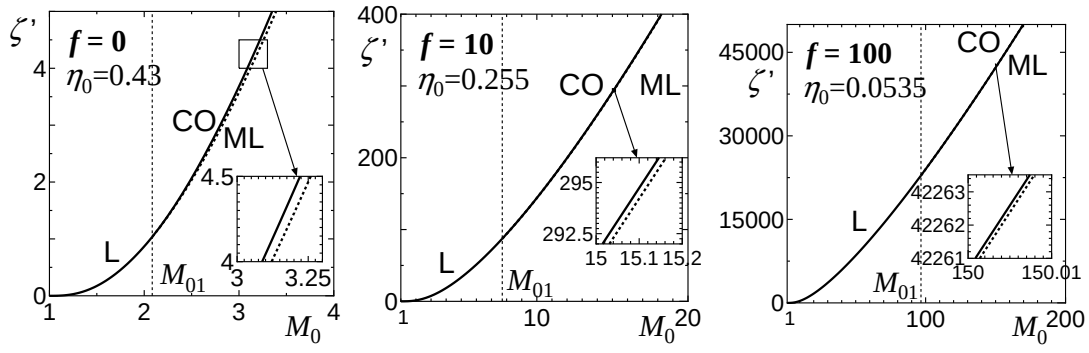

Figure 2.7: Dependence of the dimensionless entropy production rate, ς' ($= \frac{\varsigma}{\eta_0 c_0}\frac{m}{k_B}$) on the unperturbed Mach number, M_0, for three different values of the internal degrees of freedom, f, ($f = 0, 10, 100$) according to the possibilities P-1 (dotted curve) and P-2 (solid curve). The unperturbed packing fraction η_0 is in the region **B**.

tion, we may adopt the coexistence-Hugoniot (the possibility P-2) as the physically relevant solution for a hard-sphere system with internal motion. According to this, hereafter, we will confine our analysis to the study of only the possibility P-2.

2.5 Classification of shock-induced liquid/solid phase transitions

In section 2.3.4, we stated that, for any given f, a shock-induced liquid-solid phase transition may occur only when the unperturbed packing fraction lies in the region **X** (see Fig. 2.4). In this section, we study the fine structure of this region: we divide it into three subregions and we motivate this subdivision pointing out the different features of these three subregions in terms of shock admissibility. Let us pay attention to the following three cases, covering all the possible relations between the unperturbed Mach number, M_0, and the perturbed packing fraction, η_1, in the region **X**:

(i) The unperturbed Mach number, M_0, is a monotonically increasing function of the perturbed packing fraction, η_1. Therefore, the characteristic Mach numbers M_{01} and M_{02} satisfy the inequality $M_{01} < M_{02}$ (cf. case (α) in Fig. 2.10).

(ii) The unperturbed Mach number, M_0, is not a monotonically increasing function of the perturbed packing fraction, η_1, and there is a packing fraction η_c ($\eta_L < \eta_c < \eta_S$) such that $M_0 = M_{01}$ when $\eta_1 = \eta_c$. The inequality $M_{01} < M_{02}$ still holds in this case (cf. case (β) in Fig. 2.10).

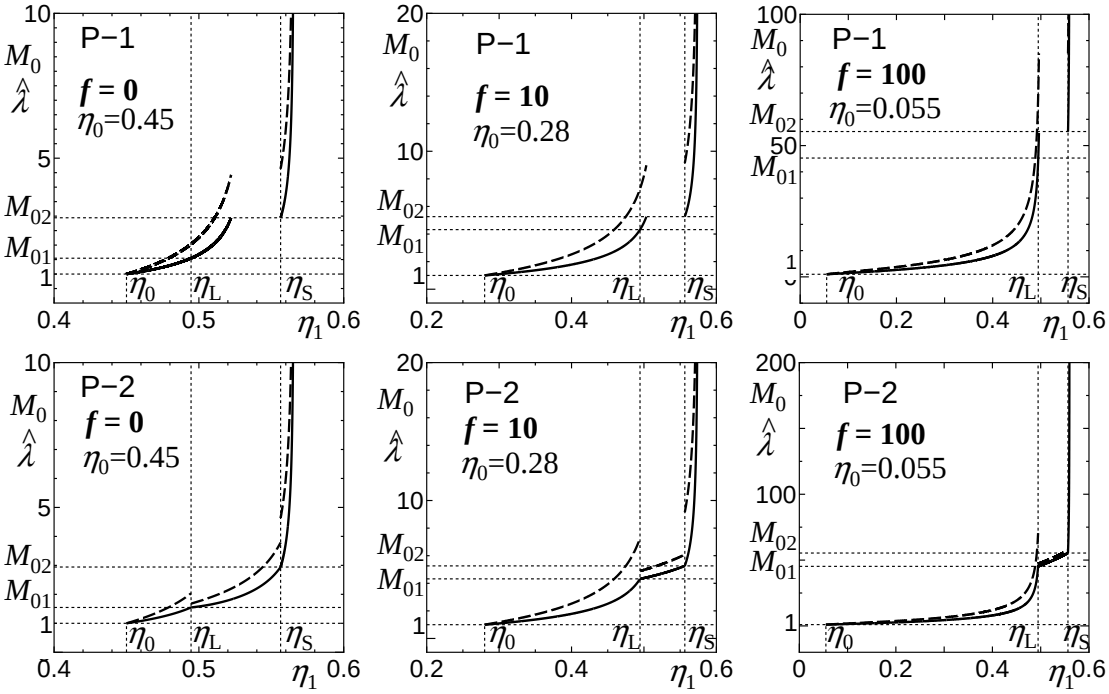

Figure 2.8: Dependence of the unperturbed Mach number, M_0, (solid curve) and of the dimensionless characteristic speed, $\hat{\lambda}$, (dashed curve) on the perturbed packing fraction η_1 for three different values of the internal degrees of freedom, f, ($f = 0, 10, 100$) according to the possibilities P-1 (above) and P-2 (below). The unperturbed packing fraction η_0 is in the region **X**.

(iii) The unperturbed Mach number, M_0, is not a monotonically increasing function of the perturbed packing fraction, η_1, as in the case (ii), but the packing fraction η_c satisfies, in this case, the inequality $\eta_c > \eta_S$. The inequality $M_{01} > M_{02}$ holds in this case (cf. cases (γ) and (δ) in Fig. 2.10).

We can prove that the boundary between the cases (i) and (ii) is characterized by the condition that the characteristic unperturbed Mach number M_{01} is equal to the characteristic speed estimated by using the L-CO Hugoniot conditions, $\hat{\lambda}^{CO}$, at the freezing point η_L:

$$M_{01} = \hat{\lambda}^{CO}\Big|_{\eta_L}. \tag{2.11}$$

The boundary between the cases (ii) and (iii) is given by the condition:

$$M_{01} = M_{02}. \tag{2.12}$$

By using the conditions (2.11) and (2.12) we realize that the region **X** may be divided into three distinct subregions **C**, **D** and **Y**, which correspond to the cases

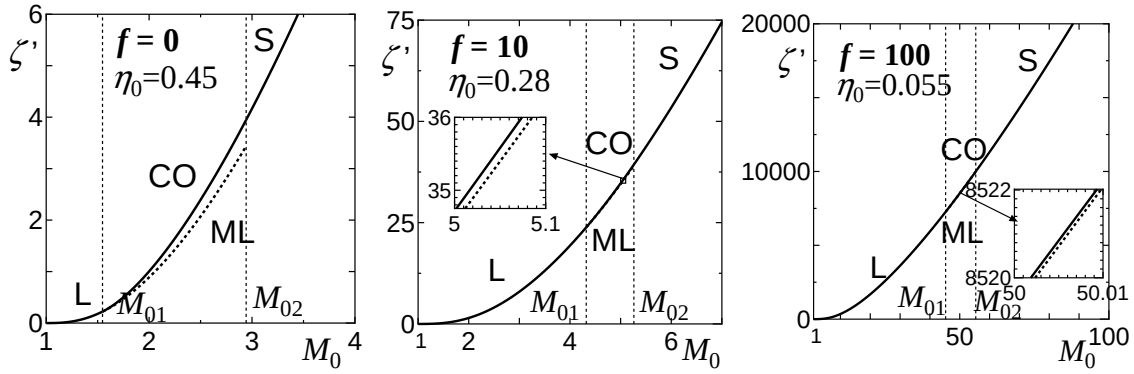

Figure 2.9: Dependence of the dimensionless entropy production rate, ς' ($= \frac{\varsigma}{\eta_0 c_0}\frac{m}{k_B}$) on the unperturbed Mach number, M_0, for three different values of the internal degrees of freedom, f, ($f = 0, 10, 100$) according to the possibilities P-1 (dotted curve) and P-2 (solid curve). The unperturbed packing fraction η_0 is in the region **X**.

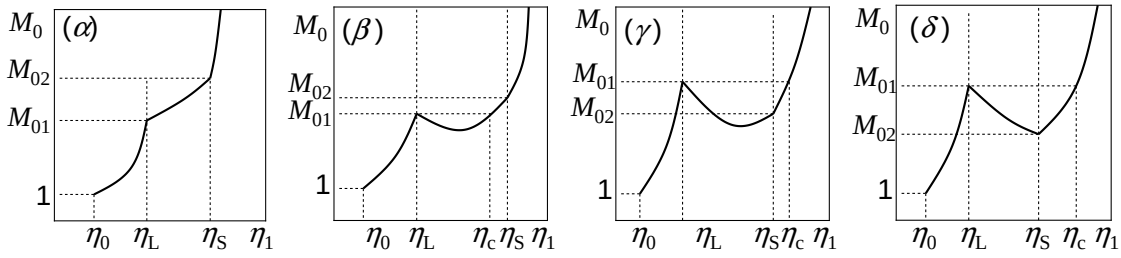

Figure 2.10: Schematic representations of typical cases of the relationship between the unperturbed Mach number M_0 and the perturbed packing fraction η_1 in the region **X**

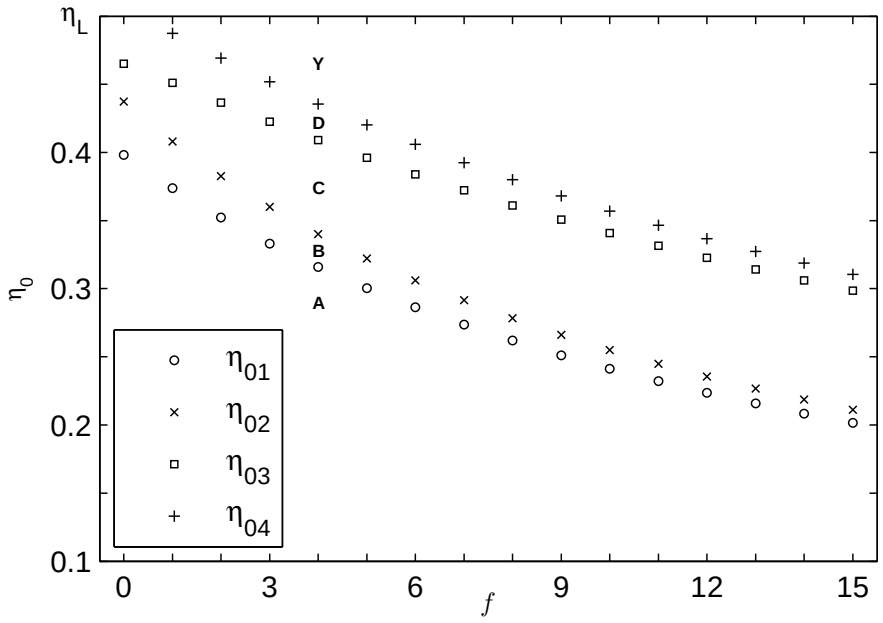

Figure 2.11: The region **X** may be divided into the three subregions **C**, **D** and **Y**.

(i), (ii) and (iii), respectively, as shown in Fig. 2.11. In fact, for any $f > 0$, there exists an unperturbed packing fraction, η_{03}, for which the condition (2.11) is satisfied and, analogously, there exists an unperturbed packing fraction, η_{04}, for which the condition (2.12) is satisfied; all the unperturbed packing fraction such that $\eta_{02} < \eta_0 < \eta_{03}$ belong to the case (i), all the ones such that $\eta_{03} < \eta_0 < \eta_{04}$ belong to the case (ii) and all those such that $\eta_{04} < \eta_0 < \eta_L$ belong to the case (iii). When $f = 0$, it turns out that the condition (2.12) is never satisfied; in this case any unperturbed packing fraction such that $\eta_{03} < \eta_0 < \eta_L$ belong to the case (ii). So, region **C**$= \{(f, \eta_0) : f \in \mathbb{N}, \eta_{02} < \eta_0 < \eta_{03}\}$, region **D**$= \{(f, \eta_0) : f \in \mathbb{N}_+, \eta_{03} < \eta_0 < \eta_{04}\} \cup \{(f, \eta_0) : f = 0, \eta_{03} < \eta_0 < \eta_L\}$ and region **Y**$= \{(f, \eta_0) : f \in \mathbb{N}_+, \eta_{04} < \eta_0 < \eta_L\}$.

We summarize the characteristic features of the regions **C**, **D** and **Y** in detail by studying the case $f = 10$, pointing out that the results are qualitatively valid for any $f > 0$.

- Region **C**. The dependence of the unperturbed Mach number, M_0, and of the dimensionless characteristic speed, $\hat{\lambda}$, on the perturbed packing fraction, η_1, in a typical case ($\eta_0 = 0.28$) is shown in Fig. 2.12. We notice that, from the Liu conditions, any compressive shock wave ($\eta_1 > \eta_0$) is admissible. In other words, by using a single compressive shock, we can obtain any stable perturbed state

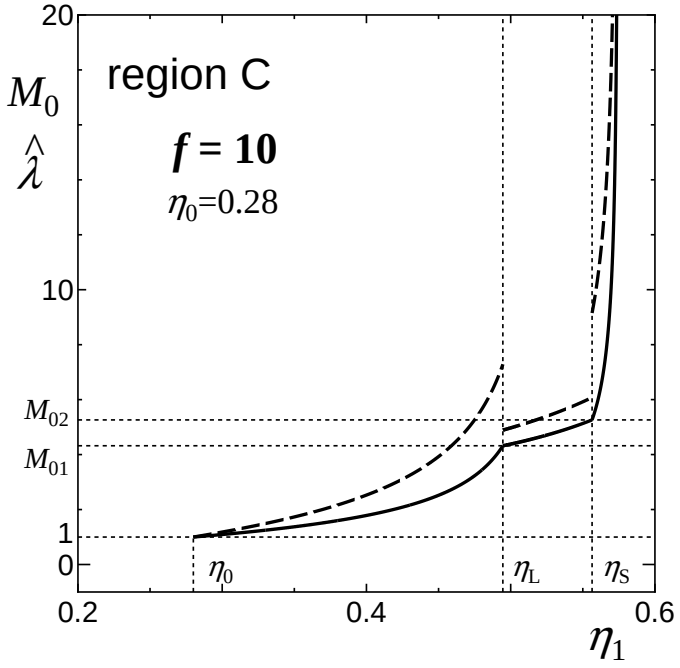

Figure 2.12: Typical dependence of the Mach number M_0 (solid curve) and the dimensionless characteristic speed $\hat{\lambda}$ (broken curve) on the perturbed packing fraction, η_1. Any shock wave with a perturbed state ($\eta_1 > \eta_0$) is stable.

in any phase (liquid phase, coexistence and solid phase). The same property of the admissibility for a single shock was already found in the case of $f = 0$ presented in the paper [83].

- Region **D**. The dependence of the unperturbed Mach number, M_0, and of the dimensionless characteristic speed, $\hat{\lambda}$, on the perturbed packing fraction, η_1, in the case with $\eta_0 = 0.35$ is shown in Fig. 2.13. The intersection point between M_0 and $\hat{\lambda}$ in the coexistence region is the local minimum point of M_0. A noticeable point is that, from the Liu conditions, a shock wave with a perturbed packing fraction such that $\eta_0 < \eta_1 < \eta_L$ and $\eta_1 > \eta_c$ is admissible, while a shock wave with a perturbed packing fraction such that $\eta_L < \eta_1 < \eta_c$ is not admissible. That is to say, it is impossible to reach a perturbed state with the packing fraction in the part of the coexistence region $\eta_L < \eta_1 < \eta_c$ through a stable shock. In the next section we will study the stability of a shock wave numerically and will confirm the above results.

  If an initial shock is in the above-mentioned inadmissible region, such a shock eventually splits into several waves composed of shock waves, rarefaction waves

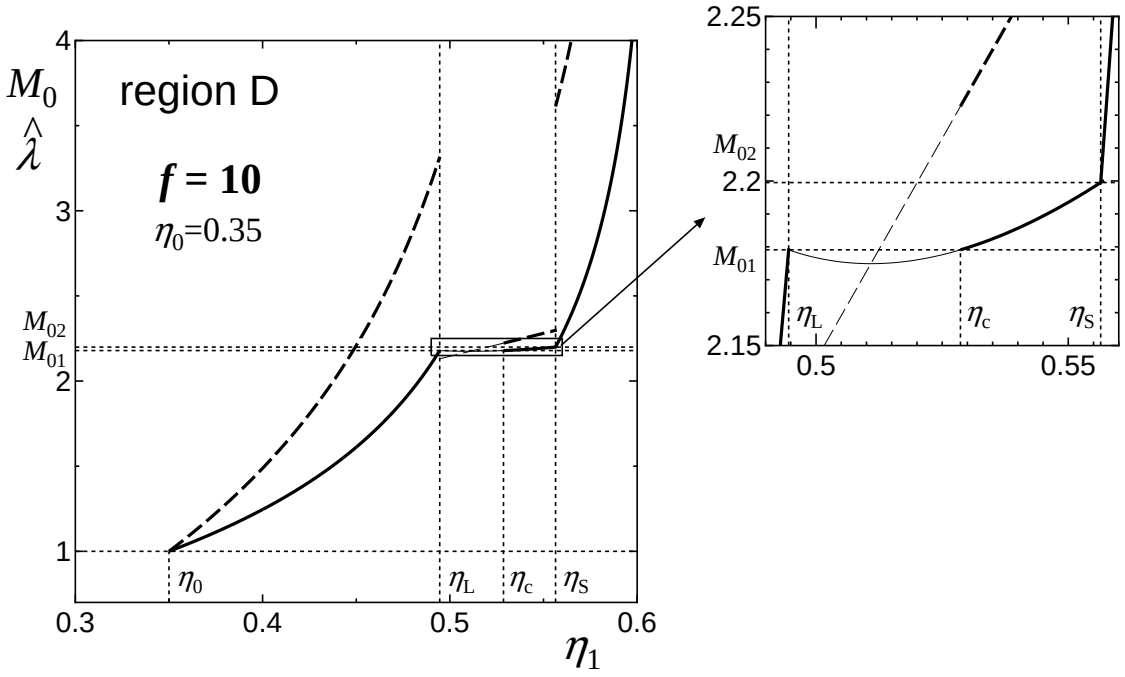

Figure 2.13: Typical dependence of the Mach number M_0 (solid curve) and the dimensionless characteristic speed $\hat{\lambda}$ (broken curve) on the perturbed packing fraction, η_1. A shock wave with the perturbed packing fraction, η_1, in the region, $\eta_0 < \eta_1 < \eta_L$ and $\eta_1 > \eta_c$, is stable (boldfaced part of the curve M_0), while a shock wave with a perturbed packing fraction such that $\eta_L < \eta_1 < \eta_c$ is unstable (lightfaced part of the curve M_0).

and constant states in the course of its propagation. Some typical numerical examples of the shock splitting and composite waves occurred thereby will be shown also in the next section. Shock splitting phenomena in a gas [69–71] and in a solid [57] have already been studied.

- Region **Y**. Let us discuss the region **Y** that is characteristic of a hard sphere system with internal degrees of freedom $f \geq 1$. Typical dependence of the Mach number, M_0, and the dimensionless characteristic speed, $\hat{\lambda}$, on the packing fraction η_1 is shown in Fig. 2.14 and Fig. 2.15 (see cases (γ) and (δ) in Fig. 2.10). The unperturbed Mach number, M_0, has a local minimum point in the coexistence region (see Fig. 2.14) or it is monotonically decreasing, as η_1 increases, all over the coexistence region (see Fig. 2.15). As far as a stable single shock is concerned, we can study both cases simultaneously.

  From the Liu conditions, a shock wave with a perturbed state in the region $\eta_0 < \eta_1 < \eta_L$ and $\eta_1 > \eta_c$ is admissible, while a shock wave with a perturbed

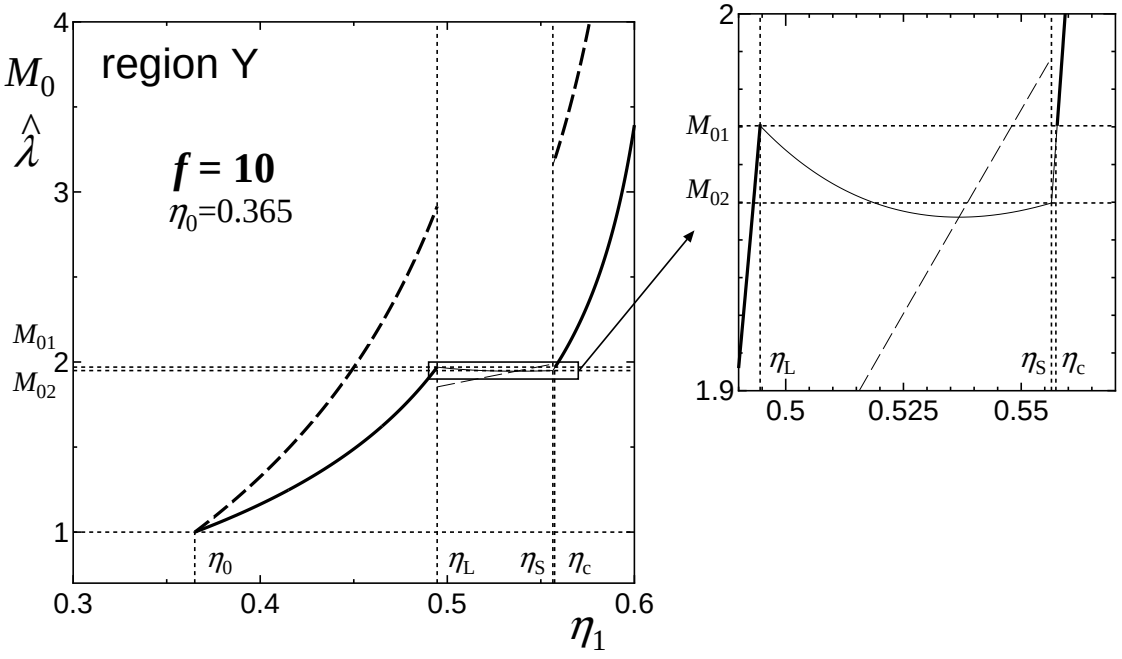

Figure 2.14: Typical dependence of the Mach number, M_0, (solid curve) and the dimensionless characteristic speed $\hat{\lambda}$ (broken curve) on the perturbed packing fraction, η_1. A shock wave with the perturbed packing fraction η_1 in the region, $\eta_0 < \eta_1 < \eta_L$ and $\eta_1 > \eta_c$, is stable (boldfaced part of the curve M_0), while a shock wave with a perturbed packing fraction, η_1, such that $\eta_L < \eta_1 < \eta_c$ is unstable (lightfaced part of the curve M_0). The unstable region includes the melting point η_S.

state in the region $\eta_L < \eta_1 < \eta_c$ is not admissible. As in the Region **D**, it is impossible to reach a perturbed state with the packing fraction in the region $\eta_L < \eta_1 < \eta_c$ through a single stable shock. However, it should be noticed that the unstable region in this case includes the melting point η_S and therefore includes a part of the Hugoniot locus in thermodynamically stable solid phase. Therefore a shock wave may be unstable even though the perturbed state is in thermodynamically stable solid phase. This is one of remarkable features of the dynamic phase transitions found in the present analysis. In material syntheses, for example, this new fact may become important because we have now noticed that there are thermodynamic stable states which cannot be reached by a single shock.

In the next section we will study numerically the stability of a shock wave and the shock splitting.

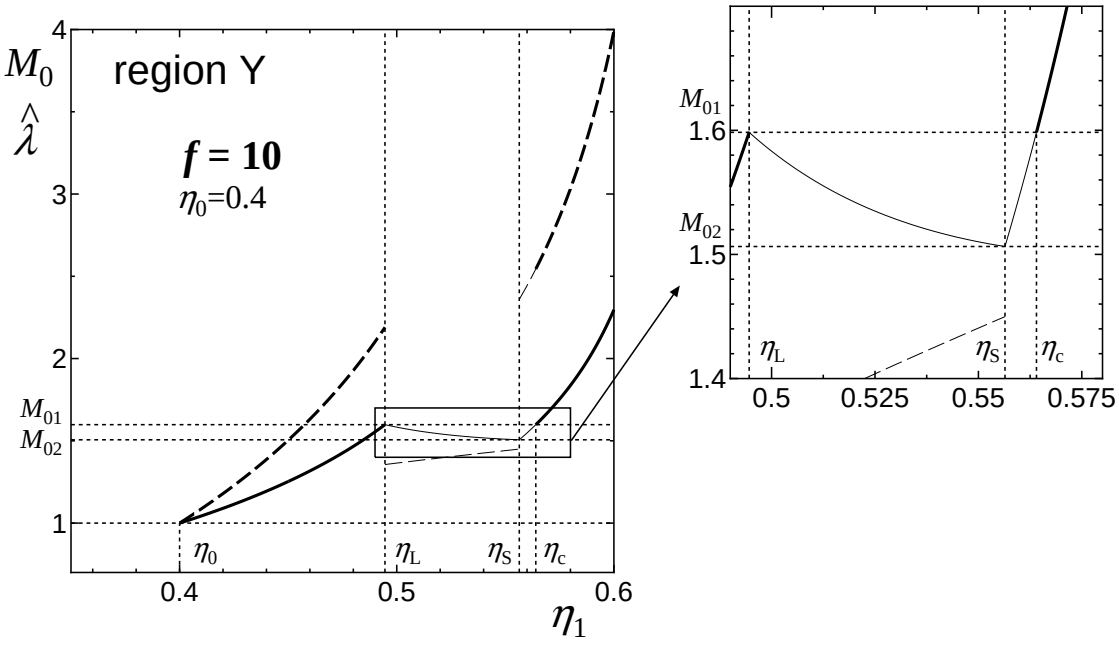

Figure 2.15: Typical dependence of the Mach number, M_0, (solid curve) and the dimensionless characteristic speed $\hat{\lambda}$ (broken curve) on the perturbed packing fraction, η_1. A shock wave with the perturbed packing fraction η_1 in the region, $\eta_0 < \eta_1 < \eta_L$ and $\eta_1 > \eta_c$, is stable (boldfaced part of the curve M_0), while a shock wave with η_1 in the region $\eta_L < \eta_1 < \eta_c$ is unstable (lightfaced part of the curve M_0). The unstable region includes the melting point η_S.

2.6 Numerical analysis

In the previous sections, we have used the Liu conditions in our analysis. Rigorously speaking, the Liu conditions require the constitutive equations to be smooth, so they are not applicable when the Hugoniot loci cross neighborhoods of perturbed states with packing fractions equal to η_L or η_S, because the equations of state are not smooth when $\eta = \eta_L$ and $\eta = \eta_S$. In these cases, the numerical approach plays a major role showing that the results concerning the shock admissibility are the same as if the Liu conditions were applicable.

Numerical solutions of the equations for the hard-sphere system described in Section 2.2 have been calculated in order to check the theoretical results stated in Section 2.5 and to analyze the admissibility of a shock wave when its unperturbed state lies in one of the regions labeled as **A**, **B**, **C**, **D** and **Y**.

The tool used for the computations is a MATLAB/C++ general-purpose code useful for the numerical solution of hyperbolic systems of balance and/or conserva-

tion laws which has been recently developed by some of the authors [85,86]. The tool allows the user to choose the suitable algorithm among a wide variety of available algorithms. For the case being, the selected algorithm is based on a fourth-order Central Runge-Kutta (CRK) scheme recently proposed by Pareschi et al. [87], which turned out to be stable and sound for a wide range of hyperbolic systems of conservation laws, including the case of locally linearly degenerate fields.

When the unperturbed state, $\mathbf{u}_0$, belongs to either of the regions **A**, **B** and **C**, the Liu conditions give the same results as the Lax conditions and it turns out that all the states $\mathbf{u}_1$ lying on the admissible branch of the Hugoniot locus passing through the given state $\mathbf{u}_0$ are connected to $\mathbf{u}_0$ by an admissible shock wave, i.e., all the compressive shocks are admissible. This well-known theoretical result has been checked by means of numerical calculations and some representative results are shown in Fig. 2.16 for the cases of $\mathbf{u}_0$ belonging to the regions **A**, **B** and **C**. For each of these three cases, given an unperturbed state $\mathbf{u}_0 \equiv (\eta_0, v_0, p_0\omega/m)$, we show the profile of η, as a function of x at $t = 0.2$ which comes from a Cauchy initial data of Riemann type in which the discontinuity between the unperturbed state $\mathbf{u}_0$ and the perturbed state $\mathbf{u}_1$ is located at $x = 0$. The value of the internal degrees of freedom is set to $f = 10$.

For the case **A**, the packing fraction of the considered unperturbed state is $\eta_0 = 0.2$; for the case **B**, the packing fraction is $\eta_0 = 0.255$ and, finally, for the case **C** we set $\eta_0 = 0.28$. All the calculations have been performed with $v_0 = 0$ and $p_0\omega/m = 0.3$. In all these cases the packing fractions of the perturbed states, η_1, for which numerical results are presented are graphically shown in Fig. 2.16(a,c,e) by means of black circles.

From the corresponding η profiles, obtained numerically and given in Fig. 2.16(b,d,f), we may claim that the shock wave appears to be acceptable for any of the perturbed state that we have examined.

The numerical analysis of the admissibility of a shock waves whose unperturbed state lies in the region **D** is presented in Fig. 2.17 for $\eta_0 = 0.35$. In this case, the Lax conditions are not applicable and the Liu conditions become necessary in order to analyze the admissibility of shocks. The range of the η_1 values for which the Liu conditions allow to claim that the shock is not admissible corresponds to the region under the horizontal thin line in Fig. 2.17(b), that is $\eta_L < \eta_1 < \eta_c$, while the values of η_1 outside this interval ($\eta_0 \leq \eta_1 \leq \eta_L$ and $\eta_1 \geq \eta_c$) give admissible shocks.

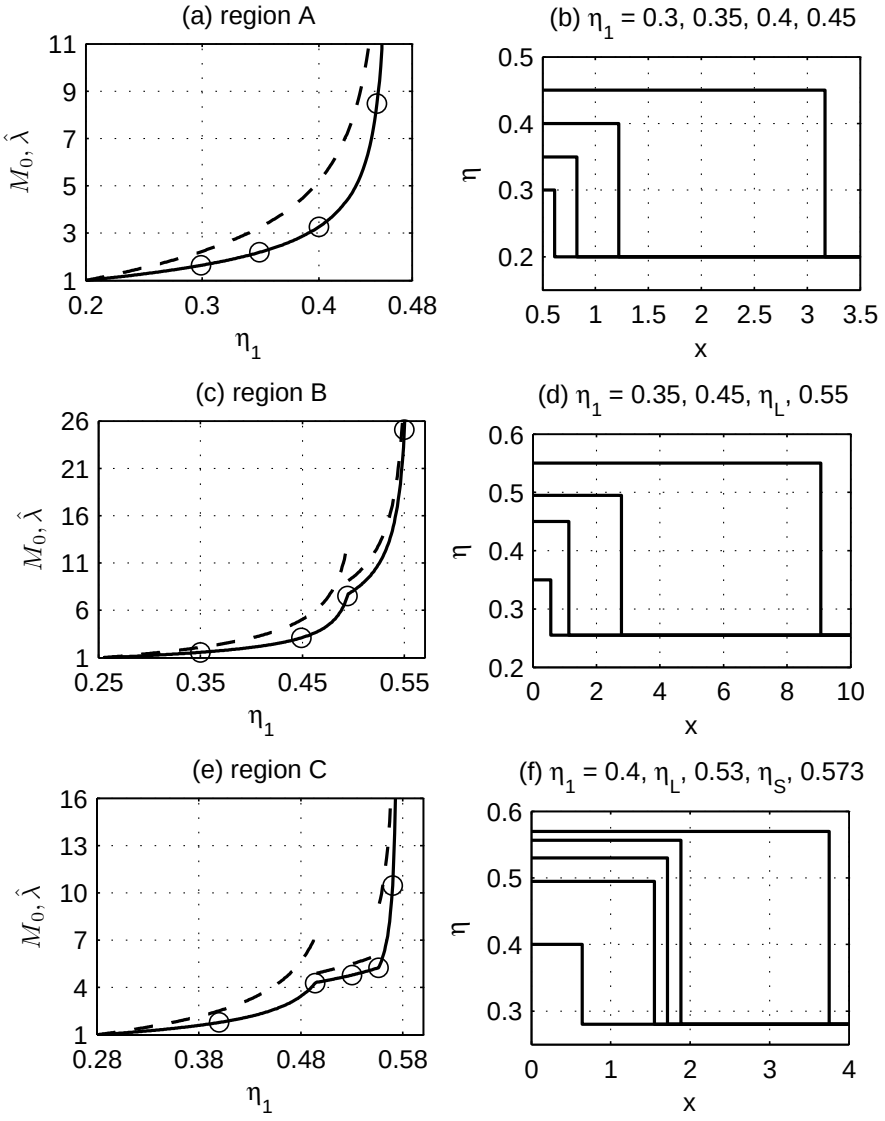

Figure 2.16: Left figures: M_0 and $\hat{\lambda}$ as functions of η_1 for unperturbed states defined by: v_0=0, $p_0\omega/m$=0.3 and (a) η_0=0.2 (Region **A**); (c) η_0=0.255 (Region **B**); (e) η_0=0.28 (Region **C**). Right figures: η profiles obtained numerically as solutions of the Riemann problem with unperturbed states defined above and perturbed states indicated by the black circles in the left figures: (b) $\eta_1 = 0.3, 0.35, 0.4, 0.45$; (d) $\eta_1 = 0.35, 0.45, \eta_L \simeq 0.4946, 0.55$; (f) $\eta_1 = 0.4, \eta_L \simeq 0.4946, 0.53, \eta_S \simeq 0.5564, 0.573$.

The numerical solutions, presented here for a set of perturbed states whose packing fraction spans all the regions of interest, confirm the theoretical results, as may be appreciated from the profiles of the packing fraction, η, shown in Fig. 2.17(c–f).

Numerical results concerning the case in which the unperturbed state $\mathbf{u}_0$ lies in the region **Y** are presented in Fig. 2.18. In this case, as pointed out in Section 2.5, a shock wave with a perturbed packing fraction, η_1, in the solid branch ($\eta_1 > \eta_S$)

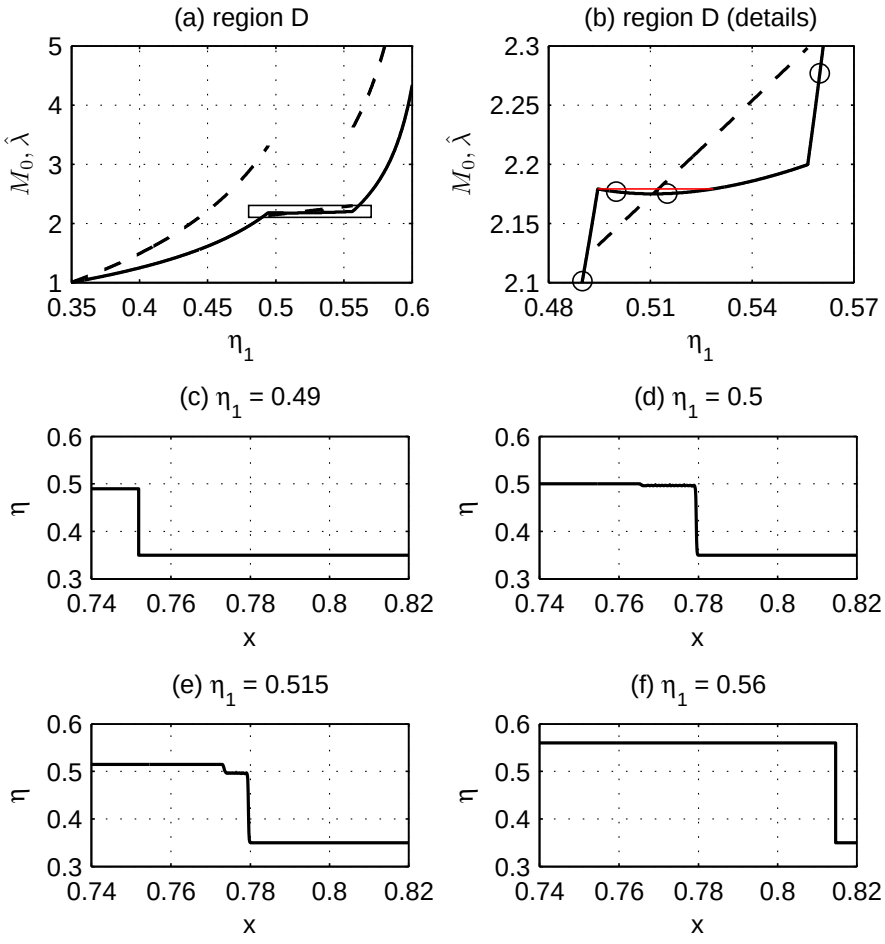

Figure 2.17: Region **D**: (a) M_0 and $\hat{\lambda}$ as functions of η_1 for an unperturbed state defined by: η_0=0.35, v_0=0, $p_0\omega/m$=0.3; (b) Blow-up of the boxed region in part (a) of the figure; (c–f): η profiles obtained numerically as solutions of the Riemann problem with unperturbed states defined above and perturbed states indicated by the black circles in part (b) of the figure: $\eta_1 = 0.49, 0.5, 0.515, 0.56$.

may be not acceptable, as well as all the shock waves with packing fractions in the coexistence region ($\eta_L < \eta_1 < \eta_S$). In fact, from the Liu conditions, we obtain that a shock is admissible if $\eta_0 \leq \eta_1 \leq \eta_L$ or $\eta_1 \geq \eta_c > \eta_S$. This means that all the perturbed states lying on the Hugoniot locus through $\mathbf{u}_0$ such that $\eta_S < \eta_1 < \eta_c$ ($\eta_S \simeq 0.5564$, $\eta_c \simeq 0.5576$) are not acceptable. These results are confirmed by the numerical solutions, as may be appreciated from Fig. 2.18(c–f).

It is worth noting that, in the presented cases of non-admissible shocks (i.e. the cases in Fig. 2.17(d,e) and in Fig. 2.18(d,e)), the η profiles show the so-called *shock splitting* phenomenon, i.e. the wave profile is made up with a combination of shock waves, rarefaction waves and constant states, depending on the particular values of

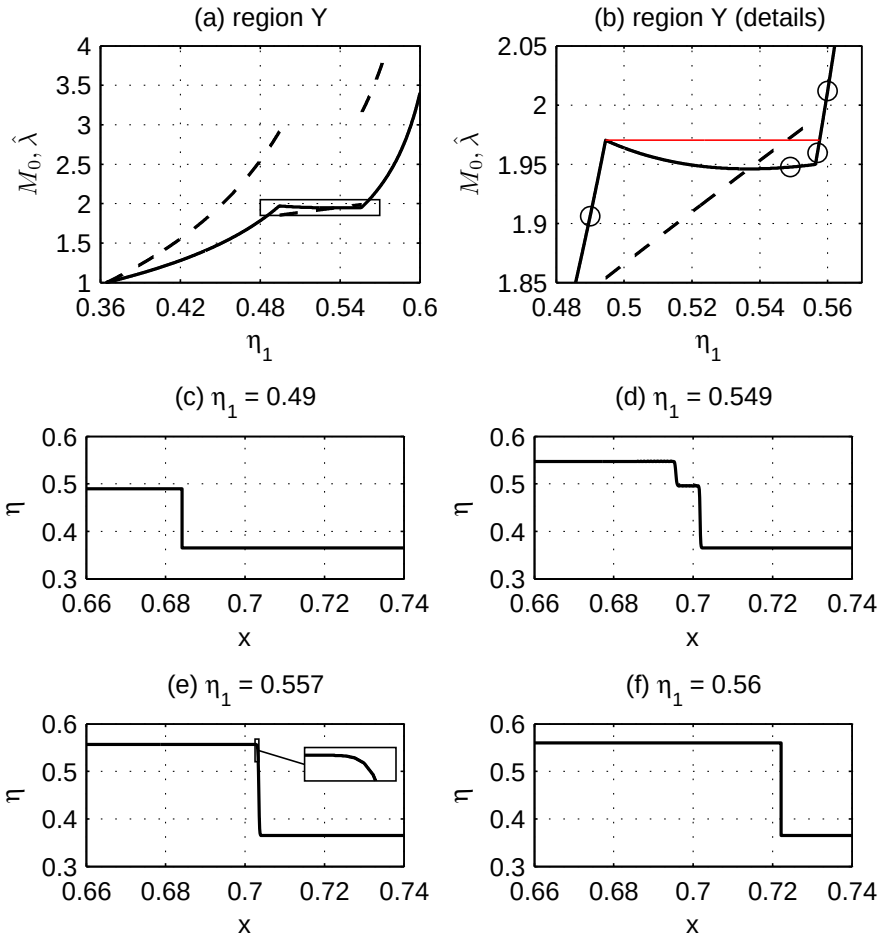

Figure 2.18: Region **Y**: (a) M_0 and $\hat{\lambda}$ as functions of η_1 for an unperturbed state defined by: η_0=0.365, v_0=0, $p_0\omega/m$=0.3; (b) Blow-up of the boxed region in part (a) of the figure; (c–f): η profiles obtained numerically as solutions of the Riemann problem with unperturbed state defined above and perturbed states indicated by the black circles in part (b) of the figure: $\eta_1 = 0.49, 0.549, 0.557, 0.56$.

the unperturbed and perturbed states.

2.7 Summary and concluding remarks

From the analysis of the RH conditions, we have found the distinct regions **A**, **B**, **C**, **D** and **Y** in the plane of the unperturbed packing fraction η_0 and the internal degrees of freedom f (Fig. 2.11). It is interesting to note that region **Y** can be observed only if $f \geq 1$, that is, if there is an internal motion.

The characteristic features of the regions **A** to **C** have already been discussed through studying the cases of no internal motion (i.e. $f = 0$) in the paper [83]. The

regions **D** and **Y** are essentially new findings in the present paper. By applying the Liu conditions to the cases in the regions **D** and **Y** we have made clear the admissible condition for a stable single shock wave. Even if a perturbed state is thermodynamically stable, it is not always stable dynamically, that is, it may be unstable with respect to a dynamical perturbation. In such an unstable case we can observe the so-called shock splitting phenomena as shown in the numerical analysis in section VI.

Lastly let us summarize the concluding remarks as follows:

(i) In the present analysis, our study is mainly limited within analyzing stable shock waves. If we want to study the time-evolution of an unstable single shock in detail, we should divide the region **Y** into more subregions in order to classify such time-evolutions properly (see, for example, the cases (γ) and (δ) in Fig. 2.10 both of which belong to the same region **Y**). The subject is left for a future work.

(ii) This remark is concerned with an experiment that seems to be possible to check the present theory. That is, an experiment on shock wave phenomena in a system of fullerenes C_{60}. We can expect to observe shock-induced liquid-solid phase transitions in this system. Their experimental data can be compared with the present results of a suitable non-zero value of f. However, the success of such an experiment is not so much sure at present because the liquid phase of the system has not been observed clearly until now [88–90].

Chapter 3

A new type of shock in real gases: a compressive upper shock

3.1 Introduction

The compressive shocks, inducing phase transitions, may be called *compressive lower shocks*, since they have the feature, common to all the compressive shocks described in the literature, that the density of the perturbed state is larger than the density of the unperturbed state and, as the shock strength increases (for instance, the *perturbed* pressure, i.e., the pressure of the perturbed state), the perturbed density increases as well, approaching *from below* the value corresponding to the minimal allowed specific volume (i.e., they are *compressive lower shocks*).

In this chapter, we prove that there exists a very thin region in the ρp plane, characterized by low values of density and pressure, near the gas/liquid coexistence curve, which we call $\tilde{\mathbf{C}}$, in which an admissible compressive shock has the unusual property that as the strength of the shock increases, the perturbed density approaches the limit value *from above* and, as a consequence, as the strength of shock increases, the perturbed density decreases [93]. In the following, we shall discuss this new kind of shocks, which may be called *compressive upper shocks*, and we identify completely the region $\tilde{\mathbf{C}}$ which depends on the internal degrees of freedom of a constituent molecule. Hopefully, these new findings may provide some useful indications for experimentalists.

For simplicity we adopt a real gas modeled by the van der Waals equation which can be regarded as the simplified model of the system of hard-spheres with attractive force. It was pointed out that there exists a region in the space of the states such that when the unperturbed state, $\mathbf{u}_0$, belongs to this region, the Hugoniot locus

for $\mathbf{u}_0$, which we denote as $\mathcal{H}(\mathbf{u}_0)$, crosses the coexistence curve, $\mathcal{C}_{coe}$, and phase transitions may be allowed.

3.2 The van der Waals model and the Rankine-Hugoniot conditions

The van der Waals caloric and thermal equations of state are given by:

$$\begin{aligned} e &= RT/\delta - a\rho, \\ p &= RT\,\rho/(1-b\rho) - a\rho^2, \end{aligned} \tag{3.1}$$

where e, p, ρ and T are, respectively, the specific internal energy, pressure, density and temperature; $\delta = R/c_v$, $R = k_B/m$, being k_B the Boltzmann constant, m the mass of a constituent molecule and c_v the specific heat capacity at constant volume related to the internal degrees of freedom. The material-dependent constants a and b represent, respectively, a measure of the attraction between molecules and the effective volume of a molecule.

We consider a shock wave propagating in a perfect fluid described by the one-dimensional hyperbolic system of the Euler equations with the constitutive equations given in (3.1). The shock, propagating with velocity U_s, divides the space into two subspaces: the unperturbed state (or upstream state), $\mathbf{u}_0$, and the perturbed state (or downstream state), $\mathbf{u}_1$ which are, respectively, the states before and after the shock. The field $\mathbf{u}_1 \in \mathcal{H}(\mathbf{u}_0)$, i.e., it is the solution of the Rankine-Hugoniot (RH) conditions. For later convenience, it is useful to introduce the dimensionless variables

$$\begin{gathered} \hat{\rho} = \rho/\rho_{cr}, \qquad \hat{p} = p/p_{cr}, \qquad \hat{T} = T/T_{cr}, \\ \hat{e} = (\rho_{cr}/p_{cr})\,e, \quad \hat{v} = \sqrt{\rho_{cr}/p_{cr}}\;v, \quad \hat{c} = \sqrt{\rho_{cr}/p_{cr}}\;c, \end{gathered}$$

where v is the velocity of the fluid and $c = \sqrt{(\partial p/\partial\rho)_S}$ is the sound velocity (being S the specific entropy). In the above expressions, $\rho_{cr} = 1/(3b)$, $p_{cr} = a/(27b^2)$ and $T_{cr} = 8a/(27Rb)$ are respectively, the values of the mass density, pressure and temperature at the *critical point*.

Focusing on non-characteristic shocks (i.e., discarding the so called *contact discontinuities*) in the present case, it is well known that a shock satisfying the Rankine-

Hugoniot conditions of the Euler system reads

$$\begin{aligned}
\hat{v}_1 &= \hat{c}_0 M_0 \frac{\hat{\rho}_1 - \hat{\rho}_0}{\hat{\rho}_1}, \\
\hat{p}_1 &= \hat{p}_0 + \hat{c}_0^2 M_0^2 \frac{\hat{\rho}_0 \left(\hat{\rho}_1 - \hat{\rho}_0\right)}{\hat{\rho}_1}, \\
M_0 &= \frac{1}{\hat{c}_0} \sqrt{\frac{2\hat{\rho}_1}{\hat{\rho}_0 \left(\hat{\rho}_1 - \hat{\rho}_0\right)} \left(\hat{p}_1 - \frac{\hat{\rho}_0 \hat{\rho}_1 \left(\hat{e}_1 - \hat{e}_0\right)}{\hat{\rho}_1 - \hat{\rho}_0}\right)},
\end{aligned} \tag{3.2}$$

where $M_0 = (U_s - v_0)/c_0$ is the unperturbed Mach number. In the following, we shall consider only shocks propagating in the positive x direction ($M_0 > 0$) and, due to Galilean invariance, we shall also assume, without any loss of generality, $v_0 = 0$.

We restrict ourselves to considering the unperturbed state in the gas region, the dimensionless internal energy and sound velocity in the unperturbed state, respectively, $\hat{e}_0$ and $\hat{c}_0$, are given by:

$$\begin{aligned}
\hat{e}_0 &= \left(\hat{p}_0 + 3\hat{\rho}_0^2\right)\left(3 - \hat{\rho}_0\right) / \left(3\delta\hat{\rho}_0\right) - 3\hat{\rho}_0, \\
\hat{c}_0 &= \sqrt{3\left(1+\delta\right)\left(\hat{p}_0 + 3\hat{\rho}_0^2\right) / \left(3\hat{\rho}_0 - \hat{\rho}_0^2\right) - 6\hat{\rho}_0}.
\end{aligned} \tag{3.3}$$

The internal energy in the perturbed state, $\hat{e}_1$, depends on the phase in which the perturbed state is: if it belongs to the gas or liquid phase, we have

$$\hat{e}_1 = \left(\hat{p}_1 + 3\hat{\rho}_1^2\right)\left(3 - \hat{\rho}_1\right) / \left(3\delta\hat{\rho}_1\right) - 3\hat{\rho}_1 \tag{3.4}$$

which, inserted into Eq. $(3.2)_3$, yields

$$\begin{aligned}
M_0 &= (\sqrt{6\hat{\rho}_1}/\hat{c}_0)\sqrt{N/D}, \\
N &= \hat{p}_0(1+\delta) + \hat{\rho}_0\hat{\rho}_1(\hat{\rho}_1 + \hat{\rho}_0 + 3\delta - 3), \\
D &= \hat{\rho}_0(2\hat{\rho}_0(3 - \hat{\rho}_1) + 3\delta(\hat{\rho}_0 - \hat{\rho}_1)).
\end{aligned} \tag{3.5}$$

When the perturbed state goes into the gas/liquid coexistence region which is bounded by the coexistence curve, $\mathcal{C}_{coe}$, the relation $(5.6)_1$ is still to be used in the unperturbed state, but the expression of $\hat{e}_1$ given in (3.4) for the perturbed state, must be replaced by [94]:

$$\hat{e}_1 = \frac{(\hat{p}_1 + 3\hat{\rho}_G^2)(3 - \hat{\rho}_G)}{3\delta\hat{\rho}_G} - 3\left(\hat{\rho}_G + \hat{\rho}_L - \frac{\hat{\rho}_G\hat{\rho}_L}{\hat{\rho}_1}\right), \tag{3.6}$$

where $\hat{\rho}_G$ and $\hat{\rho}_L$ are, respectively, the densities of the gas and liquid phases at pressure $\hat{p}_1$. Taking into account that the chemical potential and the pressure are the same in the two phases, $\hat{\rho}_G$ and $\hat{\rho}_L$ are implicitly obtained by the following

conditions:

$$\begin{aligned} 3\left(\hat{\rho}_G-\hat{\rho}_L\right)\left(6-\hat{\rho}_G-\hat{\rho}_L\right)+\left(3-\hat{\rho}_G\right)\left(3-\hat{\rho}_L\right) \\ \left(\hat{\rho}_G+\hat{\rho}_L\right)\ln\left(\frac{\hat{\rho}_L(3-\hat{\rho}_G)}{\hat{\rho}_G(3-\hat{\rho}_L)}\right)=0, \\ \hat{p}_1=\hat{\rho}_G\hat{\rho}_L\left(3-\hat{\rho}_G-\hat{\rho}_L\right). \end{aligned} \tag{3.7}$$

Moreover, (4.21) has to be replaced by (3.2), (3.6) and (3.7), which, with the thermal equation of state on the coexistence curve, set up a system that can be solved by means of a suitable numerical method.

3.3 Compressive upper/lower shocks

In order to discuss the compressive upper shock, it is necessary to introduce the limit density at the strong shock limit, i.e. the limiting value of the density when the perturbed pressure, or Mach number, tends to infinity, $\hat{\rho}_1^{\infty} \equiv \hat{\rho}_1^{\infty}(\hat{\rho}_0)$. Taking into account (4.21) this value of the density is the solution of the following equation:

$$D(\hat{\rho}_0,\hat{\rho}_1)=0. \tag{3.8}$$

After introducing

$$\tilde{N}(\hat{\rho}_0,\hat{p}_0)=N(\hat{\rho}_0,\hat{p}_0,\hat{\rho}_1^{\infty}(\hat{\rho}_0)), \tag{3.9}$$

we define the region $\tilde{\mathbf{C}}$ as the region in the $\hat{\rho}\hat{p}$ plane delimited by the coexistence curve $\mathcal{C}_{coe}$ and by the curve $\tilde{\mathcal{C}}_b$ given by the following equation:

$$\tilde{\mathcal{C}}_b \equiv \ \{(\hat{\rho}_0,\hat{p}_0):\tilde{N}\left(\hat{\rho}_0,\hat{p}_0\right)=0\}. \tag{3.10}$$

It is easily seen that, for unperturbed states belonging to the region $\tilde{\mathbf{C}}$, we have $\tilde{N}(\hat{\rho}_0,\hat{p}_0)<0$, while for unperturbed states outside of $\tilde{\mathbf{C}}$, it is certainly $\tilde{N}(\hat{\rho}_0,\hat{p}_0)>0$. Moreover, $D(\hat{\rho}_0,\hat{\rho}_1)>0$ for $\hat{\rho}_0<\hat{\rho}_1<\hat{\rho}_1^{\infty}$ and $D(\hat{\rho}_0,\hat{\rho}_1)<0$ for $\hat{\rho}_1>\hat{\rho}_1^{\infty}$. Therefore, if the initial unperturbed state is chosen in $\tilde{\mathbf{C}}$, we have

$$\lim_{\hat{\rho}_1\to(\hat{\rho}_1^{\infty})^-} N/D=-\infty, \qquad \lim_{\hat{\rho}_1\to(\hat{\rho}_1^{\infty})^+} N/D=+\infty,$$

and the opposite situation is met when the unperturbed state is chosen outside of $\tilde{\mathbf{C}}$. Let $\mathbf{C}$ be the region in the $\hat{\rho}\hat{p}$ plane such that when the unperturbed sate belongs to this region, its Hugoniot locus crosses the coexistence curve. Therefore, we have the situation sketched in Fig.3.1: Given two unperturbed states, A_0 and B_0, with the same $\hat{\rho}_0$, such that $A_0\in\tilde{\mathbf{C}}$ and $B_0\in\mathbf{C}\setminus\tilde{\mathbf{C}}$, the corresponding Hugoniot loci

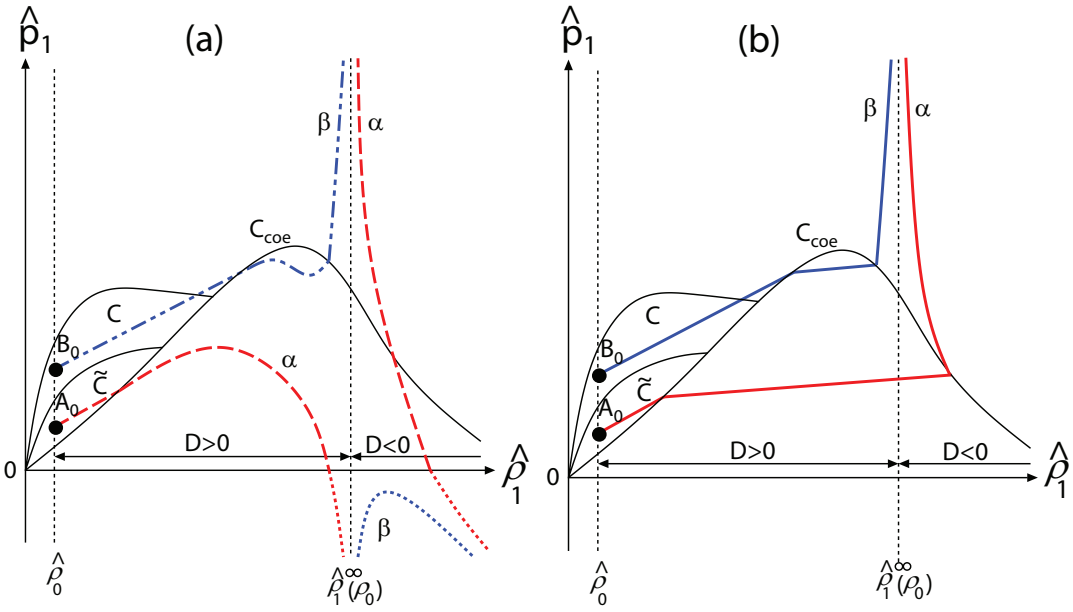

Figure 3.1: Schematic representation of Hugoniot loci, $\mathcal{H}(\mathbf{u}_0)$, without phase transition (a) and with phase transitions (b). The Hugoniot loci without and with phase transition are obtained inserting in Eqs. (3.2), respectively, Eq. (3.4) and Eq. (3.6).

obtained ignoring the phase transition, i.e., calculated by means of Eqs. (3.2), (5.6) and (3.4), are represented in Fig. 3.1(a) by, respectively, the curves α and β (the states with a negative pressure are physically meaningless and they correspond to complex values of Mach numbers). On the other hand, since both the Hugoniot loci meet the coexistence curve, the shock induces a phase transition and the curves α and β sketched in Fig. 3.1(a) must be replaced by those shown in Fig. 3.1(b), calculated by Eqs. (3.2), (5.6), (3.6) and (3.7). We observe that the shock with the unperturbed state B_0 is a usual *compressive lower shock* and the one associated to the unperturbed state A_0 is a *compressive upper shock*.

As is clearly seen from the above discussion, we can conclude that the gas $\rightarrow$ liquid phase transition is necessary for observing the compressive upper shock.

It is worth observing that, when we come to the study of compressive upper shocks, the perturbed pressure is not a single valued function of the perturbed density (this can be easily seen in Fig.3.1), so the perturbed pressure $\hat{p}_1$ is a more suitable parameter as the strength of the shock than the perturbed density $\hat{\rho}_1$.

3.4 Admissibility of shock waves

According to the theory of hyperbolic systems, not every solution of the Rankine-Hugoniot conditions corresponds to a physically meaningful shock wave. Thus, we need a criterion to select which states $\mathbf{u}_1 \in \mathcal{H}(\mathbf{u}_0)$ are the perturbed states that, together with $\mathbf{u}_0$ form *admissible* shocks. Since admissible shocks propagate with no change in shape when they are given as initial data, these solution are sometimes called *stable shocks*. It is well-known that not all the shock waves that correspond to the solutions of the RH conditions are admissible and that the Liu condition [44–46] should be satisfied in order that an initial shock can be stable and then can propagate.

The Liu condition asserts that a shock wave is admissible if and only if its velocity of propagation is not decreasing as we move on the RH curve starting from the unperturbed state, $\mathbf{u}_0$, towards a given perturbed state, $\mathbf{u}_1$:

$$s(\mathbf{u}_0, \tilde{\mathbf{u}}) \leq s(\mathbf{u}_0, \mathbf{u}_1) \qquad \forall \tilde{\mathbf{u}} \in \text{RH curve through } \mathbf{u}_0.$$

If the Liu conditions are not satisfied, the shock will become *unstable*, or *inadmissible*. It is well known that the Liu condition implies the Lax condition, and at least for moderate shocks, the entropy growth, and therefore stable shocks satisfy the second law of the thermodynamics (see, e.g. [8]). Conversely, the entropy growth is not sufficient to imply the Liu condition, and we need an additional condition [8,46].

In view of checking the admissibility of the compressive upper shock, we need to plot U_s (or, equivalently, in this case, M_0) as a function of the strength of the shock, i.e. $\hat{p}_1$. From Fig. 3.2, obtained for a typical unperturbed state in the region $\tilde{\mathbf{C}}$, it may be appreciated that compressive shocks are always admissible, except for an interval of values of the shock strength which corresponds to the part of $\mathcal{H}(\mathbf{u}_0)$ spanning the coexistence region and part of the liquid region (gas $\rightarrow$ liquid shock-induced phase transitions are thus allowed, but gas $\rightarrow$ coexistence state phase transitions are not permitted).

3.5 Numerical analysis

The numerical analysis carried out by means of a numerical code elsewhere presented [85,86], based on a modification of a central Runge-Kutta (CRK) scheme [87], confirms the theoretical predictions. Choosing the same values of the unperturbed

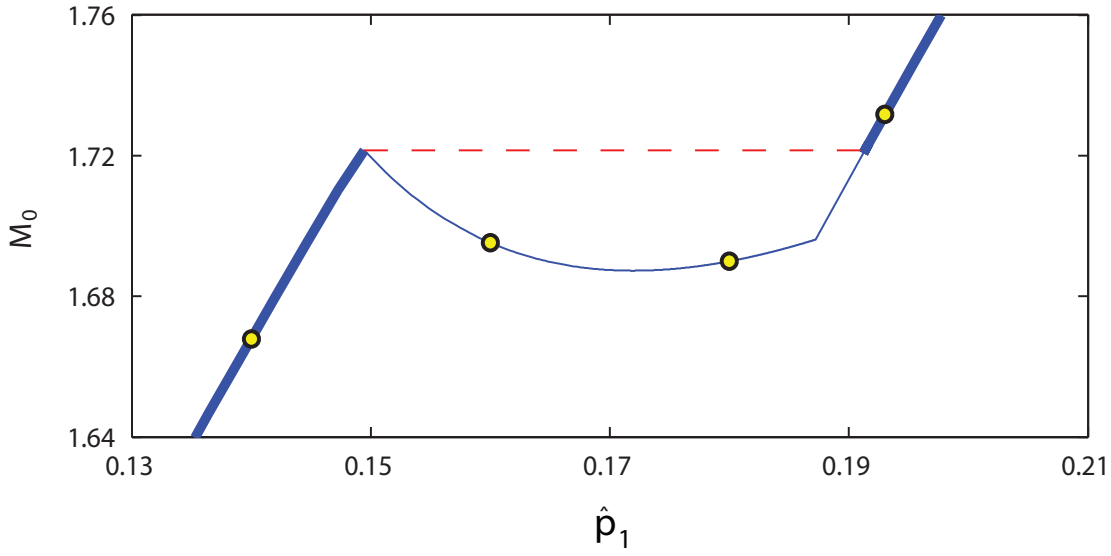

Figure 3.2: Mach number, M_0, as a function of the perturbed pressure, $\hat{p}_1$ ($\hat{p}_0 = 0.05$, $\hat{\rho}_0 = 0.03$, $\delta = 0.01$). The dots represent the perturbed states for which numerical calculations are shown in Fig. 3.3. The thick part of the curve represents admissible shocks, and the part under the horizontal line represents inadmissible ones.

state as in Fig. 3.2, shock profiles for several perturbed states are given in Fig. 3.3. These wave profiles are obtained by solving a Riemann problem for each pair of perturbed/unperturbed states connected to the Euler equations with the equations of state (3.1). Since the computational domain must be finite, as usual some artificial boundaries are introduced: absorbing boundary conditions are here imposed in order to avoid spurious (unphysical) reflections of the outgoing waves. The instant time at which the wave profiles are shown is arbitrarily chosen as $\hat{t}$=0.3. Since in a Riemann problem the shock instability appears immediately after the initial time (i.e., at t=0^+), any choice of the instant time would be acceptable, taken into account that the larger the time, the more appreciable is the (possible) shock instability (the numerical computations were actually performed for much longer times and the above-mentioned value of $\hat{t}$ was selected as a compromise solution between the requirement of having reasonably appreciable shock instabilities and the requirement of plotting clear wave profiles). From Fig. 3.3(b,c) it is possible to observe that when a single shock wave is unstable, the $\hat{\rho}$ profiles show the so-called *shock splitting* phenomenon, i.e., the wave profile is made up with a combination of shock waves, rarefaction waves and constant states, depending on the particular values of the unperturbed and the perturbed states.

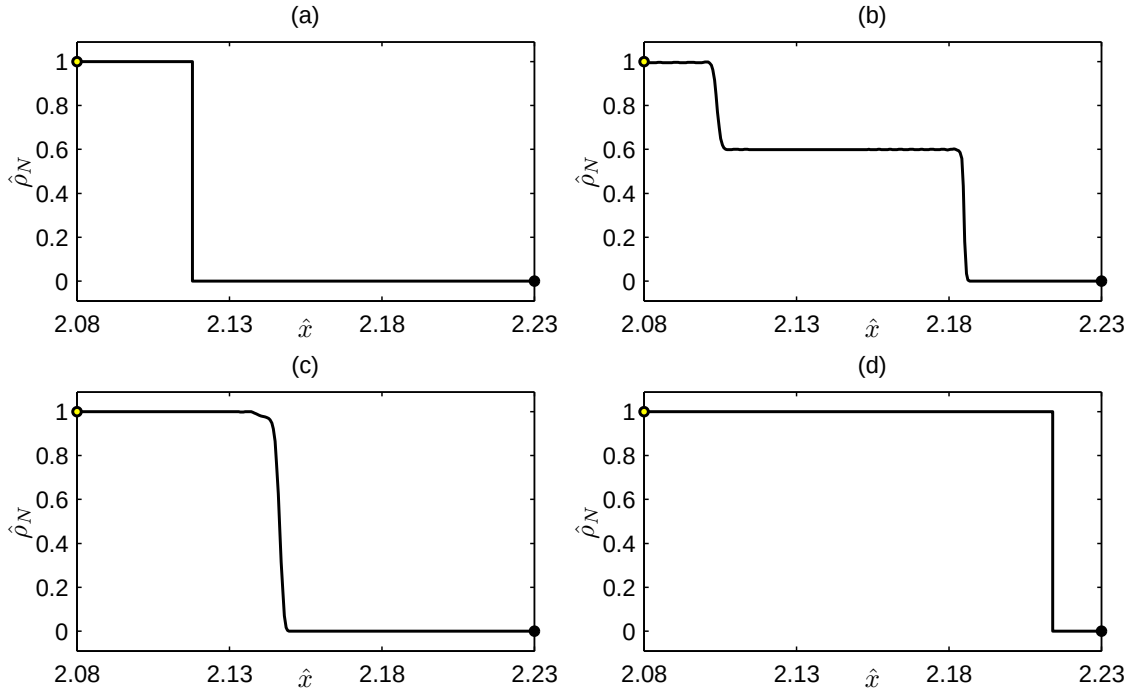

Figure 3.3: Normalized density profiles, $\hat{\rho}_N = (\hat{\rho} - \hat{\rho}_0) / (\hat{\rho}_1 - \hat{\rho}_0)$ versus dimensionless space, $\hat{x} = x/L$ (L is a characteristic length), for the perturbed states represented by the dots in Fig. 3.2: (a) $\hat{p}_1 = 0.14$; (b) $\hat{p}_1 = 0.16$; (c) $\hat{p}_1 = 0.18$; (d) $\hat{p}_1 = 0.193$ ($\hat{p}_0 = 0.05$ and $\hat{\rho}_0 = 0.03$). The profiles are obtained for $\hat{t} = 0.3$, where $\hat{t}$ is a dimensionless time ($\hat{t} = t/L\sqrt{\rho_{cr}/p_{cr}}$).

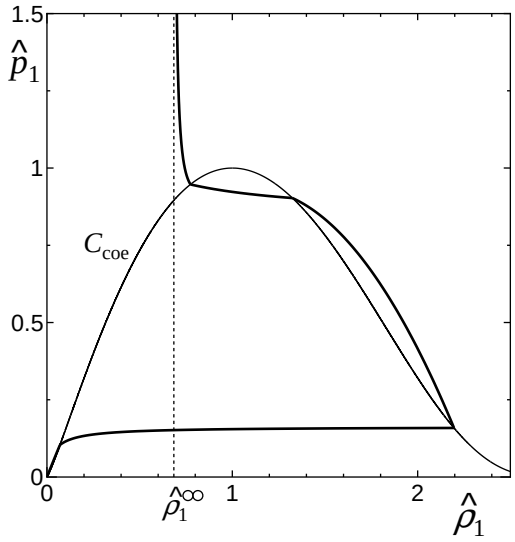

Figure 3.4: The Hugoniot locus for $\delta = 0.01, \hat{\rho}_0 = 0.00440616, \hat{p}_0 = 0.0067$. Dependence of the perturbed pressure on the perturbed density.

We finally note that some Hugoniot loci for unperturbed states in region **C**, have the possibility to cross twice the liquid branch of the coexistence curve. As seen in Fig. 3.4, with the increase of the shock parameter, the perturbed state on the Hugoniot locus moves in gas $\rightarrow$ liquid $\rightarrow$ gas phase, which is an extremely unusual behavior never reported before as far as we know. The study of this *double* gas $\rightarrow$ liquid $\rightarrow$ gas phase change, including the study of the shock admissibility, will be the subject of a forthcoming paper.

In order to study the features of the region $\tilde{\mathbf{C}}$, it is useful to write down the expression of $\tilde{\mathcal{C}}_b$, obtained from the expression of the density at the strong shock limit (see Eqs. (4.21) and (3.8)),

$$\hat{\rho}_1^{\infty} = 3\hat{\rho}_0(2+\delta)/\left(2\hat{\rho}_0 + 3\delta\right),$$

and making use of Eqs. (3.9), (3.10) and (4.21). In the $\hat{\rho}\hat{p}$ plane, the curve $\tilde{\mathcal{C}}_b$ is described by:

$$\hat{p}_0 = \frac{3\hat{\rho}_0^2(2+\delta)\left(3\delta\left(3-4\hat{\rho}_0\right) - 9\delta^2 - 2\hat{\rho}_0^2\right)}{(1+\delta)\left(3\delta + 2\hat{\rho}_0\right)^2}.$$

In Fig. 3.5, the region $\tilde{\mathbf{C}}$ is shown, together with the coexistence curve $\mathcal{C}_{coe}$. It turns out to be interesting to study the dependence of the region $\tilde{\mathbf{C}}$ on δ. This study leads to the understanding that if δ is larger than the critical value $\delta \simeq 0.103$, the region $\tilde{\mathbf{C}}$ is empty, therefore, $\delta \lesssim 0.103$ is the necessary condition for observing a compressive upper shock. It is also possible to prove that the area of the region

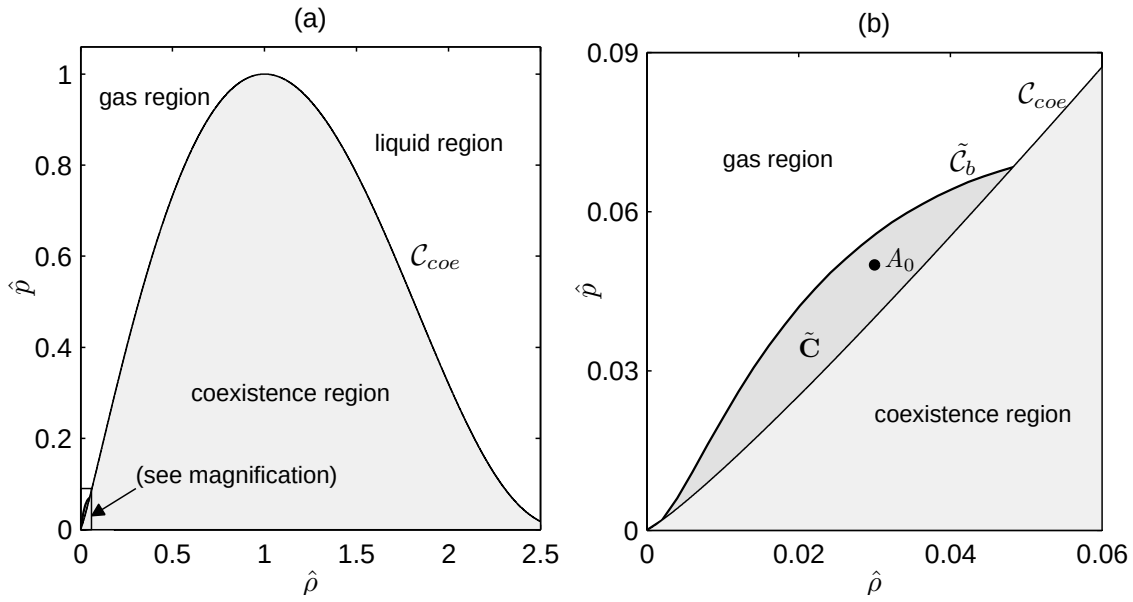

Figure 3.5: Gas region, coexistence region and $\tilde{\mathbf{C}}$ region (bounded by $\tilde{\mathcal{C}}_b$ and $\mathcal{C}_{coe}$ curves) for $\delta = 0.01$. The black dot represents the unperturbed state, A_0, used for the numerical calculations showed in Fig. 3.2 and in Fig. 3.3.

$\tilde{\mathbf{C}}$ is maximum when $\delta \simeq 0.042$; this means that compressive upper shocks may be observed even for a gas whose molecules have several constituent atoms. In a review paper [47], several real gases with δ satisfying above conditions are studied.

3.6 Summary and concluding remarks

We found the new type of shock wave, which has unusual property that, when the perturbed pressure increases, the perturbed density decreases, in a van der Waals fluid by theoretical and numerical analysis.

We emphasize that this new type of shock is not restricted to the van der Waals fluid. Since we have verified that the same type of shock exists in a hard-sphere system with attractive forces (details will be shown in the next chapter [97]), we are allowed to assert that this new shock is typical of real gases.

Chapter 4

Shock waves in a polytropic hard-sphere system with attractive force

4.1 Introduction

In the present chapter, as the subsequence of the studies discussed in the previous chapters, we will analyze shock wave phenomena in systems of hard spheres with attractive forces [97]. The present model based on the perturbation method developed in the theory of liquid-state physics [78–80] was firstly proposed in [95] as a suitable model to predict the physical quantities at the triple point. The validity and the usefulness have been confirmed through the theoretical prediction of the physical values at the critical point [96] and also many examples.

As the essential feature of the present model, this model can explain three phases, namely, gas, liquid and solid phases within a unified way. As it is expected, we will see that this model can explain the results obtained in a van der Waals model and also in a hard-sphere system. Furthermore, we will make clear the conditions for the shock-induced phase transitions and the admissibility of shock waves. Especially we will concentrate on shock-induced phase transition from gas phase to solid phase.

The purpose of the present chapter is to study shock waves and shock-induced phase transition in a system of hard-spheres with attractive force. To be more specific, we will study the following three points in detail: (i) the dependence of the solution of RH conditions on the attractive force, (ii) the admissibility of shock waves, and (iii) possibility of shock-induced phase transitions.

4.2 The system of hard spheres with attractive force

In this section, we summarize the equations of state for a system of hard-spheres with attractive force and the static properties of the present model.

4.2.1 Caloric and thermal equation of state

By using mean field theory, we can introduce the effect of attractive force as a perturbation from a hard-sphere system [95, 96]. The effect of the attractive force for specific internal energy, Δe, can be specified as follows:

$$\Delta e = -\frac{a}{m^2}\rho, \tag{4.1}$$

where a is positive constant which represents the strength of attractive force ($a \geq 0$). Therefore, specific internal energy e is given by the sum of the specific internal energy for the hard-sphere system $e_{\rm HS}$ (2.1) and the correction due to the attractive force Δe as follows:

$$\begin{aligned} e &= e_{\rm HS} + \Delta e \\ &= \frac{\mathcal{D}}{2m}k_{\rm B}T - \frac{a\eta}{m\omega}. \end{aligned} \tag{4.2}$$

Similarly, the effect of the attractive force for the pressure, Δp, can be given by

$$\Delta p = -\frac{a}{m^2}\rho^2 \tag{4.3}$$

and therefore the pressure p is given by the sum of the pressure for hard-sphere system $p_{\rm HS}$ (2.3) and the correction Δp as follows:

$$\begin{aligned} p &= p_{\rm HS} + \Delta p \\ &= \frac{\eta}{\omega}k_{\rm B}T\Gamma(\eta) - \frac{a\eta^2}{\omega^2}. \end{aligned} \tag{4.4}$$

Note that the corrections due to the attractive force (4.1) and (4.3) have the same form of the correction adopted in a van der Waals system [see the equations of state for a van der Waals fluid (3.1)]. Since the repulsive effect for a hard-sphere system are more precise than the repulsive effect for a van der Waals system, the present system can also be regarded as the modified model not only for a hard-sphere system and also for a van der Waals model.

4.2.2 Critical point and the law of corresponding states

Due to the attractive force, there exist not only liquid and solid phases but also gas phase in the present model and therefore the present model has the critical point

and the triple point. The conditions for the critical point are given by

$$\left(\frac{\partial p}{\partial \eta}\right)_T = 0, \quad \left(\frac{\partial^2 p}{\partial \eta^2}\right)_T = 0.$$

Inserting the thermal equation of state (4.4) to the critical condition, we obtain the critical packing fraction $\eta_{\rm c}$, the critical temperature $T_{\rm c}$ and critical pressure $p_{\rm c}$ as follows:

$$\eta_{\rm c} \sim 0.1301, \qquad T_{\rm c} = A_T \frac{a}{k_{\rm B}\omega}, \qquad p_{\rm c} = A_p \frac{a}{\omega^2}, \tag{4.5}$$

where A_T and A_p are proportional constants ($A_T \sim 0.09421$, $A_p \sim 0.004401$). For the later convenience, we introduce the dimensionless quantities as follows:

$$\tilde{T} = \frac{T}{T_{\rm c}}, \quad \tilde{p} = \frac{p}{p_{\rm c}}. \tag{4.6}$$

Inserting these dimensionless quantities to the thermal equation of state (4.4), we can obtain the dimensionless equation which is independent of the constant of the strength of attractive force a as follows:

$$\frac{A_p \tilde{p}}{A_T \tilde{T}} = \eta\Gamma(\eta) - \frac{\eta^2}{A_T \tilde{T}}.$$

We will call this relation as *the law of corresponding state* for the present system.

4.2.3 Coexistence conditions and phase diagram

Let us discuss the coexistence conditions for the present system. We will consider the coexistence state consisting of the two state which have the different phases and will refer the two states as the state C1 and state the C2, respectively. For example, when we consider gas and liquid coexistence state, the phase of the state C1 and the phase of the state C2 are gas and liquid phases, respectively. Hereafter, the subscript C1 and C2 means quantities in the the state C1 and state C2, respectively.

In general, the coexistence condition between the state C1 and the state C2 can be given by two conditions with common temperature. First condition is the equality of the specific Gibbs free energies expressed as follows:

$$g(\eta_{C1}, T) = g(\eta_{C2}, T), \tag{4.7}$$

where g is the specific Gibbs free energy defined by $g \equiv e - Ts + p/\rho$ with s being the specific entropy. Second condition is the equality of the pressures represented by

$$p(\eta_{C1}, T) = p(\eta_{C2}, T). \tag{4.8}$$

These general coexistence conditions will be written explicitly by using the thermal and caloric equations of state which depend on the phases of the state C1 and the state C2.

Now we discuss the gas/liquid coexistence condition. Note that both of gas and liquid phase can be obtained from the equation of state with the Γ^{L} branch because the packing fractions of both of gas and liquid at the gas/liquid coexistence state are less than η_{0L}, where η_{0L} and η_{0S} represent the packing fraction at the freezing and melting points of a hard-sphere system without attractive force, respectively.

Inserting the caloric and thermal equations of state (4.2), (4.4) to the Gibbs relation,

$$\mathrm{d}s = \frac{1}{T}\mathrm{d}e + \frac{p}{T}\mathrm{d}\left(\frac{1}{\rho}\right), \tag{4.9}$$

we can obtain the specific entropy as follows:

$$ds = \frac{k_{\mathrm{B}}}{m}\left(\frac{\mathcal{D}}{2}\frac{\mathrm{d}T}{T} - \frac{\Gamma(\eta)}{\eta}\mathrm{d}\eta\right).$$

Integrating this equation, we obtain

$$s - s_a = \frac{k_{\mathrm{B}}}{m}\left(\frac{\mathcal{D}}{2}\frac{T}{T_a} - \ln\frac{\eta}{\eta_a} - \int_{\eta_a}^{\eta}\frac{\chi^{\mathrm{L}}(\eta)}{\eta}\mathrm{d}\eta\right),$$

where subscript a means the reference state. Adopting the state in a rarefied limit ($\eta_a \to 0$) for the reference state, the specific entropy s can be given by

$$s = \frac{k_{\mathrm{B}}}{m}\left(\frac{\mathcal{D}}{2}T - \ln\eta - \int_0^{\eta}\frac{\chi^{\mathrm{L}}(\eta)}{\eta}\mathrm{d}\eta\right). \tag{4.10}$$

Inserting (4.10) with the caloric and thermal equations of state (4.2) and (4.4) to the general coexistence conditions (4.7) and (4.8), we can obtain the coexistence condition of gas / liquid coexistence state as follows:

$$\begin{cases} 2(\eta_{\mathrm{L}} - \eta_{\mathrm{G}}) - A_T\tilde{T}\left(\displaystyle\int_{\eta_{\mathrm{G}}}^{\eta_{\mathrm{L}}}\frac{\Gamma^{\mathrm{L}}(\eta)}{\eta}\mathrm{d}\eta + \Gamma^{\mathrm{L}}(\eta_{\mathrm{L}}) - \Gamma^{\mathrm{L}}(\eta_{\mathrm{G}})\right) = 0, \\ \dfrac{A_T}{A_p}\tilde{T}\eta_{\mathrm{L}}\Gamma^{\mathrm{L}}(\eta_{\mathrm{L}}) - \dfrac{\eta_{\mathrm{L}}^2}{A_p} = \dfrac{A_T}{A_p}\tilde{T}\eta_{\mathrm{G}}\Gamma^{\mathrm{L}}(\eta_{\mathrm{G}}) - \dfrac{\eta_{\mathrm{G}}^2}{A_p}. \end{cases} \tag{4.11}$$

In order to discuss liquid / solid or gas / solid coexistence condition, we have to pay attention to the fact that the thermal equation of state consists of three branch. Depending on the packing fraction, the reference specific entropy should be specified. The specific entropy at $\eta_{0\mathrm{L}}$ is given by

$$s_{0\mathrm{L}} = \frac{k_{\mathrm{B}}}{m}\left(\frac{\mathcal{D}}{2}\ln T - \ln\eta_{0\mathrm{L}} - \int_0^{\eta_{0\mathrm{L}}}\frac{\chi^{\mathrm{L}}}{\eta}\mathrm{d}\eta + C\right).$$

Using the relation $\Gamma^{\mathrm{CO}}(\eta) = \eta_{0\mathrm{L}}\Gamma^{\mathrm{L}}(\eta_{0\mathrm{L}})/\eta$ in the case that the packing fraction is between $\eta_{0\mathrm{L}}$ and $\eta_{0\mathrm{S}}$, the specific entropy at $\eta_{0\mathrm{S}}$ can be obtained as follows:

$$s_{0\mathrm{S}} = s_{0\mathrm{L}} - \frac{k_{\mathrm{B}}}{m}\eta_{0\mathrm{L}}\Gamma^{\mathrm{L}}(\eta_{0\mathrm{L}})\left(\frac{1}{\eta_{0\mathrm{L}}} - \frac{1}{\eta_{0\mathrm{S}}}\right).$$

Adopting $s_{0\mathrm{S}}$ as the reference specific entropy, the specific entropy of the solid branch can be calculated as follows:

$$s_{\mathrm{S}} = s_{0\mathrm{S}} - \frac{k_{\mathrm{B}}}{m}\int_{\eta_{0\mathrm{S}}}^{\eta_{\mathrm{S}}}\frac{\Gamma^{\mathrm{S}}(\eta)}{\eta}\mathrm{d}\eta. \tag{4.12}$$

Inserting (4.12) with the caloric and thermal equations of state (4.2), (4.4) to the general coexistence conditions (4.7), the coexistence condition of gas / solid or liquid / solid coexistence state can be summarized as follows:

$$\begin{cases} 2(\eta_{\mathrm{S}} - \eta_{\mathrm{G,L}}) - A_T\tilde{T}\Bigg[\displaystyle\int_{\eta_{\mathrm{G,L}}}^{\eta_{0\mathrm{L}}}\frac{\Gamma^{\mathrm{L}}(\eta)}{\eta}\mathrm{d}\eta - \eta_{0\mathrm{L}}\Gamma^{\mathrm{L}}(\eta_{0\mathrm{L}})\left(\frac{1}{\eta_{0\mathrm{S}}} - \frac{1}{\eta_{0\mathrm{L}}}\right) \\ \qquad\qquad + \Gamma^{\mathrm{S}}(\eta_{\mathrm{S}}) - \Gamma^{\mathrm{L}}(\eta_{\mathrm{G,L}})\displaystyle\int_{\eta_{0\mathrm{S}}}^{\eta_S}\frac{\Gamma^{\mathrm{S}}(\eta)}{\eta}\mathrm{d}\eta\Bigg] = 0, \\ \dfrac{A_T}{A_p}\tilde{T}\eta_{\mathrm{G,L}}\Gamma^{\mathrm{L}}(\eta_{\mathrm{G,L}}) - \dfrac{\eta_{\mathrm{G,L}}^2}{A_p} = \dfrac{A_T}{A_p}\tilde{T}\eta_{\mathrm{S}}\Gamma^{\mathrm{S}}(\eta_{\mathrm{S}}) - \dfrac{\eta_{\mathrm{S}}^2}{A_p}, \end{cases} \tag{4.13}$$

where $\eta_{\mathrm{G,L}}$ means η_{G} or η_{L}. Note that the both of gas / solid and liquid / solid coexistence conditions are given by the conditions (4.13). When the temperature is higher than the triple point temperature (the value will be determined in the following), these conditions represent the liquid / solid coexistence conditions. When the temperature is lower than the triple point temperature these conditions represent the gas / solid coexistence conditions.

The coexistence curves can be obtained using the gas / liquid coexistence conditions (4.11), the liquid / solid and gas / solid coexistence conditions (4.13), respectively. Figure 4.1 shows that the phase diagram in the dimensionless pressure - packing fraction plane.

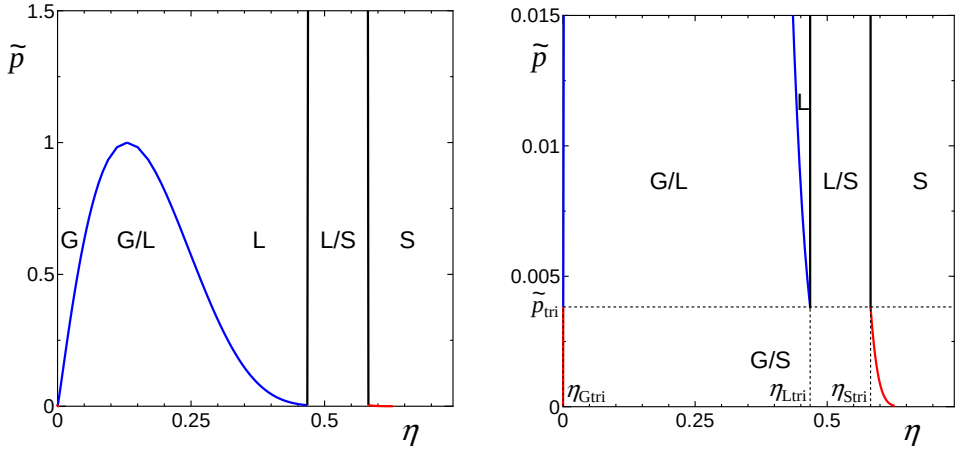

Figure 4.1: Left: The phase diagram in the $\tilde{p}$ - η plane. G, L, S, G / L, L / S and G / S mean the gas, liquid, solid, gas / liauid coexistence, liquid / solid coexistence, gas / solid coexistence phases, respectively. Right: blowup of the low pressure region in the left side.

For the completeness, the phase diagram in the $\tilde{p}$—$\tilde{T}$ plane are also shown in Fig. 4.2.

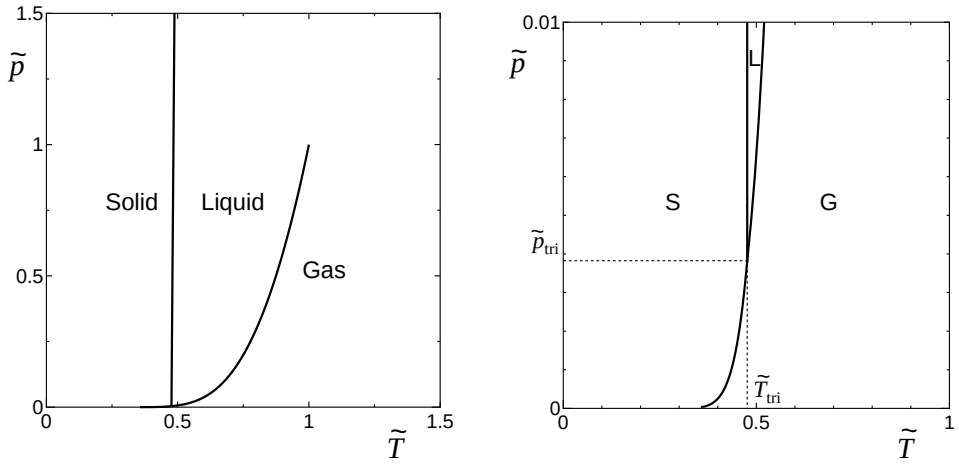

Figure 4.2: Left: The phase diagram in the $\tilde{p}$ - $\tilde{T}$ plane. G, L and S represent gas, liquid and solid phases, respectively. Right: blowup of the low pressure region in the left side.

The triple point can be obtained as the cross point between the gas / liquid coexistence curve and the liquid / solid coexistence curve because the both coexistence conditions (4.11) and (4.13) should be satisfied at the triple point. From these conditions, the temperature $\tilde{T}_{\rm t}$ and the pressure $\tilde{p}_{\rm t}$ at the triple point are given by

$$\tilde{T}_{\rm t} \simeq 0.4763, \quad \tilde{p}_{\rm t} \simeq 0.003824.$$

The packing fractions at the triple point are summarized as follows:

$$\eta_{\mathrm{Gtri}} \simeq 0.0003776, \qquad \eta_{\mathrm{Ltri}} \simeq 0.4677, \qquad \eta_{\mathrm{Stri}} \simeq 0.5821,$$

where η_{Gtri}, η_{Ltri} and η_{Stri} are the coexistence packing fraction of the gas part, liquid part and solid part at the pressure of the the triple point, respectively (See. Fig. 4.1).

4.3 The system of Euler equations and the Rankine-Hugoniot conditions

Hereafter we study shock-induced phase transitions and shock admissibility focusing on one-dimensional waves (plane waves) traveling only along the x direction.

4.3.1 The system of Euler equations

The system of Euler equations, which descrive the conservation of mass, momentum and energy for a compressible fluid in the one-dimensional case, can be expressed as follows:

$$\mathbf{u}_t + \mathbf{F}_x(\mathbf{u}) = 0, \tag{4.14}$$

where the subscripts (time t and position x) denote partial differentiation. The density $\mathbf{u}$ and the flux $\mathbf{F}$ are defined by

$$\mathbf{u} = \begin{pmatrix} \rho \\ \rho v \\ \rho e + \frac{1}{2}\rho v^2 \end{pmatrix}, \qquad \mathbf{F} = \begin{pmatrix} \rho v \\ \rho v^2 + p \\ \left(\rho e + \frac{1}{2}\rho v^2 + p\right) v \end{pmatrix} \tag{4.15}$$

with v being the velocity.

4.3.2 Local exceptionality condition

The characteristic velocities of the system of Euler equations (4.14) and (4.15) are given by

$$\lambda^{(1)} = v - c, \qquad \lambda^{(2)} = v, \qquad \lambda^{(3)} = v + c. \tag{4.16}$$

Focusing on the wave associated to $\lambda \equiv \lambda^{(3)}$, the locus of the states such that $\nabla\lambda = 0$ can be obtained as follows:

$$\rho \left(\frac{\partial^2 p}{\partial \rho^2}\right)_s + 2\left(\frac{\partial p}{\partial \rho}\right)_s = 0. \tag{4.17}$$

Hereafter we will call the curve obtained by (4.17) as the Local Exceptionality (LE) curve.

Figure 4.3 shows the LE curves obtained from the condition (4.17) for several f.

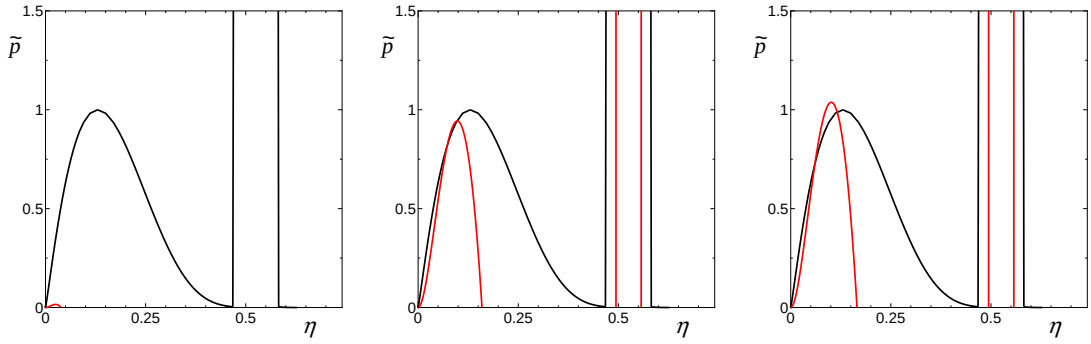

Figure 4.3: Local exceptionality curve and the coexistence curve for $f = 0$ (left), $f = 50$ (center), $f = 100$ (right).

It can be seen from Fig. 4.3 that LE curves appears only in the gas phase only when the internal degrees of freedom are enough large. This results are same as the ones in a the van der Waals system and also in a hard-sphere system.

4.4 The Rankine-Hugoniot conditions

Let us discuss the Rankine-Hugoniot relations fot a system of the hard-spheres with attractive force. The system of Euler equations (4.14) and (4.15) admits a plane shock wave provided that the jump of the physical quantities between the states before and after the shock front satisfies the Rankine-Hugoniot (RH) conditions,

$$-U_{\mathrm{s}}[\![\mathbf{u}]\!] + [\![\mathbf{F}(\mathbf{u})]\!] = 0, \tag{4.18}$$

where U_s is the propagation velociy of the shock front and $[\![\psi]\!] = \psi_1 - \psi_0$ represents the jump of a generic quantity ψ across the shock front, being ψ_1 the quantity in the state after the shock *(perturbed state)* and ψ_0 in the state before the shock *(unperturbed state)*. The conditions (4.18) are explicitly written by using the packing

fraction η instead of the mass density ρ as follows:

$$\begin{aligned} -U_{\mathrm{s}}[\![\eta]\!] + [\![\eta v]\!] &= 0, \\ -U_{\mathrm{s}}[\![\eta v]\!] + \left[\!\!\left[\eta v^2 + \frac{p\omega}{m}\right]\!\!\right] &= 0, \\ -U_{\mathrm{s}}\left[\!\!\left[\eta e + \frac{1}{2}\eta v^2\right]\!\!\right] + \left[\!\!\left[\left(\eta e + \frac{1}{2}\eta v^2 + \frac{p\omega}{m}\right) v\right]\!\!\right] &= 0. \end{aligned} \tag{4.19}$$

The unperturbed Mach number M_0 is defined by

$$M_0 \equiv \frac{U_{\mathrm{s}} - v_0}{c_0},$$

where the quantities with the subscript 0 are the so-called *unperturbed quantities*, i.e. the quantities evaluated in the unperturbed state (analogously, the quantities with the subscript 1 are evaluated in the perturbed state and are called *perturbed quantities*) and c is the sound velocity given by

$$c = \sqrt{\left(\left.\frac{\partial p}{\partial \rho}\right|_{\mathrm{s}}\right)} \tag{4.20}$$

with s being the specific entropy.

Using the Gibbs relation (4.9), we can obtain the explicit expression of the unperturbed sound speed as follows:

$$c_0 = \sqrt{\frac{-2a\mathcal{D}\eta_0 + k_{\mathrm{B}}T_0[2\Gamma_0^2 + \mathcal{D}(\Gamma_0 + \Gamma_0'\eta_0)]\omega}{\mathcal{D}m\omega}},$$

where Γ_0 and Γ_0' is defined by

$$\Gamma_0 \equiv \Gamma(\eta_0), \qquad \Gamma_0' \equiv \left.\frac{\mathrm{d}\Gamma(\eta)}{\mathrm{d}\eta}\right|_{\eta=\eta_0}.$$

Hereafter, we will focus on the case that the unperturbed state lies in gas or liquid phases, therefore, Γ_0 is always Γ^{L}.

4.4.1 Rankine-Hugoniot conditions in the case that both unperturbed and perturbed state are not coexistence state

Now we discuss the case that the both the unperturbed and the perturbed state are not coexistence state. Since the equations of state for gas, liquid, and solid phases have the same form[see (4.2) and (4.4)], althogh the expressions of the function $\Gamma(\eta)$ are different, we write down the RH conditions in the unified way. Depending on the perturbed packing fraction, suitable Γ should be chosen.

Inserting the equations of state to the general form of the RH conditions (4.19), we can obtain the expressions of RH conditions for the present system as follows:

$$\begin{aligned}
\hat{v} &\equiv \frac{v}{c_0} \\
&= M_0 \left(1 - \frac{1}{\hat{\eta}}\right), \\
\hat{p} &\equiv \frac{p}{p_0} \\
&= 1 + \frac{M_0^2(\hat{\eta}-1)\{2\mathcal{D}\eta_0 - A_T\tilde{T}_0[2\Gamma_0^2 + \mathcal{D}(\Gamma_0 + \Gamma_0'\eta_0)]\}}{\mathcal{D}\hat{\eta}(\eta_0 - A_T\tilde{T}_0\Gamma_0)} \\
M_0 &= \sqrt{\frac{\mathcal{D}\hat{\eta}\{\eta_0(\hat{\eta}-1)[2\Gamma(\hat{\eta}-1) - \mathcal{D}(\hat{\eta}+1)] + A_T\tilde{T}_0[2\Gamma\Gamma_0(\hat{\eta}-1) - \mathcal{D}(\Gamma_0 - \Gamma\hat{\eta})]\}}{(\hat{\eta}-1)[\Gamma(\hat{\eta}-1) - \mathcal{D}]\{2\mathcal{D}\eta_0 - A_T\tilde{T}_0[2\Gamma_0^2 + \mathcal{D}(\Gamma_0 + \Gamma_0'\eta_0)]\}}}
\end{aligned} \tag{4.21}$$

$$\begin{aligned}
\hat{T} &\equiv \frac{T}{T_0} \\
&= \frac{\eta^2 + \hat{p}(A_T\tilde{T}_0\eta_0\Gamma_0 - \eta_0^2)}{A_T\tilde{T}_0\eta\Gamma}
\end{aligned}$$

4.4.2 Rankine-Hugoniot conditions in the case that only perturbed state are coexistence state

Let us discuss the RH conditions in the case that only the perturbed state is coexistence state. We assume that coexistence states consist of two different phases as we discussed in 4.2.3.

We introduce a parameter α that specify a coexistence tate by the definition that α is the ratio of the state C2 in the coexistence state. Because of the additivity of the specific volume, the total packing fraction in the coexistence state is given by

$$\frac{1}{\eta(\alpha)} \equiv \frac{1-\alpha}{\eta_{C1}} + \frac{\alpha}{\eta_{C2}}.$$

Similarly, the total specific internal energy is given by

$$e(\alpha) = (1-\alpha)e_{C1} + \alpha e_{C2}$$

with e_{C1} and e_{C2} being

$$\begin{aligned}
e_{C1} &= \frac{\mathcal{D}}{2m}k_{\mathrm{B}}T - \frac{a\eta_{C1}}{m\omega}, \\
e_{C2} &= \frac{\mathcal{D}}{2m}k_{\mathrm{B}}T - \frac{a\eta_{C2}}{m\omega}.
\end{aligned}$$

The pressures are common between two states as follows:

$$p = \frac{\eta_{C1}}{\omega} k_{\mathrm{B}} T \Gamma_{C1}(\eta_{C1}) - \frac{a\eta_{C1}^2}{\omega^2} \left(= \frac{\eta_{C2}}{\omega} k_{\mathrm{B}} T \Gamma_{C2}(\eta_{C2}) - \frac{a\eta_{C2}^2}{\omega^2} \right).$$

Inserting these relations to the RH conditions (4.18), we obtain following expressions:

$$\hat{v} = M_0 \left(1 - \frac{1}{\eta(\alpha)} \right),$$

$$\begin{aligned} \hat{T} = \frac{1}{A_T \mathcal{D} \tilde{T}_0 \Gamma_{C1} \eta_{C1} \eta(\alpha)} \Big\{ & \mathcal{D} \left[2M_0^2 \eta_0^2 (\eta_0 - \eta(\alpha)) + \eta(\alpha)(\eta_{C1}^2 - \eta_0^2) \right] \\ & + A_T \tilde{T}_0 \eta_0 \Big[2M_0^2 \Gamma_0^2 (\eta(\alpha) - \eta_0) \\ & + \mathcal{D}(\Gamma_0 \eta(\alpha) - M_0^2 (\Gamma_0 + \Gamma_0' \eta_0)(\eta_0 - \eta(\alpha))) \Big] \Big\}, \end{aligned}$$

$$\begin{aligned} M_0 = \Bigg[& \frac{1}{(\eta(\alpha) - \eta_0)[\Gamma_{C1} \eta_{C1} (\eta_0 - \eta(\alpha)) + \mathcal{D} \eta_0 \eta(\alpha)]} \\ & \times \frac{\mathcal{D}\eta(\alpha)}{\{2\mathcal{D}\eta_0 - A_T \tilde{T}_0 [2\Gamma_0^2 + \mathcal{D}(\Gamma_0 + \Gamma_0' \eta_0)]\}} \\ & \times \Bigg(\{\mathcal{D}(\eta_{C1}^2 - \eta_0^2)\eta(\alpha) - 2\Gamma_{C1}\eta_{C1}[\eta_0^2 - 2\eta_0\eta(\alpha) + \eta(\alpha)(\eta_{C1} - \alpha\eta_{C1} + \alpha\eta_{C2})] \\ & - A_T \tilde{T}_0 \{\mathcal{D}\Gamma_{C1}\eta_{C1}\eta(\alpha) - \Gamma_0 [2\Gamma_{C1}\eta_{C1}(\eta_0 - \eta(\alpha)) + \mathcal{D}\eta_0\eta(\alpha)]\} \Bigg) \Bigg]^{\frac{1}{2}}. \end{aligned}$$

Combining these RH conditions with the coexistence conditions (4.11) and (4.13) we can obtain the Hugoniot curves even in the case that the perturbed state is coexistence state. This system should be solved by means of the suitable numerical scheme.

4.5 Shock-induced phase transitions

4.5.1 Gas → Liquid phase transition

We discuss the shock-induced phase transition from the gas phase to the liquid phase (gas → liquid phase transition). Now we assume that the unperturbed state is in the gas phase, however, not near from the triple points. If not, the shock-induced phase transition from the gas phase to the solid phase (gas → solid phase transition) may occur. We will make clear the condition to observe these kinds of phase transitions later.

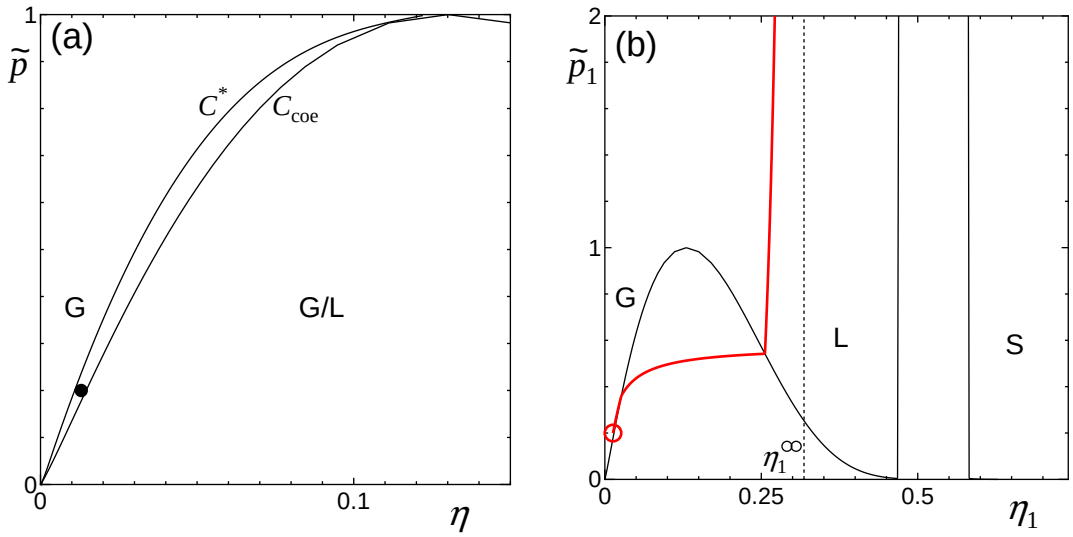

Figure 4.4: (a) The C^* curve for $f = 100$. The gas / liquid coexistence curves $C_{\rm coe}$ are also shown. (b) The RH curves in the $\tilde{p} - \eta$ plane for the unperturbed state ($\eta_0 = 0.013$, $\tilde{p}_0 = 0.2$) shown by the mark in the figure (a).

In order to analyze the shock-induced gas $\rightarrow$ liquid phase transition, the curve C^* introduced in the paper [94] is useful. The curve C^* consists of the unperturbed states whose Hugoniot curves are tangent to the coexistence curve. The unperturbed state $\mathbf{u}_0 \in C^*$ can be expressed by

$$\begin{cases} \tilde{p}_{\rm C}(\eta_1) = \tilde{p}_{\mathcal{H}}(\eta_1, \tilde{\mathbf{u}}_0), \\ \dfrac{\partial \tilde{p}_{\rm C}}{\partial \eta}(\eta_1) = \dfrac{\partial \tilde{p}_{\mathcal{H}}}{\partial \eta}(\eta_1, \tilde{\mathbf{u}}_0) \end{cases} \tag{4.22}$$

with $\tilde{p}_{\rm C}$ and $\tilde{p}_{\mathcal{H}}$ being the gas/liquid coexistence curve given by (4.11) and the gas $\rightarrow$ gas RH curve, respectively. If the unperturbed state lies in the region delimited by the curve C^* and the gas/liquid coexistence curve, the Rankine-Hugoniot curve can across the coexistence curve, therefore, gas $\rightarrow$ liquid phase transition may occur.

Fig. 4.4 shows the RH curves for $f = 100$, $\eta_0 = 0.013$, $\tilde{P}_0 = 0.2$ in the $\tilde{p} - \eta$ plane as a typical example of the shock-induced gas $\rightarrow$ liquid phase transition. With the increase of the strength of the shock, the phase of the perturbed state becomes from gas phase to gas / liquid coexistence phase and to liquid phase. Therefore, gas $\rightarrow$ liquid phase transition may be observed.

It is also easily seen from Fig. 4.4 that there is the limit packing fraction η_1^∞ to which the perturbed packing fraction approaches when the strength of the shock wave tends to infinite (the perturbed pressure or the Mach number tends to infinite).

This value of the packing fraction can easily be obtained from Eq. (4.21) as follows:

$$\Gamma(\hat{\eta}^{\infty} - 1) - \mathcal{D} = 0, \tag{4.23}$$

where $\hat{\eta}^{\infty} \equiv \eta_1^{\infty}/\eta_0$. In the present case, the unperturbed state and the perturbed state are in gas or liquid phase and therefore, the packing fraction at the strong shock limit can be given by

$$\Gamma^{\mathrm{L}}(\hat{\eta}^{\infty} - 1) - \mathcal{D} = 0. \tag{4.24}$$

In the present system, the compressive upper shocks, which were discovered in a van del Waals system in Chap. 3 [93], can also be observed. This shock has an unusual property that when the perturbed pressure increases, the perturbed packing fraction may decreases and tends to the limit packing fraction η_1^{∞}. Compressive upper shocks exist in the case that the unperturbed state lies in the region $\tilde{C}$ delimited by the coexistence curve and by the curve $\tilde{C}_{\mathrm{b}}$, which consists of the unperturbed state satisfying the condition that the numerator of Mach number is zero at the limit packing fraction. The unperturbed state $\mathbf{u}_0 \in \tilde{C}_{\mathrm{b}}$ can be given by

$$\eta_0(\hat{\eta}-1)[2\Gamma^{\mathrm{L}}(\hat{\eta}-1)-\mathcal{D}(\hat{\eta}+1)]+A_T\tilde{T}_0[2\Gamma^{\mathrm{L}}\Gamma_0^{\mathrm{L}}(\hat{\eta}-1)-\mathcal{D}(\Gamma_0^{\mathrm{L}}-\Gamma^{\mathrm{L}}\hat{\eta})]\Big|_{\eta_1=\eta_1^{\infty}} = 0. \tag{4.25}$$

Figure 4.5 shows that the dependence of the perturbed pressure on the perturbed density for $f = 100$, $\eta_0 = 0.0033$, $\tilde{p}_0 = 0.05$ as a typical Rankine-Hugoniot curve of compressive upper shock and the region $\tilde{C}$.

We can see from Fig. 4.5 that the unperturbed state is inside both the curve $\tilde{C}$ and the curve C^* and that the unperturbed state used in Fig. 4.4 is outside the curve $\tilde{C}$. As is predicted, the phase of the unperturbed state becomes from gas phase to gas / liquid coexistence phase and to liquid phase and after the phase transition the perturbed density decreases as the perturbed pressure increases.

It is worth noting that the results obtained in the present model can explain all the results obtained in a van der Waals fluid. There exist not only shock-induced phase transitions but also the other real-gas effects can be discussed. For example, negative shock waves can be observed if the unperturbed state lies in the region delimited by the coexistence curve and the locally exceptional curve which is shown in the Fig. 4.3. Furthermore, from the Liu condition, it can be easily shown that a shock wave may be inadmissible. However, the detailed discussions are omitted here for simplicity. We just emphasize that these facts mean that the present model can be a suitable modified model of the van der Waals model.

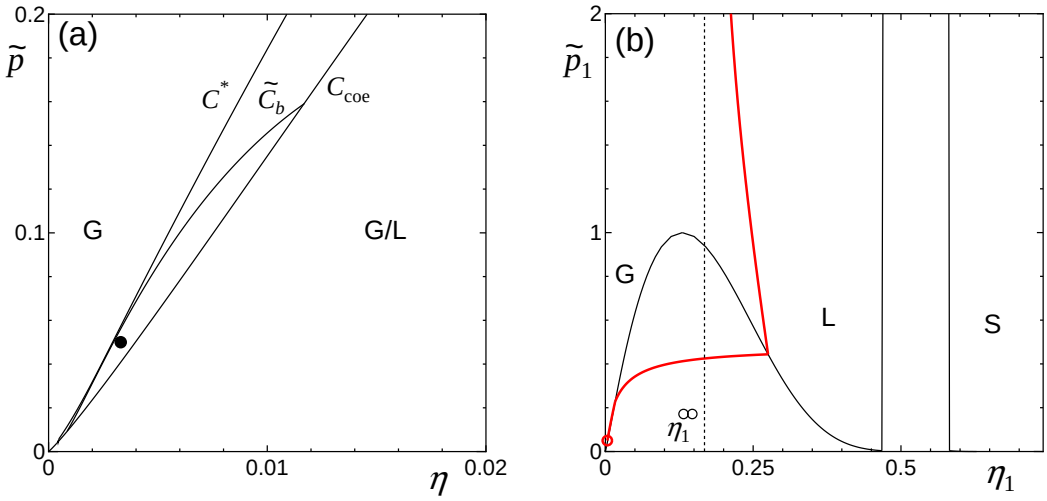

Figure 4.5: (a) The C^* curve and $\tilde{C}_{\rm b}$ curve for $f = 100$. The gas / liquid coexistence curve $C_{\rm coe}$ is also shown. (b) The RH curves in the $\tilde{p} - \eta$ plane for the unperturbed state ($\eta_0 = 0.0033$, $\tilde{p}_0 = 0.05$) shown by the mark in the figure (a).

4.5.2 Liquid → solid phase transition

Now we discuss the case that the unperturbed state lies in liquid phase. For the analysis of the shock-induced phase transition from liquid phase to solid phase (liquid → solid phase transition), the critical packing fraction η_{02} introduced in the papers [83, 84] is useful. η_{02} is the unperturbed packing fraction whose perturbed packing fraction approaches to η_{0S} at the strong shock limit. From the Eq. (4.23), the limit packing fraction is given by

$$\Gamma^{\rm S}(\hat{\eta}^\infty - 1) - \mathcal{D} = 0 \tag{4.26}$$

and therefore, η_{02} can be expressed as follows:

$$\eta_{02} = \eta_{0S}\frac{\Gamma^{\rm S}(\eta_{0\rm S})}{\mathcal{D} + \Gamma^{\rm S}(\eta_{0\rm S})}.$$

If the unperturbed packing fraction is greater than η_{02}, the RH curve can reach the solid phase, therefore, liquid → solid phase transition can be observed. The condition to observe compressive upper shocks is that the unperturbed state lies in the region $\tilde{C}_2$ delimited by the coexistence curve and the curve $\tilde{C}_{\rm b2}$, which consists of the unperturbed state satisfying the condition that the numerator of Mach number is zero at the limit packing fraction, given by

$$\eta_0(\hat{\eta}-1)[2\Gamma^{\rm S}(\hat{\eta}-1)-\mathcal{D}(\hat{\eta}+1)]+A_T\tilde{T}_0[2\Gamma^{\rm S}\Gamma_0^{\rm L}(\hat{\eta}-1)-\mathcal{D}(\Gamma_0^{\rm L}-\Gamma^{\rm S}\hat{\eta})]\Big|_{\eta_1=\eta_1^\infty} = 0. \tag{4.27}$$

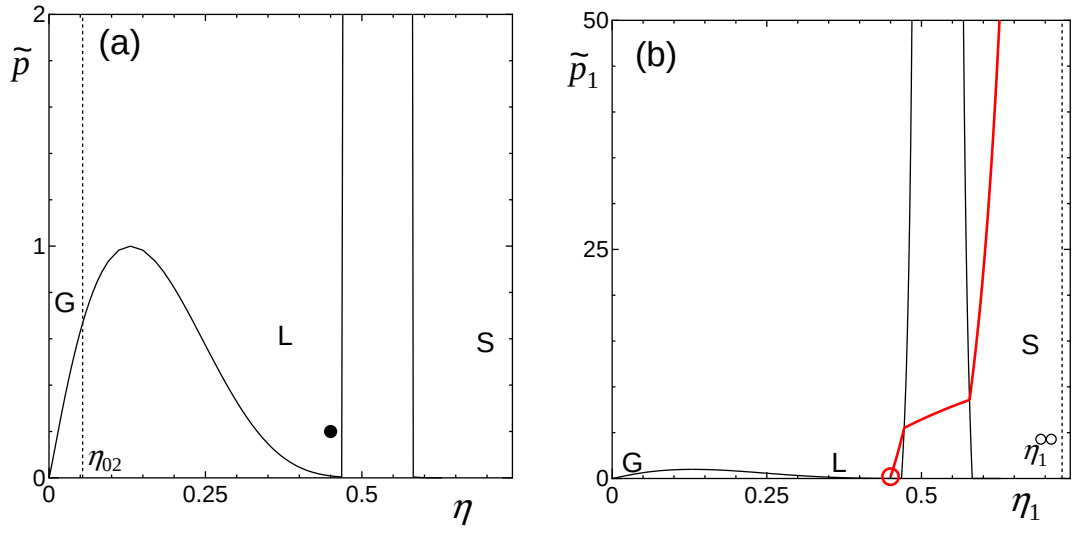

Figure 4.6: (a) The η_{02} curve for $f = 100$. The coexistence curves $C_{\rm coe}$ is also shown. (b) The RH curves in the $\tilde{p} - \eta$ plane for the unperturbed state ($\eta_0 = 0.2$, $\tilde{p}_0 = 0.45$) shown by the mark in the figure (a).

Note that the difference between the condition of $\tilde{C}_{\rm b}$ (4.25) and the condition of $\tilde{C}_{\rm b2}$ (4.27) is the Γ at the perturbed state. It can be easily shown that the region $\tilde{C}_2$ lies only in the rare region in the gas state. Compressive upper shocks can never be observed when the unperturbed state is in liquid state.

Fig. 4.6 shows the RH curves for $f = 100$, $\eta_0 = 0.45$, $\tilde{P}_0 = 0.2$, as a typical example of the shock-induced liquid $\rightarrow$ solid phase transition. From Fig. 4.6, we can easily confirm that the unperturbed packing fraction η_0 is larger than η_{02} and that liquid $\rightarrow$ solid phase transition can be observed with the increase of the strength of the shock.

As is expected, the results obtained in the present model can explain all the results obtained in a hard-sphere model. Therefore, we can conclude that the present model is a suitable modified model of the hard-sphere system. It can be seen from the Fig. 4.3 that negative shocks can never be observed when the unperturbed state is in liquid phase. It can also be seen that a single shock wave can be unstable from the Liu condition.

4.5.3 Gas $\rightarrow$ solid phase transition

Now we discuss the shock-induced phase transition from gas phase to solid phase (gas $\rightarrow$ solid phase transition). This is essentially new phenomenon which can not be

analyzed by both a van der Waals fluid and a hard-sphere model. In order to analyze the gas → solid phase transition, we introduce the curve consists of the unperturbed states whose Hugoniot cross the coexistence curve at the triple point. Hereafter we call this curve as C_2^* and the unperturbed state $\mathbf{u}_0 \in C_2^*$ can be expressed as follows:

$$\begin{cases} \tilde{p}_{\mathrm{C}}(\eta_1) = \tilde{p}_{\mathcal{H}}(\eta_1, \tilde{\mathbf{u}}_0), \\ \eta_1 = \eta_{\mathrm{Gtri}} \end{cases} \tag{4.28}$$

with $\tilde{p}_{\mathrm{C}}$ and $\tilde{p}_{\mathcal{H}}$ being the gas/solid coexistence curve given by (4.13) and the gas → gas RH curve, respectively.

If the unperturbed state is in the region delimited by the curve C_2^* and the gas/solid coexistence curve, the Hugoniot curve will cross the coexistence curve, therefore, gas → solid phase transition may occur. Figure 4.7 shows that the typical Hugoniot curve accompanying gas → solid phase transition. From Fig. 4.7, we can see that the unperturbed state is inside the curve C_2^*, the curve $\tilde{C}_{\mathrm{b}}$ and $\tilde{C}_{\mathrm{b}2}$. With the increase of the strength of the shock (the perturbed pressure), the perturbed packing fraction also increase and the phase of the unperturbed state will firstly become from gas phase to gas / solid coexistence phase and to the solid phase. After that, the perturbed density decrease and the phase of the perturbed state becomes from the solid phase to the solid / liquid coexistence and to the liquid phase as the the perturbed pressure increases. From the Liu condition, a shock wave with the perturbed pressure such that $p_0 < p_1 < p_{\mathrm{G}}$ and $p_1 > p_{c(S)}$ is stable while a shock wave with the perturbed pressure such that $p_{\mathrm{G}} < p_1 < p_{c(S)}$ is unstable. We discovered that there exists a compressive upper shock accompanying gas → solid phase transition.

Figure 4.8 shows the other typical Hugoniot curve of compressive lower shock accompanying gas → solid phase transition. From Fig. 4.8, we can see that the unperturbed state is inside the curve C_2^* curve, however, is outside the curve $\tilde{C}_{\mathrm{b}2}$. With the increase of the strength of the shock (the perturbed pressure), the perturbed packing fraction also increase and the phase of the unperturbed state will become from gas phase to gas / solid coexistence phase and to solid phase. From the Liu condition, a shock wave with the perturbed packing fraction such that $\eta_0 < \eta_1 < \eta_{\mathrm{G}}$ and $\eta_1 > \eta_{c(S)}$ is stable while a shock wave with the perturbed packing fraction such that $\eta_{\mathrm{G}} < \eta_1 < \eta_{c(S)}$ is unstable. We can conclude that gas → solid phase transition can also be induced by a compressive lower shock wave.

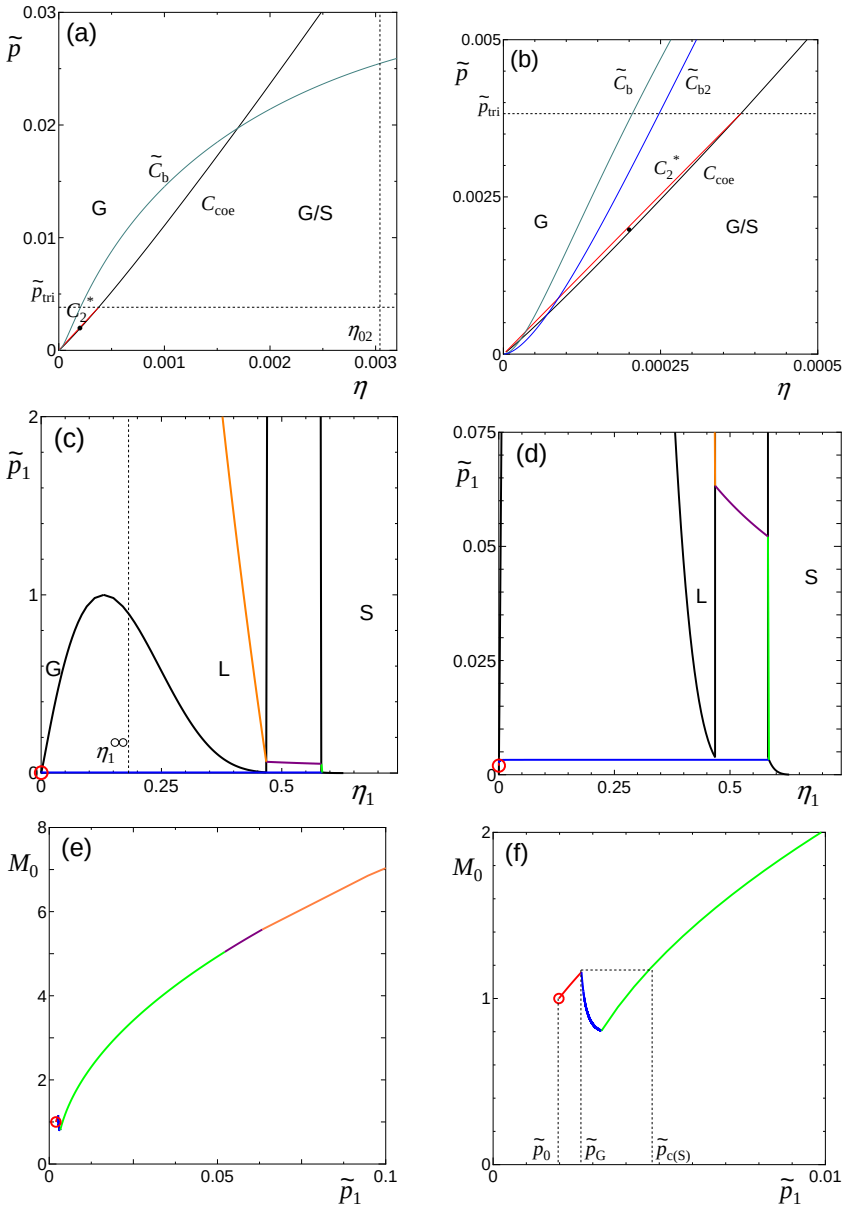

Figure 4.7: (a) The C_2^* curve and $\tilde{C}_b$ curve for $f = 2000$. The gas / solid and gas / liquid coexistence curves C_{coe} are also shown. (b) blowup of the low pressure region in part (a) of the figure. $\tilde{C}_{b2}$ curve is also shown. (c) The RH curves in the $\tilde{p} - \eta$ plane for the unperturbed state ($\eta_0 = 0.0002$, $\tilde{p}_0 = 0.00198$) shown by the mark in the figures (a) and (b). (d) blowup of the low pressure region in part (c) of the figure. (e) The RH curves in the $M_0 - \tilde{p}$ plane for the same unperturbed state. (f) blowup of the low pressure region in part (e) of the figure.

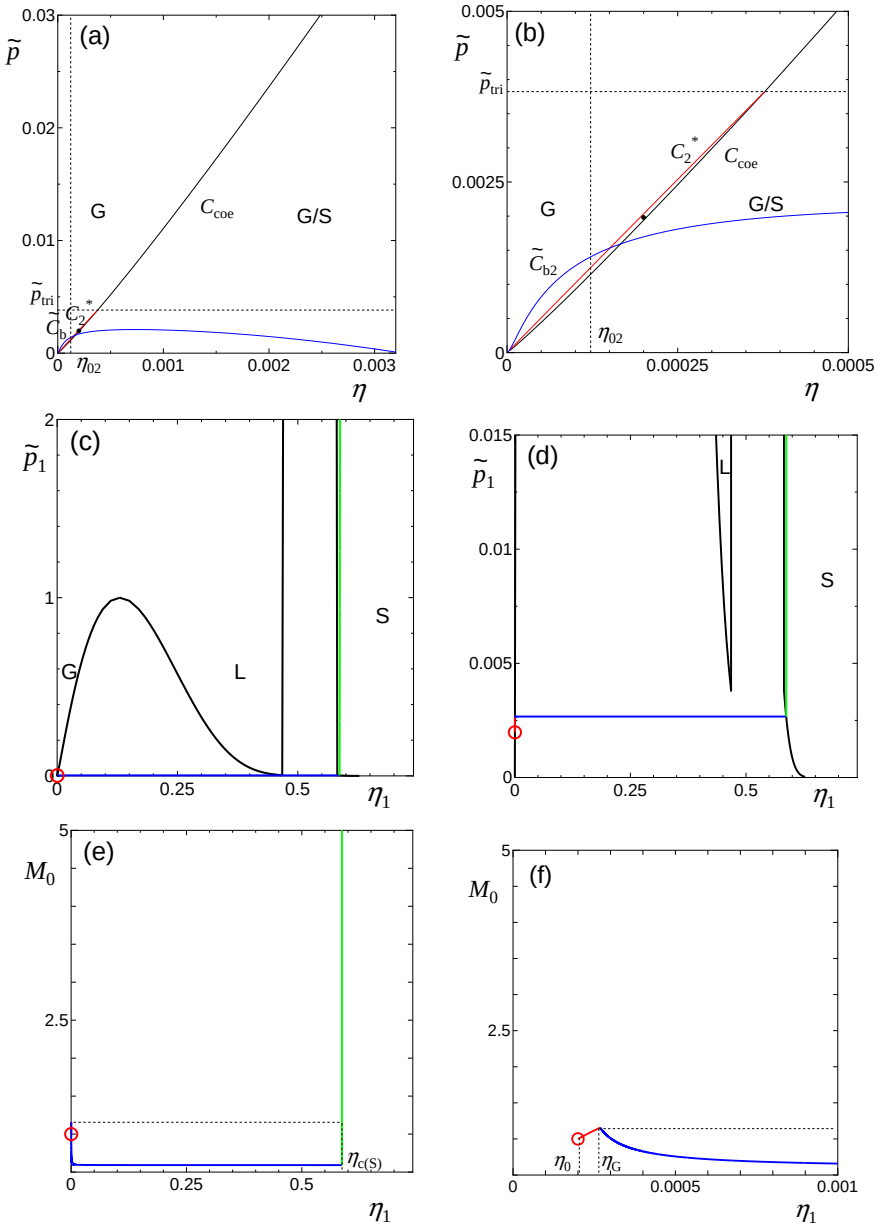

Figure 4.8: (a) The C_2^* curve and $\tilde{C}_{\rm b}$ curve for $f = 50000$. The gas / solid and gas / liquid coexistence curves $C_{\rm coe}$ are also shown. (b) blowup of the low pressure region in part (a) of the figure. $\tilde{C}_{\rm b}$ curve is also shown. (c) The RH curves in the $\tilde{p}-\eta$ plane for the unperturbed state ($\eta_0 = 0.0002$, $\tilde{p}_0 = 0.00198$) shown by the mark in the figures (a) and (b). (d) blowup of the low pressure region in part (c) of the figure. (e) The RH curves in the $M_0 - \eta$ plane for the same unperturbed state. (f) blowup of the low pressure region in part (e) of the figure.

4.5.4 Gas → liquid → solid phase transition

Now we discuss the case that both gas → liquid and liquid → solid phase transitions can be observed as increase of the shock strength. This is also essentially new phenomena which can not be analyzed by both a van der Waals fluid and a hard-sphere system. For observing this kind of shock, both conditions of gas → liquid and liquid → solid phase transitions must be satisfied. These conditions are that the unperturbed state lies in the region delimited by the C^* curve and by the gas / liquid coexistence curve *and* the unperturbed packing fraction is greater than η_{02}

Fig. 4.9 shows the RH curves for $f = 1000$, $\eta_0 = 0.06$, $\tilde{P}_0 = 0.8$, as a typical example of the shock-induced gas → liquid → solid phase transition. From Fig. 4.9, we can see that the unperturbed state satisfy the above-mentioned condition for Gas → liquid → solid phase transition. With the increase of the strength of the shock (the perturbed pressure), the perturbed packing fraction also increase and the phase of the perturbed state will become from the gas phase to the gas / liquid coexistence phase → liquid phase → liquid / solid coexistence phase → solid phase. From the Liu condition, a shock wave with the perturbed packing fraction such that $\eta_0 < \eta_1 < \eta_{\rm G}$, $\eta_{c(L)} < \eta_1 < \eta_{\rm L(S)}$ and $\eta_1 > \eta_{c(S)}$ is stable while a shock wave with the perturbed packing fraction such that $\eta_{\rm G} < \eta_1 < \eta_{c(L)}$ and $\eta_{\rm L(S)} < \eta_1 < \eta_{c(S)}$ is unstable. We can conclude that gas → solid phase transition can also be observed in this case.

4.6 Summary and concluding remarks

From the analysis of the Rankine-Hugoniot conditions based on the system of hard-spheres with attractive force, we have made clear the conditions for the shock-induced phase transitions.

We confirmed that the Rankine-Hugoniot (RH) curves, which are the loci of the unperturbed states satisfying the RH conditions, are qualitatively same as the RH curves obtained in a van der Waals system in the case that shock-induced gas → liquid phase transition occurs. Similarly it was also shown that the RH curves for the present system can explain the RH curves obtained in the hard-sphere system when shock-induced liquid → solid phase transition appears. These facts support the validity of the present analysis based on the present model as a extended version of both of a van der Waals model and a hard-sphere model.

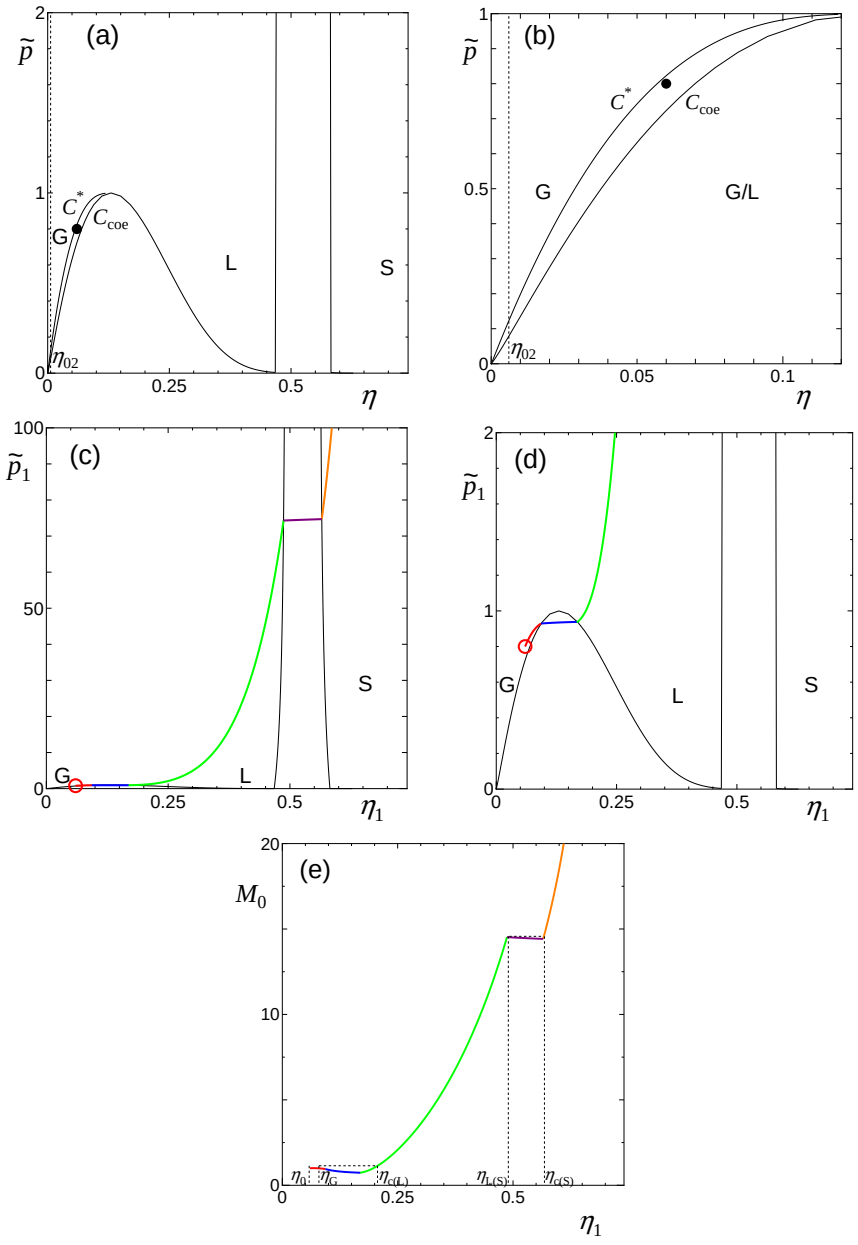

Figure 4.9: (a) The C^* curve and η_{02} curve for $f = 1000$. The gas / solid and gas / liquid coexistence curves $C_{\rm coe}$ are also shown. (b) blowup of the low pressure region in part(a) of the figure. $\tilde{C}_{\rm b}$ curve is also shown. (c) The RH curves in the $\tilde{p} - \eta$ plane for the unperturbed state ($\eta_0 = 0.06$, $\tilde{p}_0 = 0.8$) shown by the mark in the figures (a) and (b). (d) blowup of the low pressure region in part (c) of the figure. (e) The RH curves in the $M_0 - \eta_1$ plane for the same unperturbed state.

In addition to the above-mentioned shock-induced phase transitions, the condition for the gas → solid phase transition has been discussed. In the present model, there exist three phases, namely, gas, liquid and solid phases, therefore, we can also analyze this kind of phase transition. Two possible scenarios of the gas → solid phase transition has been presented. First one is that gas → gas / solid coexistence → solid phase transition are induced as the shock strength increase. Second one is that gas → gas / liquid coexistence → liquid → liquid / solid coexistence → solid phase transition are induced with the increase of the shock strength.

The admissibility of a shock wave was also studied by using the mathematical stability condition, namely, the Liu condition. It is shown that the shock waves may admissible even if gas → solid phase transition is induced by shock waves. Therefore, we can conclude that a shock wave can induce the gas → solid phase transition in the present model and the both scenarios are acceptable.

Lastly let us summarize the concluding remarks as follows:

(I) Concerning the observation of gas → solid phase transition, the required number of internal degrees of freedom are different between the first scenerio and the second scenerio. The first scenario needs aroud 2,000 internal degrees of freedom, however, the second scenario needs only around 20 internal degrees of freedom. Within the analysis based on the present model, we can conclude that the second scenerio is more hopeful for observation by experiments.

(II) Heretofore we adopted the polytropic models where the specific heat with constant volume is constant. For the next step, we can construct more realistic model by introducing the non-polytropic effect to the present model. The shock waves in a non-polytropic hard-sphere system will be analyzed in the next chapter [91].

Chapter 5

Shock waves in a non-polytropic hard-sphere system

5.1 Introduction

Shock-induced phase transitions in a hard-sphere system were studied in detail [83, 84] by adopting a special caloric equation of state (*P-model* below). The *P-model* is characterized by the caloric equation of state (the thermal equation of state is shown in the next section):

$$e = \frac{k_B T}{2m}(3 + f), \tag{5.1}$$

where e is the specific internal energy, k_B is the Boltzmann constant, T is the absolute temperature, m is the mass of a particle and the constant f corresponds to the internal degrees of freedom of a particle. In the derivation of Eq. (5.1), we have assumed that all the excited internal modes satisfy the equipartition law of energy in classical statistical mechanics. As a consequence the specific heat at fixed volume c_V is constant and the system is polytropic.

Zhao et al. [83] studied shock-induced phase transitions in a hard-sphere system with the caloric equation of state (5.1) with no internal degree of freedom, that is, $f = 0$. The Rankine-Hugoniot (RH) conditions and the admissibility (stability) of a shock wave are analyzed and classified explicitly.

In Chap. 2, we made a similar analysis of a system of hard spheres with internal degrees of freedom [84]: $f > 0$. The important role of the internal motions in the shock-induced phase transitions is quantitatively made clear. It is also shown that, due to the effect of non-zero f, a new type of instability of shock waves can exist.

Although many interesting facts are newly found, the validity range of these analyses basing on the *P-model* is limited due to the assumption of the equipartition

law of energy, which is satisfied for a system in a high temperature. The order of magnitude of the characteristic temperature for internal rotational modes of a molecule is 10^2K while that for internal vibrational modes is 10^3K. If we want to study the shock wave phenomena in a wider temperature range, for example, from a room temperature to the temperature above 10^3K, a more realistic model that can describe the excitation process of the internal modes depending on the temperature is mandatory.

To this end, we adopt the *NonP-model* with the caloric equation of state [80]:

$$e = \frac{k_B T}{m}\left(\frac{3+I_r}{2} + \sum_{i=1}^{I_v} \frac{T_i/T}{\exp(T_i/T)-1}\right), \tag{5.2}$$

where I_r is the degrees of freedom for the internal rotational modes of a molecule, I_v is that for the internal vibrational modes, and T_i is the characteristic temperature of the i-th vibrational mode. Here the contribution to e from the vibrational modes is temperature-dependent, while that from the rotational modes is assumed to be temperature-independent for simplicity. The specific heat c_V is now temperature-dependent and the system is non-polytropic. In the high-temperature limit, the *NonP-model* approaches the *P-model* with $f = I_r + 2I_v$.

Shock wave phenomena in non-polytropic gases, such as in a van der Waals gas, have been extensively studied, see for example [92]. However, few studies have been made for shock-induced phase transitions in a non-polytropic system.

The purpose of the present chapter is, through analyzing a simple model, to demonstrate explicitly the importance of the non-polytropic effect on the shock-induced phase transitions, especially on the RH conditions and on the admissibility of a shock wave [91] .

5.2 Non-polytropic hard-sphere system and Rankine-Hugoniot conditions

In order to grasp the essential feature of the non-polytropic effect, we adopt a simplified *NonP-model* by assuming that all vibrational modes possess a common characteristic temperature T^*: $T_1 = T_2 = \cdots = T_{I_v} = T^*$.

The caloric and thermal equations of state are, respectively, expressed by

$$\begin{aligned} e &= \frac{k_B T}{m}\left(\frac{3+I_r}{2} + I_v \frac{T^*/T}{\exp(T^*/T)-1}\right), \\ \frac{p\omega_0}{k_B T} &= \eta\Gamma(\eta), \end{aligned} \tag{5.3}$$

where p is the pressure and η ($= \rho\omega_0/m$) is the packing fraction with ρ being the mass density and ω_0 the volume of a hard sphere. For definiteness, we adopt $I_r = 2$ hereafter. The function $\Gamma(\eta)$ for liquid phase and solid phase is given by [80, 82]:

$$\begin{aligned} \Gamma^L(\eta) &= 1 + \frac{4\eta + 1.016112\eta^2 + 1.109056\eta^3}{1 - 2.245972\eta + 1.301008\eta^2}, \\ \Gamma^S(\eta) &= 1 + \frac{1}{(\sqrt{2}\pi/(6\eta))^{1/3} - 1}, \end{aligned} \tag{5.4}$$

where superscripts L and S stand for the liquid phase and solid phase, respectively.

It is worth noting that we can easily show that the caloric equation of state $(5.3)_1$ is thermodynamically compatible to the thermal equation of state $(5.3)_2$ that is valid for both *P-model* and *NonP-model* by checking the integrability condition.

Let us analyze a one-dimensional problem of a shock wave with the propagation speed s, which divides the space into two subspaces. The state before the shock (unperturbed state) is denoted by $\mathbf{u}_0$ and the state after the shock (perturbed state) by $\mathbf{u}_1$, where $\mathbf{u} \equiv (\rho, \varrho v, \varrho e + \varrho v^2/2)$ with v being the flow velocity. Hereafter the same meaning of the suffixes 0 and 1 as above will be assumed. It is convenient to introduce the dimensionless quantities:

$$\begin{gathered} \hat{\eta} = \frac{\eta}{\eta_0}, \quad \hat{p} = \frac{p}{p_0}, \quad \hat{T} = \frac{T}{T_0}, \quad \hat{v} = \frac{v}{c_0}, \\ \hat{e} = \frac{e}{k_B T_0/m}, \quad \hat{c} = \frac{c}{\sqrt{k_B T_0/m}}, \quad \hat{c}_V = \frac{c_V}{k_B/m}, \end{gathered}$$

where $c = \sqrt{(\partial p/\partial \rho)_S}$ is the sound speed with S being the specific entropy.

As is well-known, besides the usual contact shock, the RH conditions, which are derived from the Euler equations and the constitutive Eq. (5.3), admit the following solution:

$$\begin{aligned} \hat{v}_1 &= M_0(1 - \frac{1}{\hat{\eta}_1}), \\ \hat{p}_1 &= 1 + \hat{c}_0^2 M_0^2 \frac{\hat{\eta}_1 - 1}{\Gamma(\eta_0)\hat{\eta}_1}, \\ M_0 &= \frac{\hat{\eta}_1}{\hat{c}_0(\hat{\eta}_1 - 1)} \sqrt{2\left(\hat{e}_1 - \hat{e}_0 - \Gamma(\eta_0)\frac{\hat{\eta}_1 - 1}{\hat{\eta}_1}\right)}, \end{aligned} \tag{5.5}$$

where $M_0 = (s - v_0)/c_0)$ is the unperturbed Mach number. Here shock waves are restricted to those with $M_0 > 0$ such that it propagates, say, along the positive x-direction. We have assumed in the above solution that $v_0 = 0$ without any loss of generality due to the Galilean invariance.

In order to study shock-induced phase transitions, it is necessary to adopt an

unperturbed state in the liquid phase [83, 84]. Therefore $\Gamma(\eta_0) = \Gamma^L(\eta_0)$ and

$$\begin{aligned} \hat{e}_0 &= \frac{3+I_r}{2} + I_v \frac{\hat{T}^*}{\exp[\hat{T}^*]-1}, \\ \hat{c}_0 &= \sqrt{\frac{\Gamma(\eta_0)^2}{\hat{c}_{V0}} + \Gamma(\eta_0) + \eta_0 \left(\frac{\partial \Gamma(\eta)}{\partial \eta}\right)_{\eta=\eta_0}}, \end{aligned} \tag{5.6}$$

where

$$\hat{c}_{V0} = \frac{3+I_r}{2} + I_v \frac{\hat{T}^{*2}\exp[\hat{T}^*]}{(\exp[\hat{T}^*]-1)^2}.$$

On the other hand, the perturbed state may be any one of liquid state, solid state, or liquid/solid-coexistence (L/S) state. The dimensionless specific internal energy of a perturbed state can be expressed, irrespective of its phase, by

$$\hat{e}_1 = \frac{3+I_r}{2}\hat{T}_1 + I_v \frac{\hat{T}^*}{\exp[\hat{T}^*/\hat{T}_1]-1}. \tag{5.7}$$

The relationship between $\hat{T}_1$ and $\hat{p}_1$ is as follows: If the perturbed state is a liquid or solid state,

$$\hat{T}_1 = \frac{\hat{p}_1 \Gamma^L(\eta_0)}{\hat{\eta}_1 \Gamma(\eta_1)|_{\eta_1=\hat{\eta}_1\eta_0}} \tag{5.8}$$

with $\Gamma(\eta_1) = \Gamma^L(\eta_1)$ (see Eq. $(5.4)_1$) for a liquid state and $\Gamma(\eta_1) = \Gamma^S(\eta_1)$ (see Eq. $(5.4)_2$) for a solid state. While if the perturbed state is a L/S state,

$$\hat{T}_1 = \frac{\hat{p}_1 \Gamma^L(\eta_0)}{\hat{\eta}_L \Gamma^L(\eta_L)} = \frac{\hat{p}_1 \Gamma^L(\eta_0)}{\hat{\eta}_S \Gamma^S(\eta_S)}, \tag{5.9}$$

where $\eta_L (\approx 0.4946)$ and $\eta_S (\approx 0.5564)$ are, respectively, the packing fractions at the freezing point and at the melting point [83].

Inserting Eq. (5.6), (5.7) and (5.8) (or (5.9)) into Eq. (5.5), we obtain a one-parameter family of solutions for $\hat{v}_1$, $\hat{p}_1$, $\hat{T}_1$ and M_0 in terms of $\hat{\eta}_1$ for given unperturbed state and $\hat{T}^*$.

5.3 Shock-induced phase transitions

From the solution of the RH conditions in the preceding section, we obtain RH curves in $M_0 - \eta_1$ plane as shown in Figs. 5.1, 5.2 and 5.3. If the perturbed state is a liquid state, the shock wave is called liquid-liquid shock wave ($L \to L$). In a similar way, for the other two possibilities, we call liquid-liquid/solid coexistence shock wave ($L \to L/S$) and liquid-solid shock wave ($L \to S$).

5.3.1 Crossover effect on the shock-induced phase transitions

Typical RH curves are shown in Fig. 5.1 where **NonP** is the RH curve based on the *NonP-model* in the last section, the RH curves $\mathbf{P}_\alpha$ and $\mathbf{P}_\beta$ are based on the *P-model* with $f = I_r$ and $f = I_r + 2I_v$, respectively. Here we assume $I_v = 20$, $\hat{T}^* = 30$ and $\eta_0 = 0.2$.

Because of the condition $T^* >> T_0$ in the case of Fig. 5.1, we can observe the following *crossover* of the RH curve **NonP** from $\mathbf{P}_\alpha$ to $\mathbf{P}_\beta$: For weak shocks, the role of vibrational modes in both unperturbed and perturbed states is negligible, therefore **NonP** is nearly the same as $\mathbf{P}_\alpha$. With the increase of the shock strength η_1, the perturbed temperature increases and the vibrational modes in a perturbed state are gradually excited. The RH curve **NonP**, therefore, starts to deviate from $\mathbf{P}_\alpha$. Lastly, in the strong shock limit, the perturbed temperature becomes high enough for all vibrational modes to be fully excited satisfying the classical equipartition law of energy. Therefore, **NonP** approaches $\mathbf{P}_\beta$ asymptotically.

Such a crossover may have a dramatic effect on the shock-induced phase transitions. For example, from Fig. 5.1, we notice that, although $\mathbf{P}_\alpha$ has only the possibility $L \to L$ with no phase transition, **NonP** has the $L \to L/S$ and $L \to S$ regions of the RH curve in addition to the region $L \to L$, which, of course, indicates the appearance of a shock-induced phase transition.

Therefore we obtain the new fact that the non-polytropic effect on the existence of the shock-induced phase transitions becomes to be essential in some cases.

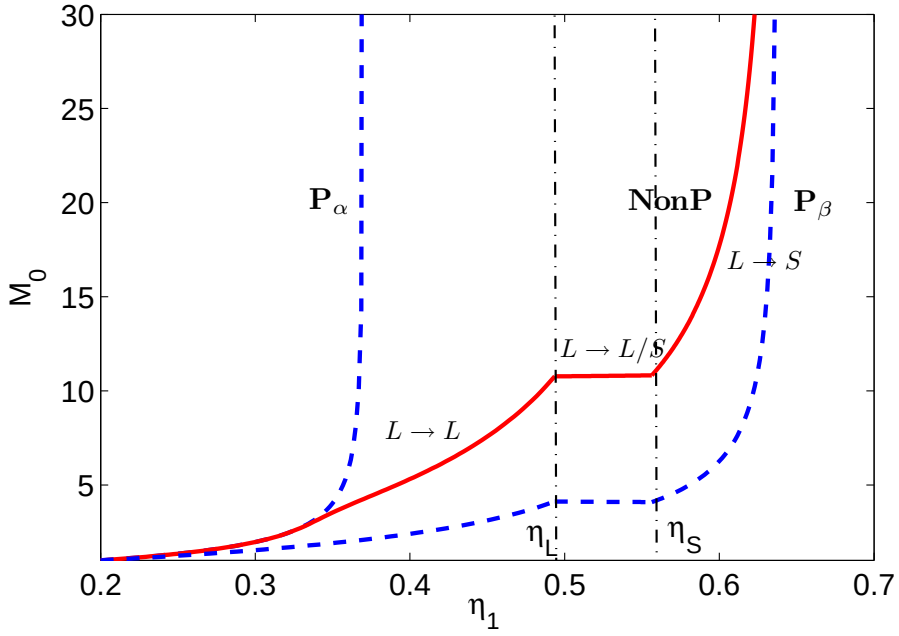

Figure 5.1: Three typical Rankine-Hugoniot curves in $M_0 - \eta_1$ plane: **NonP** (solid curve) is based on the *NonP-model* with $I_v = 20$ and $\hat{T}^* = 30$. $\mathbf{P}_\alpha$ and $\mathbf{P}_\beta$ (dashed curve) are based on the *P-model* with $f = I_r$ and $f = I_r + 2I_v$, respectively. The unperturbed packing fraction $\eta_0 = 0.2$ for all RH curves. $\eta_L (\approx 0.4946)$ and $\eta_S (\approx 0.5564)$ are, respectively, the packing fractions at the freezing and melting points.

5.3.2 Mach number at the shock-induced phase transition

The typical dependence of the RH curve **NonP** on the dimensionless temperature $\hat{T}^*$ is shown in Fig. 5.2. We can see clearly that the Mach number at the beginning of the shock-induced phase transition changes prominently with the change of the temperature $\hat{T}^*$.

Therefore we have just obtained another new fact that the non-polytropic effect on the Mach number at the beginning of the shock-induced phase transition becomes to be important in some cases like the case in Fig. 5.2. In fact, the threshold of Mach number for inducing phase transition increases monotonously with the increase of dimensionless vibrational characteristic temperature $\hat{T}^*$.

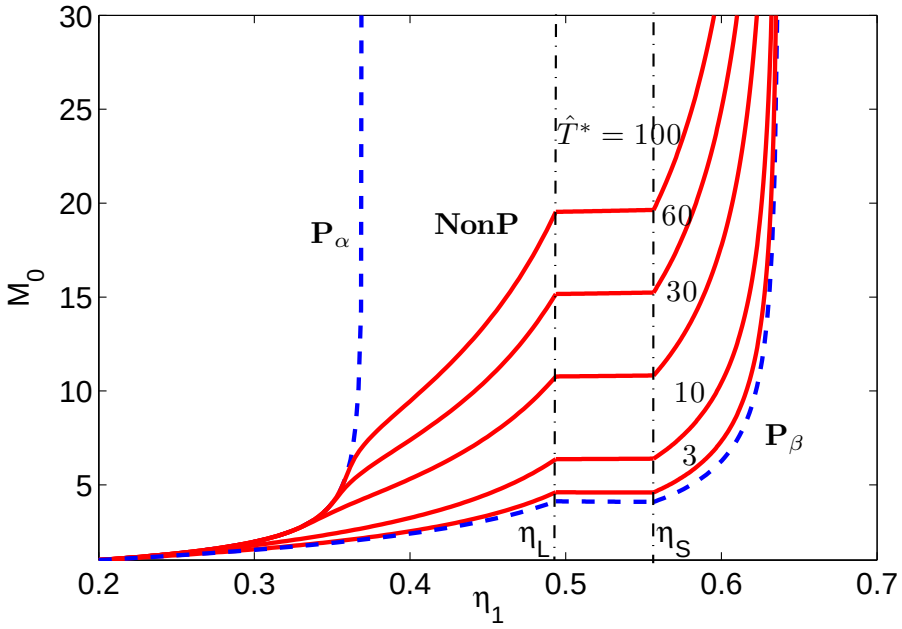

Figure 5.2: Typical dependence of the Rankine-Hugoniot curve **NonP** (solid curve) on the dimensionless temperature $\hat{T}^*$. $\mathbf{P}_\alpha$ and $\mathbf{P}_\beta$ (dashed curve) are the RH curves based on the *P-model* with $f = I_r$ and $f = I_r + 2I_v$, respectively. $I_v = 20$. $\eta_0 = 0.2$ for all RH curves.

5.4 Admissibility of shock waves

Let us study the non-polytropic effect on the *admissibility* (*stability*) of shock waves. It is well-known that not all the shock waves that correspond to the solutions of the RH conditions are admissible and that the Liu condition [44–46] should be satisfied in order that an initial shock can be stable and then can propagate.

The Liu condition asserts that a shock wave is admissible if and only if its velocity of propagation is not decreasing as we move on the RH curve starting from the unperturbed state, $\mathbf{u}_0$, towards a given perturbed state, $\mathbf{u}_1$:

$$s\left(\mathbf{u}_0, \tilde{\mathbf{u}}\right) \leq s\left(\mathbf{u}_0, \mathbf{u}_1\right) \qquad \forall \tilde{\mathbf{u}} \in \text{RH curve through } \mathbf{u}_0.$$

If the Liu conditions are not satisfied, the shock will become unstable.

The non-polytropic effect on the admissibility can be demonstrated by a typical example shown in Fig. 5.3 where we plot instead of s equivalently, M_0 as function of the strength of the shock parameter η_1. Three **NonP** curves with three different values of the characteristic temperature $\hat{T}^* = 10,\ 25,\ 60$ and the corresponding $\mathbf{P}_\beta$ curve are shown. Here we assume that $I_v = 50$, and $\eta_0 = 0.4$ for all RH curves.

The admissible regions of these RH curves are drawn by solid curves, while the inadmissible regions by dashed curves.

Remarkable points in Fig. 5.3 are summarized as follows:

(i) With the increase of the shock parameter η_1 along $\mathbf{P}_\beta$ starting from the unperturbed state with η_0, the state of an admissible shock moves in the region $L \to L$, and then jumps to the state in the region $L \to S$. Afterward it moves in the region $L \to S$ until the strong shock limit. All part of the region $L \to L/S$ and a part of $L \to S$ near the melting point η_S are in admissible.

(ii) The feature of **NonP** with $\hat{T}^* = 10$ is qualitatively the same as that of $\mathbf{P}_\beta$.

(iii) The feature of **NonP** with $\hat{T}^* = 25$ is qualitatively the same as that of $\mathbf{P}_\beta$ except that the part of the region $L \to L/S$ near the freezing point η_L now becomes to be admissible.

(iv) Whole part of the RH curve **NonP** with $\hat{T}^* = 60$ is admissible. We can show that this is true if T^* is big enough.

To sum up the non-polytropic effect on the admissibility of a shock wave plays again an important role in some cases like the case in Fig. 5.3.

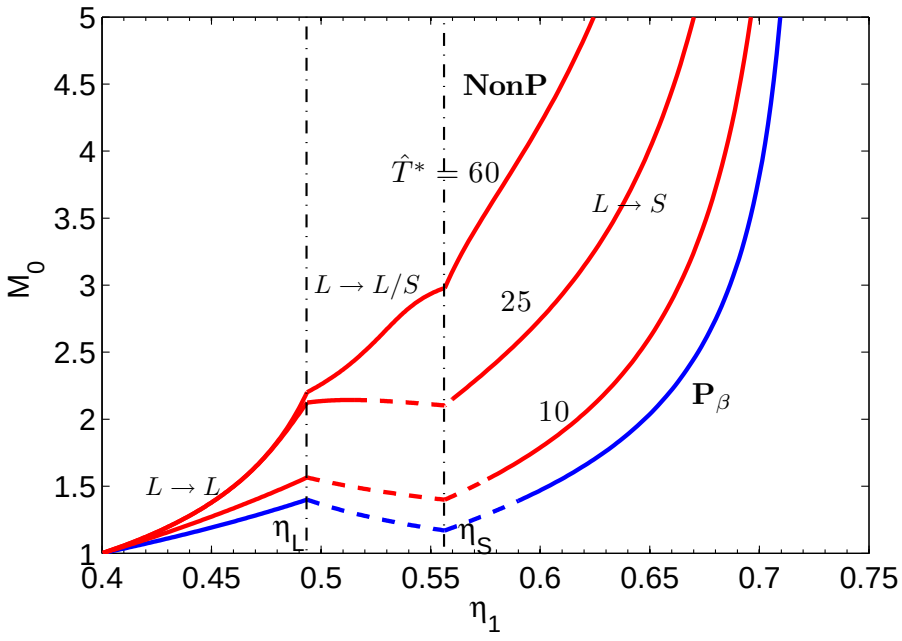

Figure 5.3: The admissible (solid line) and inadmissible (dashed line) regions for a shock wave in three RH curves of **NonP** with three different values of the characteristic temperature $\hat{T}^* = 10,\ 25,\ 60$ and the corresponding RH curve $\mathbf{P}_\beta$. $I_v = 50$. $\eta_0 = 0.4$ for all RH curves.

5.5 Conclusions

In this chapter, we analyzed the shock-induced phase transitions, especially the RH conditions and the admissibility condition in a non-polytropic hard-sphere system by adopting the simplified caloric equation of state. We have succeeded to grasp the essential feature of the non-plytropic effect on the phase transitions. The effect becomes to be more evident with the increase of $\hat{T}^*$, that is, the ratio between the characteristic temperature $T^*$of the vibrational modes and the unperturbed temperature T_0.

The present analysis can easily be extended to the analyses of the models with more realistic spectra of the internal vibrational modes which are useful for experimentalists. Result of such analyses will be reported soon.

Chapter 6

Summary and concluding remarks

In this thesis we constructed the framework of realistic model of condensed matters and by using that model, we studied real-gas effects on shock wave phenomena. In order to construct such framework, we propose the following strategy with two steps:

(i) We study shock wave phenomena in a hard-sphere system which is a good reference system of materials in liquid state.

(ii) By using all the results obtained in step (i) and by using the perturbation method developed in the theory of liquid-state physics, we study shock wave phenomena in physical systems with more realistic interatomic potential with both repulsive and attractive parts.

In Chap. 1, the applications of shock wave phenomena are summarized. It was pointed out there exist shock wave phenomena which can not be explained even qualitatively within the well-known framework of the ideal-gas model. The effects inducing such differences are called as the real-gas effects on shock wave phenomena. The typical phenomena due to the real-gas effects are shock-induced phase transitions, shock splitting phenomena and rarefaction (negative) shock waves.

In Chap. 2, we analyzed the shock waves in a polytropic hard-sphere system with and without internal degrees of freedom as a direct consequence of the previous study for a hard-sphere system. We made clear the crucial role of internal degrees of freedom on the shock-induced phase tranition from liquid phase to solid phase transition and on the admissibility of a shock wave. The complete classification of shock wave phenomena were made from the point of view of the admissibility of a shock wave. It was shown that another type of instability of a shock wave can exist even though the perturbed state is thermodynamically stable. Numerical

calculations have been performed in order to confirm the theoretical results in the case of admissible shocks and to obtain the actual evolution of the wave profiles in the case of inadmissible shocks (shock splitting phenomena).

In Chap. 3, we analyzed the new type of compressive shock wave in a van der Waals fluid which can be regarded as the simplified model of a system of hard-spheres with attractive force. This shock has a quite unusual property that when the perturbed pressure (the pressure after a shock) increases, the perturbed density decreases and tends to a limit value from above, in contrast with the ordinary well-known compressive shock in which the density tends to the limit value from below. The admissibility of a shock wave was also analyzed based on the Liu condition and we showed that this unusual shock wave can exist. The condition for this new kind of shock wave phenomena was made clear in terms of the unperturbed pressure, the unperturbed density and the internal degrees of freedom. We also pointed out the suitable parameter for the experimentalist.

In Chap. 4, we analyzed the shock waves in a system of hard-spheres with attractive force. By using this model, we can analyze shock wave phenomena in the three phases, namely, gas, liquid and solid phase, in the unified way. We confirmed that the analysis of shock wave phenomena in this model can explain the phenomena obtained in a van der Waals model and can also explain the phenomena predicted by a hard-sphere system. We analyzed the possibility of the shock-induced phase transitions. Especially it is clearly shown that the phase transition from gas phase to solid phase can be induced by a shock wave and two scenarios of such phase transitions were presented.

In Chap. 5, we analyzed the shock waves in a non-polytropic hard-sphere system where heat capacity depends on the temperature. We showed that this temperature dependence may affect on the admissibility of a shock wave strongly. The effect becomes to be more evident with the increase of the ratio between the characteristic temperature of the vibrational modes and the unperturbed temperature.

In Chap. 6, which is the present chapter, we present the summary and concluding remarks.

Lastly let us summarize the concluding remarks as follows:

(I) The usefulness of the series of the present studies is shown clearly. We have constructed the theoretical framework of the studies of shock wave phenomena in condensed matters and therefore we can also construct more realistic models by

introducing more detailed interatomic potential as the sequel to the present studies in order to make our theoretical predictions more precise.

(II) Only shock-induced phase transition from liquid phase to solid phase can be observed in the present model. Inverse transition can never be observed. It should be emphasized that this does not mean that there are no phase transitions in a solid under shock compression [9, 49–51, 53–60, 62]. We expect that these shock-induced phase transitions may be explained within the framework of more realistic models by using our strategy.

(III) We have concentrated on the conditions for typical real-gas effects on shock wave phenomena. The detailed analysis and the classification are still remained as the future subjects. For example, when shock splitting phenomena can be observed, the classification of the wave profiles remains for future subject.

(IV) We have discovered the new type of shock wave phenomena, that is, the compressive upper shock wave, in a van der Waals fluid in Chap. 3. This shock wave can also be observed in more realistic system consisted of hard-spheres with attractive force. Therefore we can conclude that the compressive upper shock wave is not restricted in the particular model and that this shock wave is another typical real-gas effect on shock wave phenomena.

(V) The theoretical studies of the shock structures in real gases also remained as the future subject. It is known that the theoretical prediction by the Navier-Stokes and Fourier theory is not valid for strong shock waves and new theories which have larger validity ranges are needed. The extended thermodynamics (ET) is the one of such theories. Until now the validity of ET has been confirmed only in rarefied gases. We expect that the shock structures in real gases can provide us useful information for the development of ET.

(VI) In this thesis the effects of chemical reactions were neglected and only planar shock waves were analyzed for simplicity. The detonation shock waves and the dimensionality dependence of shock wave phenomena also remain as future subjects.

Acknowledgement

The present study has been carried out at Department of Scientific and Engineering Simulation, Nagoya Institute of Technology, Japan.

The author wishes to express his deepest thanks to his supervisor, Professor Masaru Sugiyama (Nagoya Institute of Technology), for the genuine encouragement and the invaluable advice through the present study and all his studies.

The author also sincerely appreciates Professor Toshiyuki Gotoh (Nagoya Institute of Technology), Professor Shuji Ogata (Nagoya Institute of Technology) and Professor Hiroaki Nakamura (NationalInstitute for Fusion Science) who provide him with constructive guidance during the discussion of this work.

The author would like to thank his collaborators, Professor Tommaso Ruggeri (Research Center of Applied Mathematics, University of Bologna, Italy), Professor Zhao Nanrong (Sichuan University, People's Republic of China) and Doctor Andrea Mentrelli (Research Center of Applied Mathematics, University of Bologna, Italy), for their essential contributions to the present study.

The author thanks Mr. Kaname Motoshita and all members of Sugiyama laboratory for their kind help.

The author wishes to express his hearty thanks to his wife, parents and all of his family members for continuous encouragement and their warm understanding.

The present study was partially supported by Japan Society of Promotion of Science (JSPS) No. 08J08281.

References

[1] G. Ben-dor, O. Igra and T. Elperin (Eds.), *Handbook of shock waves* Vol.1 Theoretical, Experimental, and Numerical Techniques, Academic Press, (2001).

[2] G. Ben-dor, O. Igra and T. Elperin (Eds.), *Handbook of shock waves* Vol.2 Shock Wave Interactions and Propagation, Academic Press, (2001).

[3] G. Ben-dor, O. Igra, T. Elperin and A. Lifshitz (Eds.), *Handbook of shock waves* Vol.3 Chemical Reactions in Shock Waves and Detonations, Academic Press, (2001).

[4] I. Müller and T. Ruggeri, *Rational extended thermodynamics*, Springer-Verlag, New York, (1998).

[5] S. Chapman and T. G. Cowling, *The mathematical theory of non-uniform gases*, Cambridge University Press, Cambridge, (1970).

[6] H. Struchtrup, *Macroscopic transport equations for rarefied gas flows, Approximation methods in kinetic theory*, Springer-Verlag, Berlin, Heidelberg (2005).

[7] G. B. Whitham, *Linear and nonlinear waves*, John Wiley and Sons, New York, (1974).

[8] C. Dafermos, *Hyperbolic Conservation Laws in Continuum Physics*, 3rd Edition, Springer Verlag, Berlin Heidelberg (2010).

[9] G. E. Duvall and R. A. Graham, Rev. Mod. Phys. **49**, 523 (1977).

[10] J. R. Asay and M. Shahinpoor (Eds.), *High-pressure shock compression of solids*, Springer-Verlag, New York, (1992).

[11] R. A. Graham, *Solids under high-pressure shock compression, Mechanics, Physics, and Chemistry*, Springer-Verlag, New York, (1992).

[12] A. B. Sawaoka (Eds.), *Shock waves in materials science*, Springer-Verlag, Tokyo, (1993).

[13] L. Davison, D. Grandy and M. Shahinpoor (Eds.), *High-pressure shock compression of solids II*, Springer-Verlag, New York, (1996).

[14] L. Davison and M. Shahinpoor (Eds.), *High-pressure shock compression of solids III*, Springer-Verlag, New York, (1997).

[15] L. Davison, Y. Horie and M. Shahinpoor (Eds.), *High-pressure shock compression of solids IV*, Springer-Verlag, New York, (1997).

[16] L. Davison, Y. Horie and T. Sekine (Eds.), *High-pressure shock compression of solids V*, Springer-Verlag, New York, (2002).

[17] Y. Horie, L. Davison and N. N. Thadhani (Eds.), *High-pressure shock compression of solids VI*, Springer-Verlag, New York, (2002).

[18] V. E. Fortov, L. V. Al'tshuler, R. F. Trunin and A. I. Funtikov (Eds.), *High-pressure shock compression of solids VII*, Springer-Verlag, New York, (2003).

[19] E. Jouguet, La Science aerienne **3**, 138 (1934).

[20] L. D. Landau and E. M. Lifshitz, *Fluid mechanics*, Pergamon Press, London, Second Edition (1987).

[21] L. E. Henderson, "General laws for propagation of shock waves through matter", in Handbook of Shock Waves, Vol. 1 - Theo- retical, Experimental, and Numerical Techniques, edited by G. Ben-Dor, O. Igra, and T. Elperin (Academic Press, 2001) pp. 143 - 183.

[22] H. M. Mott-Smith, Phys. Rev. **82**, 885 (1951).

[23] D. Gilbarg and D. Paolucci, J. Rat. Mech. Anal. **2**, 617 (1953).

[24] P. K. Khosla, J. Eng. Math. **3**, 289 (1969)

[25] T. Ruggeri, Phys. Rev. E **47**, 4135 (1993).

[26] W. Weiss, Phys. Rev. E **52**, R5760 (1995).

[27] T. Ruggeri, Transport Theory and Stat. Phys. **25**, 567 (1996).

[28] Guy Boillat and Tommaso Ruggeri, Continuum Mech. Thermodyn. **10**, 285 (1998).

[29] O. G. Buzykln, V. S. Galkin and V. I. Nosik, Fluid Dynamics **33**, 433 (1998).

[30] F. J. Uribe, M. Torrilhon and W. Weiss, Phys. Rev. Lett. **81**, 2044 (1998).

[31] Y. G. Ohr, Phys. Fluids **13**, 2105 (2001).

[32] J. D. Au, M. Torrilhon and W. Weiss, Phys. Fluids **13**, 2423 (2001).

[33] M. Torrilhon and H. Struchtrup, J. Fluid Mech. **513**, 171 (2004).

[34] W. Griffith, D. Brickl and V. Blackman, Phys. Rev. **102**, 1209 (1956).

[35] M. Linzer and D. F. Hornig, Phys. Fluids **12** 1661 (1963).

[36] H. Alsmeyer, J. Fluid. Mech. **74**, 497 (1976).

[37] J. W. Swegle D. E. Grady, J. Appl. Phys. **58**, 692 (1985).

[38] W. G. Hoover, Phys. Rev. Lett. **42**, 1531 (1979).

[39] B. L. Holian, W. G. Hoover, B. Moran and G. K. Straub, Phys. Rev. A **22**, 2798 (1980).

[40] E. Salomons and M. Mareschel, Phys. Rev. Lett. **69** 269 (1992).

[41] S. I. Anisimov, V. V. Zhakhovskii and V. E. Fortov, JETP Lett. **65**, 755 (1997).

[42] V. V. Zhakhovskii, K. Nishihara, S. I. Anisimov, JETP Lett. **66**, 99 (1997).

[43] P. D. Lax, Comm. Pure Appl. Math. **10**, 537 (1957).

[44] T.-P. Liu, J. Math. Anal. Appl. **53**, 78 (1976).

[45] T.-P. Liu, Memoir, American Mathematical Society **240**, 12 (1981).

[46] T.-P. Liu and T. Ruggeri, Acta Mathematicae Applicatae Sinica, English Series **1**, 1 (2003).

[47] G. E. A. Meier: *Liquefaction shock waves. In Shock Wave Science and Technology Reference Library, Vol. 1. Multiphase Flows I* (Ed. M. E. H. van Dongen), Chap. 7, pp. 231-267, Springer, Berlin Heidelberg, (2007).

[48] A. Matsuda, K. Kondo and K. G. Nakamura, J. Chem. Phys. **124**, 054501 (2006).

[49] C. S. Yoo, N. C. Holmes, M. Ross D. J. Webb and C. Pike, Phys. Rev. Lett. **70**, 3931 (1993).

[50] C. Dai, X. Jin, X. Zhou, J. Liu and J. Hu, J. Phys. D: Appl. Phys. **34**, 3064 (2001).

[51] R. S. Hixson and J. N. Fritz, Phys. Rev. Lett. **62**, 637 (1989).

[52] M. Woo and I. Greber, AIAA J. **37**, 215 (1999).

[53] A. B. Belonoshko, Science **275**, 955 (1997).

[54] J. W. Jeong, I. Lee and K. J. Chang, Phys. Rev. B **59**, 329 (1999).

[55] J. W. Jeong and K. J. Chang, J. Phys. Condens. Matter **11**, 3799 (1999).

[56] S. N. Luo, T. J. Ahrens, T. Çağin, A. Strachan, W. A. Goddard III and D. C. Swift, Phys. Rev. B **68**, 134206 (2003).

[57] K. Kadau, T. C. Germann, P. S. Lomdahl, B. L. Holian, Science **296**, 1681 (2002).

[58] S. N. Luo, T. J. Ahrens, Phys. Earth and Planetary Interiors **143-144**, 369 (2004).

[59] L. V. Al'tshuler, Zh. Prikl. Mekh. Tekh. Fiz. **4**, 93 (1978).

[60] M. Ross, Phys. Rev. A **8**, 1466 (1973).

[61] P. A. Thompson, "Liquid-vapor adiabatic phase changes and related phenomena", in *Nonlinear Waves in Real Fluids*, edited by A. Kluwick (Springer, 1991) Chap. 6, pp. 147 - 213.

[62] D. G. Morris, J. Appl. Phys. **51**, 2059 (1980).

[63] P. A. Thompson and K. C. Lambrakis, J. Fluid Mech. **60** 187 (1973).

[64] C. Zamfirescu, A. Guardone, and P. Colonna, "Admissibility region for rarefaction shock waves in dense gases", J. Fluid Mech. **599**, 363 (2008).

[65] A. Guardone, C. Zamfirescu, and P. Colonna, "Maximum intensity of rarefaction shock waves for dense gases", J. Fluid Mech. **642**, 127 (2010).

[66] A. A. Borisov, AL. A. Borisov, S. S. Kutateladze, and V. E. Nakoryakov, J. Fluid Mech. **126**, 59 (1983).

[67] S. S. Kutateladze, V. E. Nakoryakov, and A. A. Borisov, "Rarefaction waves in liquid and gas-liquid media", Annual Review of Fluid Mechanics **19**, 577 (1987).

[68] A. Kluwick, "Rarefaction shocks", in Handbook of Shock Waves, Vol. 1. Theoretical, Experimental, and Numerical Techniques, edited by G. Ben-Dor, O. Igra, and T. Elperin (Academic Press, 2001), Chap. 3 & 4, pp. 339 - 411.

[69] P. A. Thompson and Y. Kim, Phys. Fluids **26**, 3211 (1983).

[70] P. A. Thompson, H. Chaves, G. E. A. Maier, Y. Kim and H. Speckmann, J. Fluid Mech. **185**, 385 (1987).

[71] M. S. Cramer, J. Fluid Mech. **199**, 281 (1989).

[72] R. Menikoff and B. J. Plohr, Rev. Mod. Phys. **61**, 75 (1989).

[73] W. Dahmen, S. Müller and A. Voss, *In Analysis and Numerics for Conservation Laws, (Ed. G. Warnecke).* Springer Verlag, 137 (2005).

[74] Ya. B. Zel'dovich and Yu. P. Reizer, *Physics of Shock Waves and High-Temperature Hydrodynamic Phenomena.* (Dover 2002).

[75] J. B. Alder and T. E. Wainwright, J. Chem. Phys. **27**, 1208 (1957).

[76] J. B. Alder and T. E. Wainwright, Phys. Rev. **127**, 359 (1962).

[77] W. G. Hoover and F. H. Ree, J. Chem. Phys. **49**, 3609 (1968).

[78] J. A. Barker and D. Henderson, Rev. Mod. Phys. **48**, 587 (1976).

[79] J. P. Hansen and J. R. McDonald, *Theory of simple liquids*, Academic Press, London, (1986).

[80] A. Münster, *Statistical Thermo-dynamics*, Springer-Verlag Berlin Heidelberg New York, Vol. 2 (1974).

[81] P. A. Thompson, G. A. Carofano and Y. Kim, J. Fluid Mech. **166**, 57 (1986).

[82] L. V. Woodcock, J. Chem. Soc., Faraday Transactions **72**, 731 (1975).

[83] N. Zhao, M. Sugiyama and T. Ruggeri, J. Chem. Phys. **129**, 054506 (2008).

[84] S. Taniguchi, A. Mentrelli, N. Zhao, T. Ruggeri and M. Sugiyama, Phys. Rev. E **81**, 066307 (2010).

[85] A. Mentrelli and T. Ruggeri, Suppl. Rend. Circ. Mat. Palermo **II/78**, 201 (2006).

[86] A. Mentrelli, T. Ruggeri, M. Sugiyama and N. Zhao, Wave Motion **45**, 498 (2008).

[87] L. Pareschi, G. Puppo and G. Russo, SIAM J. Sci. Comput. **26**, 979 (2005).

[88] A. Cheng, M. L. Klein and C. Caccamo, Phys. Rev. Lett. **71**, 1200 (1993).

[89] M. H. J. Hagen, E. J. Meijer, G. C. A. M. Mooij, D. Frenkel and H. N. W. Lekkerkerker, Nature **365**, 425 (1993).

[90] L. Mederos and G. Navascués, Phys. Rev. B **50**, 1301 (1994).

[91] Y. Zheng, N. Zhao, T. Ruggeri, M. Sugiyama, S. Taniguchi, Phys. Lett. A **374**, 3315 (2010).

[92] L. Quartapelle, L. Castelletti, A. Guardone and G. Quaranta, J. Comput. Phys. **190**, 118 (2003).

[93] S. Taniguchi, A. Mentrelli, T. Ruggeri, M. Sugiyama and N. Zhao, Phys. Rev. E **82**, 036324 (2010).

[94] N. Zhao, A. Mentrelli, T. Ruggeri and M. Sugiyama (submitted).

[95] H. C. Longuet-Higgins: Mol. Phys. **8** (1964) 549.

[96] D. A. Young and B. J. Alder: Phys. Rev. A **3** (1971) 364.

[97] S. Taniguchi, N. Zhao and M.Sugiyama, "Shock-induced phase transition in systems of hard spheres with attractive force" (in preparation). The contents were partially reported at the ISWI (International Shock Wave Institute) Conference 2010 (UK).

List of Papers

Chapter 2

S. Taniguchi, A. Mentrelli, N. Zhao, T Ruggeri and M. Sugiyama:
"Shock-Induced Phase Transition in Systems of Hard Spheres with Internal Degrees of Freedom"
Phys. Rev. E Vol. 81 (2010) 066307 (13 pages).

Chapter 3

S. Taniguchi, A. Mentrelli, T. Ruggeri, M. Sugiyama and N. Zhao:
"Prediction and simulation of compressive shocks with lower perturbed density for increasing shock strength in real gases"
Phys. Rev. E Vol. 82 (2010) 036324 (5 pages).

Chapter 5

Y. Zheng, N. Zhao, T. Ruggeri, M. Sugiyama and S. Taniguchi:
"Non-polytropic effect on shock-induced phase transitions in a hard-sphere system"
Phys. Lett. A Vol. 374 (2010) pp. 3315-3318.

Other Publications

C. Curro, G. Valenti, M. Sugiyama, S. Taniguchi:
"Propagation of an acceleration wave in layers of isotropic solids at finite temperatures" Wave Motion. Vol. 46(2) (2009) pp. 108-121.

S. Taniguchi, A. Iwasaki and M. Sugiyama:
"Relationship between Maxwell Boundary Condition and Two Kinds of Stochastic Thermal Wall"
J. Phys. Soc. Jpn. Vol. 77 (2008) 124004 (5 pages).

S. Taniguchi, M. Nakamura, M. Sugiyama, M. Isobe and N. Zhao:
"Analysis of Heat Conduction Phenomena in a One-Dimensional Hard-Point Gas by Extended Thermodynamics"
Proceedings of XIV International Conference on Waves and Stability in Continuous Media (World Scientific Pub.) (2008) pp.560 — 569.

S. Taniguchi, M. Nakamura, M. Sugiyama, M. Isobe, and N. Zhao:
"Phenomenological Approach to Heat Conduction in a One-Dimensional Hard-Point Gas beyond Local Equilibrium"
J. Phys. Soc. Jpn. Vol.77 (2008) 014004 (10 pages).

S. Taniguchi, M. Nakamura, M. Isobe, N. Zhao and M. Sugiyama:
"Heat conduction problem in a one-dimensional hard-point gas: Molecular dynamics and extended thermodynamics"
Comp. Phys. Commun. Vol. 177 (2007) pp.164-165.